Investigations of Root Epidermal Cell Specification in *Arabidopsis thaliana*

by

Wenjia Wang

A dissertation submitted in partial fulfillment
of the requirements for the degree of
Doctor of Philosophy
(Molecular, Cellular, and Developmental Biology)
in the University of Michigan
2020

Doctoral Committee:

Professor John W. Schiefelbein, Chair
Professor Jairam Menon
Associate Professor Erik E. Nielsen
Associate Professor Andrzej Wierzbicki

Wenjia Wang

wangwenj@umich.edu

ORCID ID: 0000-0002-4809-251X

holidays but they've never complained a single word about it. I have received so much

support, encourage, and love from them throughout my life. I dedicate not only this

dissertation, but everything I gained to my parents.

TABLE OF CONTENTS

LIST OF FIGURES

LIST OF TABLES

ABSTRACT

Development of multicellular organisms relies on proper specification of multiple cell types. The root epidermis of *Arabidopsis thaliana* consists of root-hair and non-hair cell types, and has been used as a powerful tool to study cell specification thanks to its easy accessibility and discernable morphologies. Arabidopsis root epidermis generates a position-dependent cell pattern, underlying which is a complicated network of transcription factors. Taking advantage of a wealth of previous studies on gene regulation during Arabidopsis root epidermal cell specification, my research deciphers novel root epidermis patterning mutants emerging from genetic screenings. The ultimate goal of this dissertation is to provide deeper and novel insights into root epidermal cell specification.

The first half of my dissertation research starts from a missense mutation altering one residue of the WEREWOLF (WER) protein, a central transcription factor regulating root epidermal cell specification. WER is critical for proper specification of both root-hair and non-hair cells, but little functional analysis of this protein has been performed. My research characterizes how this missense mutation alters DNA-protein interactions and the protein-protein interactions that are essential for WER function, and how expression of WER target genes, which encode important regulators for root epidermal cell specification, is affected accordingly. The importance of this specific residue in WER is further addressed through generation of a series of substitutions at this position that

lead to a variety of disruptions in root epidermal cell patterning. Taken together, this part of my dissertation dissects WER protein function during root epidermal cell specification, and more importantly, reveals the necessity of a balanced production of multiple regulators for proper cell patterning.

The second half of my dissertation studies the effects of defective ribosome biogenesis on root epidermis development. The rationale of this research project is endorsed by observations that mutants in ribosome biogenesis factors cause a cell fate switch from root-hair cell to non-hair cell. Incorporating genetic and molecular approaches, my research identifies misregulated root epidermis cell specification regulators responsible for this unique mutant phenotype. Moreover, a novel regulatory module is identified as the connection between root epidermal cell specification and ribosomal stress responses. Therefore, my research provides original evidence for plants' ability to adjust their root hair production according to ribosome biogenesis status.

Taken together, my dissertation investigates Arabidopsis root epidermal cell specification in two distinct yet related aspects: how the robustness of cell specification is achieved under normal growth conditions, and how the plasticity of cell specification is adopted under stressed conditions.

Chapter 1

General Introduction

Root epidermis development in *Arabidopsis thaliana*

Arabidopsis primary root formation and structure

In *Arabidopsis thaliana*, formation of a primary root starts from embryogenesis (van den Berg et al. 1998; De Smet et al. 2010; Petricka et al. 2012; ten Hove et al. 2015). A zygote first undergoes asymmetric cell division: the top smaller daughter cell (future shoot end) gives rise to the proembryo; the bottom larger daughter cell (future root end) continues to divide horizontally and form a suspensor structure. The uppermost suspensor cell, named as hypophysis, continues to divide asymmetrically: the upper daughter cell gives rise to the quiescent center (QC), which contains a group of 4 cells showing little or no mitotic activities but are responsible for recruiting and maintaining stem-cell properties of adjacent cells through signaling induction (van den Berg et al. 1997; Doerner 1998; Rovere et al. 2016); the lower daughter cell gives rise to columella initials that form the future apical root cap. Meanwhile, the proembryo undergoes multiple cell divisions and contributes to initials for other root tissues. All these initials compose the root meristem surrounding the QC and ultimately define the primary root structure (Figure 1.1).

Arabidopsis primary roots display well-organized structures (Smith et al. 2012; Fisher et al. 2016). The outermost structures at root tips are the apical and lateral root

caps. The innermost structure is a stele bundle, consisting of vascular cells including pericycle, protoxylem, metaxylem, procambium, and phloem (Vaughan-Hirsch et al. 2018) (Figure 1.2). The stele bundle is surrounded by concentric single layers of endodermis, cortex, and epidermis (Figure 1.2). Endodermal and cortical cell layers arise from endodermis/cortex initials (Figure 1.1) that undergo one periclinal cell division followed by continuous horizontal cell divisions (Benfey et al. 2000). The root epidermis is generated by epidermis/lateral root cap initials (Figure 1.1) that also undergo periclinal and horizontal divisions (Kidner et al. 2000). Due to the fact that each of these cell layers results from horizontal cell divisions of a ring of initials, each layer is composed of columns of longitudinal cell files arranged side-by-side. Furthermore, given the lack of cell movement in plant tissues, the relative positions between cells from adjacent cell layers are inherited from those of their corresponding initials and therefore remain largely unchanged during later development.

From a temporal perspective, Arabidopsis primary roots can be divided into four zones defined by different developmental stages (Verbelen et al. 2006; Bargmann et al. 2013; Huang et al. 2015). The meristematic zone constitutes an approximately 250 µm range starting from the root tip (Verbelen et al. 2006). This zone is covered by root cap and features small and flat cell shapes due to rapid cell divisions (Figure 1.3). Upon exiting the meristematic stage, cells gradually cease cell division and transit into cell elongation, thus entering the elongation zone. This zone is characterized by a rapidly increasing ratio between the height and width of root cells. During later stages of cell elongation, a particular subgroup of root epidermal cells form bulges at their basal ends, which marks the start of the differentiation zone. These bulges then undergo a distinct

2

form of cell expansion named tip growth, and form root hairs (Figure 1.3). As root hairs

reach their maximum length, these cells become fully differentiated and therefore enter

the maturation stage.

Arabidopsis primary root epidermis formation and cell patterning

The Arabidopsis primary root epidermis originates from a ring of 16 lateral root

cap/epidermis initials (Dolan et al. 1993; Scheres et al. 1994; Kidner et al. 2000). Each

initial cell first divides periclinally, leaving the outer daughter cell as a lateral root cap

initial. The inner daughter cell then divides horizontally, generating the top cell as an

epidermis daughter cell and the bottom cell maintained as the original initial. Epidermis

daughter cells continue horizontal cell divisions and contribute to meristematic

epidermal cells, which continue to divide horizontally. Occasionally, some meristematic

epidermal cells also undergo anticlinal cell divisions, leading to an increase of total cell

file numbers within the root epidermis (Berger et al. 1998a). In general, Arabidopsis

seedling roots possess 16-24 longitudinal epidermal cell files, with up to 8 additional cell

files resulting from these anticlinal cell divisions.

Root epidermal cells are in direct contact with the underlying cortical cells, which

originate from endodermis/cortex initials. An endodermis/cortex initial first divides

horizontally and maintain the bottom daughter cell as the original initial cell (Benfey et

al. 2000; Fisher et al. 2016). The top daughter cell divides periclinally to generate an

inner cell for endodermis and an outer cell for cortex, both of which continue to divide

horizontally and give rise to meristematic endodermal and cortical cells (Benfey et al.

2000). Distinct from meristematic epidermal cells, meristematic cortical cells seldom

divide in an anticlinal direction. As a consequence, the cortical cell file number of an Arabidopsis primary root remains as 8 throughout development.

Since the root epidermis contains a greater number of cell files compared to root cortex, there are two possible relative positions between an epidermal cell file and its underlying cortical cell file(s): it can be located on the clefts between two cortical cell files (the H position), or above one cortical cell file (the N position). In Arabidopsis, this difference in epidermal cell positions leads to distinct developmental routes (Galway et al. 1994; Berger et al. 1998a): epidermal cells in the H-position files develop into root-hair cells, while epidermal cells in the N-position files develop into non-hair cells. In general, an Arabidopsis primary root contains 8 root-hair cell files with 1-2 non-hair cell files interspersed between each pair of them.

Root-hair cells and non-hair cells in Arabidopsis root epidermis

Apart from the appearance of root hairs, which can be easily visualized in differentiation zones, H- and N-position root epidermal cells exhibit several distinct features in earlier developmental stages. Histochemical staining revealed that H-position cells in meristematic zones exhibit higher cytoplasmic densities and delayed formation of central vacuoles compared to their neighboring cells in the N positions (Duckett et al. 1994; Galway et al. 1994). Additionally, H-position cells in late meristematic and early elongation zones possess higher numbers of U2 small nuclear ribonucleoprotein (snRNPs) particles, the essential components for spliceosomes (Boudonck et al. 1998; Patel et al. 2008). These features imply a higher level of metabolic activities in developing H-position cells than N-position cells, most likely due to higher metabolic requirements for root hair formation. Additionally, meristematic

epidermal cells in H positions divide at higher rates compared to those in N positions, resulting in a higher cell number per file (Duckett et al. 1994; Berger et al. 1998b). So far, the connection between cell division rate and root-hair/non-hair cell specification remains unclear. Nevertheless, this feature has been used as a marker to identify H-position cell files in wild-type roots.

Cellular distinctions between H- and N-position meristematic cells in root epidermis indicate that cells in different positions adopt separate developmental programs during early stages. However, this cell fate divergence is to some extent reversible. As mentioned earlier, meristematic epidermal cells occasionally undergo anticlinal divisions, and two daughter cells undergo several horizontal divisions to generate a two-cell-file epidermal clone (Berger et al. 1998a; Berger et al. 1998b) (Figure 1.4). If the anticlinal cell division happens in an H-position cell, one daughter cell will remain in the H position while the other will end up in the N position. Analysis of these types of epidermal clones revealed that the newly formed N-position files usually contain less cells than the H-position files within the same clone and express markers of early non-hair cells (Berger et al. 1998b) (Figure 1.4). Therefore, daughter cells originating from the anticlinal division quickly adopt their new cell fate according to their new cell positions. Accordingly, meristematic epidermal cells are efficiently reprogrammed during cell division and therefore can adopt a different cell fate readily.

Molecular basis for Arabidopsis root epidermal cell patterning

The unique cell patterning of Arabidopsis primary root epidermis has provided a powerful system to study the molecular basis underlying plant cell specification. After more than 20 years of research efforts, a regulatory network has been built up to

explain this position-dependent cell specification event (Schiefelbein et al. 2009; Bruex et al. 2012; Schiefelbein et al. 2014).

The central regulator of root epidermal cell patterning is a transcription factor complex containing a MYB transcription factor, basic helix-loop-helix (bHLH) transcription factors, and a WD40 repeat protein. In plants, this type of MYB-bHLH-WD40 complex is formed from variable combinations of components that are specific for different plant tissues and is involved in a wide range of cell specification events including root hair patterning, leaf trichome patterning, and hypocotyl stomata patterning (Ramsay et al. 2005) (see below). In root epidermis, the MYB-bHLH-WD40 complex is composed of WEREWOLF (WER) as the MYB component, GLABRA 3/EHANCER OF GLABRA 3 (GL3/EGL3) as the bHLH components, and TESTA TRANSPARENT GLABRA 1 (TTG1) (Schiefelbein et al. 2014) as the WD40 component.

WER belongs to the R2R3-type MYB protein family (Stracke et al. 2001). Arabidopsis R2R3-type MYB proteins possess two MYB repeats highly resembling the R2 and R3 domains in mammalian c-Myb protein, which contains three MYB repeats but only requires R2 and R3 for DNA binding (Sakura et al. 1989; Gabrielsen et al. 1991). Structural studies of mammalian c-Myb protein revealed that both R2 and R3 domains contain three α-helices, both of which have the third helices directly interacting with DNA bases (Ogata et al. 1994). The DNA-associating residues in c-Myb R2 and R3 repeats are conserved in R2 and R3 domains of WER. *In vitro* and *in vivo* studies confirmed that WER is able to bind to promoter regions of its target genes in a sequence-specific manner (Ryu et al. 2005; Kang et al. 2009; Song et al. 2011). The third α-helix in WER R2 domain is also reported as the binding site for phosphatidic acid,

6

which is necessary for nuclear localization (Yao et al. 2013). The R3 domain in WER

contains a conserved bHLH-binding motif in its first two α-helices that associates with

GL3 and EGL3 both *in vitro* and *in vivo* (Zimmermann et al. 2004; Song et al. 2011).

The R2 and R3 domains are localized at the N terminus of WER, while the C terminus

of the protein is responsible for transactivation (Lee et al. 2001).

GL3 and EGL3 are closely related bHLH transcription factors (Li et al. 2006;

Zhang et al. 2018), and they have been shown to bind to overlapping promoter regions

of their target genes (Morohashi et al. 2007; Morohashi et al. 2009). Detailed *in vitro*

analysis generally divided GL3/EGL3 proteins into several functional segments: 1) the N

terminus is responsible for binding MYB proteins; 2) the middle segment associates with

TTG1; 3) the C terminus contains a bHLH domain responsible for DNA binding and

homo-/hetero-dimerization (Payne et al. 2000; F. Zhang et al. 2003; Pattanaik et al.

2014). Additionally, another bHLH family protein, MYC1, is also involved in root

epidermal development given the synergic relationship between *myc1* and *gl3* mutants

(and between *myc1* and *egl3* mutants) (Bruex et al. 2012). However, MYC1 fails to fully

replace GL3/EGL3 functions (Zhao et al. 2012), suggesting a distinct protein function

from GL3/EGL3.

TTG1 belongs to the WD40 protein family, which features a 40-residue domain

containing signature glycine-histidine (GH) dipeptides and tryptophan-aspartate (WD)

dipeptides (Fong et al. 1986; Xu et al. 2011). Functional studies revealed that a 25-

residue region at the C terminus of TTG1 is required to bind GL3 (Payne et al. 2000).

TTG1 does not bind MYB proteins (Pattanaik et al. 2014). Instead of acting as an

executive transcription factor, TTG1 serves as a scaffolding protein within the complex

to facilitate the recruitment and association of WER and GL3/EGL3. This argument is supported by multiple studies on MYB-bHLH-WD40 complexes reporting that overexpression of bHLH proteins significantly complement *ttg1* mutant phenotypes (Lloyd et al. 1994; Payne et al. 2000; Bernhardt et al. 2003).

Given the association of WER with GL3/EGL3 and GL3/EGL3 with TTG1, these proteins have been considered to form a 'trimeric' complex in order to function (Ramsay et al. 2005). Interestingly, *in vitro* studies revealed that addition of WER weakens the interaction between GL3/EGL3 and TTG1, which raises a possibility that this complex could also occur as two counteracting complexes of WER-GL3/EGL3 and GL3/EGL3-TTG1 (Pesch et al. 2015).

Except for *TTG1*, which is constitutively expressed in all epidermal cells with little positional specificity, *WER, GL3*, and *EGL3* display position-specific expression patterns. *WER* is expressed in all epidermal cells, but with higher levels in N-position cells (Lee et al. 1999). Consistently, WER proteins accumulate preferentially in N-position cells (Ryu et al. 2005). Both *GL3* and *EGL3* are expressed preferentially in H-position cells (Bernhardt et al. 2003; Bernhardt et al. 2005). GL3 proteins translocate to adjacent N-position cells, while EGL3 proteins preferentially remain in H-position cells (Bernhardt et al. 2005; Kang et al. 2013).

During early development of root epidermis, positional cues, most likely coming from underlying cortical cells, designate the preferential formation of WER-GL3/EGL3-TTG1 complex in N-position cells, which directly induces expression of *CAPRICE* (*CPC*) gene (Ryu et al. 2005). As an R3-type MYB protein lacking the R2 domain and the transactivation domain, CPC contains the conserved bHLH-binding domain that allows

for association with GL3/EGL3 but cannot bind to the promoter regions or induce transcription (F. Zhang et al. 2003; Tominaga et al. 2007; Dubos et al. 2010; Song et al. 2011). In addition, CPC is capable of cell-to-cell movement from N- to H-position cells (Kurata et al. 2005). All these features enable CPC to serve as a lateral inhibitor from N-position cells to block WER function in their neighboring H-position cells through competitively binding to GL3/EGL3. Apart from *CPC,* the WER-GL3/EGL3-TTG1 also mediates expression of other R3-type MYB genes including *TRYPTICHON* (*TRY*) and *EHANCER OF TRY AND CPC 1* (*ETC1*) (V. Kirik et al. 2004; Simon et al. 2007). As close family members of CPC, ETC1 and TRY are considered to function redundantly with CPC (V. Kirik et al. 2004; Simon et al. 2007). Altogether, these R3-type MYB proteins efficiently inhibit formation of WER-GL3/EGL3-TTG1 complex in H-position cells.

The R3-type MYB proteins (CPC, ETC1, TRY) robustly maintain differential amounts of WER-GL3/EGL3-TTG1 complex between H and N positions. However, this lateral-inhibition mechanism is not sufficient to set up the *de novo* differences between the two cell positions. Mutant screens have identified knockout mutants of the *SCRAMBLED* (*SCM*) gene that exhibit largely randomized accumulation of WER-GL3/EGL3-TTG1 complex in root epidermis as well as position-independent root hair patterns (Kwak et al. 2005). *SCM* encodes a kinase-receptor-like protein preferentially accumulating on the membrane of H-position cells (Kwak et al. 2005; Kwak et al. 2007). Overexpressed *SCM* leads to *WER* down-regulation (Kwak et al. 2005; Kwak et al. 2007). Although the biochemical function of SCM still remains unknown, it has been proposed that SCM integrates positional cues from underlying cortical cells and sets up

initial molecular distinctions between H and N positions during early root epidermal development via inhibiting *WER* transcription in H-position cells.

Differential accumulation of WER-GL3/EGL3-TTG1 complex between H and N positions directly leads to preferential expression of *GLABRA 2* (*GL2*) in N-position cells. As another target gene of the WER-GL3/EGL3-TTG1 complex, *GL2* encodes a homeodomain-leucine-zipper transcription factor (Masucci et al. 1996a; Song et al. 2011). The GL2 protein directly binds to promoter regions and suppress expression of a series of bHLH genes including *ROOT HAIR DEFECTIVE 6* (RHD6)*, RHD6-LIKE 1* (RSL1)*, RSL2, Lj-RSL1-LIKE 1* (*LRL1*)*, LRL2* (Lin et al. 2015)*.* These bHLH transcription factors are responsible for root hair initiation and elongation (Masucci et al. 1994; Menand et al. 2007). Therefore, *GL2* expression in N-position cells inhibits formation of root hairs and results in non-hair cell specification.

Due to the determining role of GL2 in non-hair cell formation, mutants affecting *GL2* expression result in abnormal root epidermal cell patterns. In the *gl2-1* null mutant, primary roots display nearly 100% of ectopic root-hair cells in the N position, described as a 'hairy' phenotype (Masucci et al. 1996a). Both *wer-1* and *ttg1* null mutants, which largely deplete *GL2* expression, exhibit 'hairy' phenotypes (Galway et al. 1994; Lee et al. 1999). Both *gl3-1* and *egl3-1* null mutants exhibit partial decrease in *GL2* expression and thus partially 'hairy' phenotypes, with the *gl3-1* phenotype being more dramatic (Bernhardt et al. 2003). The *gl3-1 egl3-1* double mutant exhibits a total depletion of *GL2* expression and 'hairy' roots (Bernhardt et al. 2003). Interestingly, *gl3-1* and *egl3-1* single mutants both exhibit less 'hairy' phenotypes in lower parts of roots (newly formed regions) compared to upper parts (older regions), which is not observed in *gl3-1 egl3-1*

10

(Bernhardt et al. 2003). Therefore, GL3 and EGL3 proteins might partially compensate for one another during early root development. In the *cpc-1* knockout mutant, inhibition of WER-GL3/EGL3-TTG1 complex in H-position cells is largely depleted, allowing for ectopic *GL2* expression (Wada et al. 2002). Consistently, the *cpc-1* mutant exhibits approximately 70% reduction of root-hair cells in the H position, described as the largely 'hairless' phenotype (Wada et al. 1997). Addition of the *etc1-1* knockout mutant or *try-82* null mutant to the *cpc-1* single mutant enhances this phenotype to a totally 'hairless' phenotype (V. Kirik et al. 2004; Simon et al. 2007).

Taking together all these findings, a model has been proposed to explain root-hair and non-hair cell specification in Arabidopsis root epidermis (Schiefelbein et al. 2014) (Figure 1.5): At the start of root epidermal development, SCM mediates suppression of *WER* expression and causes lower amounts of WER-GL3/EGL3-TTG1 complex in H-position cells compared to N-position cells. As a consequence, N-position cells produce more R3-type MYB proteins and mediate stronger lateral inhibition in H-position cells. Eventually, a robust amount of WER-GL3/EGL3-TTG1 is maintained in N-position cells, which leads to consistent *GL2* expression and inhibition of root hair formation. By contrast, in H-position cells, formation of WER-GL3/EGL3-TTG1 is effectively inhibited, allowing for expression of root hair promoting genes.

Multiple feedback loops within regulatory network of Arabidopsis root epidermal development

A series of positive and negative feedback loops have been discovered to reinforce this regulatory network.

First, MYB23 functions in a positive feedback loop for the WER-GL3/EGL3-TTG1 complex. In N-position cells, the WER-GL3/EGL3-TTG1 complex directly induces *MYB23* expression (Kang et al. 2009). *MYB23* encodes a R2R3-type MYB protein closely related to WER (Stracke et al. 2001). Compared to *WER*, *MYB23* is expressed in much lower levels and *myb23-1* knockout mutant displays no significant disruptions in root hair patterning (Kang et al. 2009; Bruex et al. 2012), indicating the redundant role of MYB23. However, the *WER::MYB23* construct is able to rescue *wer-1* mutant, showing that MYB23 is functionally equivalent with WER in regulating root epidermal cell specification (Kang et al. 2009). Furthermore, MYB23 is shown to potentially self-promote through binding to its own promoter region (Kang et al. 2009). Therefore, MYB23 contributes to a robust amount of R2R3-type MYB proteins in N-position cells.

Second, CPC and other R3-type MYB proteins inhibit *WER* both transcriptionally and post-translationally as a negative feedback loop. In *cpc-1* mutant, a significant portion of H-position cells exhibit stronger *WER::GFP* signals compared to wild type (Lee et al. 2002). This CPC-mediated *WER* expression inhibition is independent of that mediated by SCM (Kwak et al. 2007). Therefore, CPC contributes to additional inhibition of *WER* transcription besides inhibiting the WER protein function. As was mentioned earlier, CPC protein possesses incomplete structure as a transcription factor and acts via disrupting the formation of functional MYB-bHLH-W40 complexes. Given this, it is likely that the expression of *WER* is under positive regulation by a MYB-bHLH-WD40 complex that can be inhibited by CPC. WER has been reported to not regulate its own expression (Kang et al. 2009), so there could be other MYB proteins upstream of WER involved in this process.

In H-position cells, CPC not only inhibits WER protein function, but also suppresses *WER* expression. Actually, these inhibitory effects also occur in N-position cells as well. In *cpc-1* mutant, the *GL2::GUS* reporter, as a readout for WER-GL3/EGL3-TTG1 complex activity, shows both ectopic signals in H-position cells and stronger signals in N-position cells (Simon et al. 2007). This increase in *GL2::GUS* expression level is even more dramatic in *cpc-1 try* double mutant (Simon et al. 2007). Though CPC and TRY are considered to move to H-position cells, these observations suggest that relatively low amounts of these proteins remain and restrict WER protein function in N-position cells. In this way, these R3-type MYB proteins and MYB23 provide two opposing forces to create a fine-tuned amount of active WER-GL3/EGL3-TTG1 complexes in N-position cells.

Third, SCM receives negative feedback from the WER-GL3/EGL3-TTG1 complex. Despite a regulatory role in the root epidermis, *SCM* is actually expressed in all developing root tissues except for root cap cells (Kurata et al. 2005; Kwak et al. 2008). In *wer-1* and *gl3-1 elg3-1* mutants, the *SCM::GUS* reporter exhibit signals in a wider range among multiple root tissues compared to wild type (Kwak et al. 2008), suggesting an inhibitory effect of WER-GL3/EGL3-TTG1 complex on *SCM* expression. Consistently, in *cpc-1 try* mutant, where inhibition of WER-GL3/EGL3-TTG1 complex is depleted, the *SCM* expression range is significantly narrowed (Kwak et al. 2008). Therefore, the inhibitory effects of SCM and WER-GL3-EGL3-TTG1 complex on each other help to maintain preferential accumulation of the former in H-position cells while the latter in N-position cells.

Early roles of root epidermal cell specification regulators

As described above, physiological differences between H- and N-position cells appear much earlier than root hair emergence. Therefore, regulators responsible for epidermal differentiation should act during early development stages of root epidermis. Indeed, in 'hairy' mutant *wer-1 myb23-1*, late meristematic cells in both H and N positions contain small and scattered vacuoles, which is characteristic of H-position cells in wild type (Lofke et al. 2013). In 'hairless' mutant *cpc-1 try*, both H- and N-position cells contain big and merged vacuoles resembling wild-type N-position cells (Lofke et al. 2013). Additionally, in both 'hairy' mutants (*wer-1 myb23-1* and *ttg1*) and 'hairless' mutant (*cpc-1 try*), the differences in cell numbers between H- and N-position files are not as dramatic as in wild-type roots, reflecting comparable cell division rates (Berger et al. 1998b; Lofke et al. 2013). Accordingly, these regulators are involved in early root epidermal cell specification. By contrast, in *gl2-1* and *rhd6* mutants, vacuole sizes and cell division rates in H and N positions are comparable to wild type (Masucci et al. 1996a; Berger et al. 1998b; Lofke et al. 2013), indicating that GL2 and RHD6, downstream of WER-GL3/EGL3-TTG1 complex, act later during cell differentiation.

Epigenetic regulation in root epidermal cell specification

Apart from the genetic regulations described above, root epidermal cell differentiation also involves epigenetic regulations that modulate chromatin accessibility. Three-dimensional fluorescence *in situ* hybridization (3D FISH) experiments probing *GL2* genomic sequence showed that its chromatin regions show greater accessibility in N-position cells compared to H-position cells. Consistently, the *fasciata2* (*fas2*) mutant, which disrupts chromosome packing, leads to ectopic *GL2* expression in H-position

cells (Costa et al. 2006). Therefore, specific *GL2* expression in N-position cells, which is essential for proper root hair patterning, requires not only position-dependent accumulation of WER-GL3/EGL3-TTG1 complexes, but also differential accessibilities of *GL2* genomic sequence in H- and N-position cells. Notably, in both 'hairy' mutant *wer-1* and partially 'hairless' mutant *cpc-1*, the differences in accessibilities of *GL2* genomic region between H- and N-position cells were depleted (Costa et al. 2006), suggesting that epigenetic regulations in *GL2* rely on molecular distinctions between the two positions. More interestingly, the chromatin status of *GL2* genomic region can be quickly remodeled during cell cycles (Costa et al. 2006), which may help to explain the rapid cell fate switches in epidermal clones originating from anticlinal cell divisions (described earlier). Meanwhile, a recent genome-wide analysis in root epidermis revealed a series of genomic regions showing differential accessibilities between H- and N-position cells (Maher et al. 2018), suggesting more genes other than *GL2* are epigenetically regulated during root epidermal differentiation.

The homeostasis of histone acetylation, modulated by histone acetyltransferases (HATs) and histone deacetylases (HDACs), regulates chromatin organization and affects gene expression (Shahbazian et al. 2007). Treatment of HDAC inhibitors resulted in ectopic root-hair cells in N positions (Xu et al. 2005), revealing the importance of proper histone acetylation for proper root epidermal cell specification. Later studies discovered that HDAC18 regulates expression of *CPC, WER* and *GL2* indirectly through manipulating histone acetylation within several kinase gene loci, while HDAC6 directly modifies histone acetylation within promoter regions of *ETC1* and *GL2* (Liu et al. 2013; Li et al. 2015).

Hormone signaling pathways modulate root epidermal cell differentiation

Multiple plant hormones have been reported to participate in different regulatory steps during root epidermal cell specification.

Brassinosteroid (BR) signaling has been reported to regulate multiple upstream regulators within the root epidermal cell specification network (Kuppusamy et al. 2009; Cheng et al. 2014). Externally applied BR and depletion of BR synthesis both disrupt *GL2* expression as well as root hair patterning (Kuppusamy et al. 2009; Cheng et al. 2014). More functional studies strongly suggested that a GLYCOGEN SYNTHASE KINASE-3 (GSK3)-like kinase BRASSINOTEROID INSENSITIVE 2 (BIN2), which is deactivated by BR signaling, directly phosphorylates TTG1 and EGL3 (Cheng et al. 2014). The WER-GL3/EGL3-TTG1 complex containing phosphorylated TTG1 exhibit significantly reduced regulatory activities (Cheng et al. 2014). Therefore, a BR signaling pathway appears to regulate the WER-GL3/EGL3-TTG1 complex at post-translational levels.

Ethylene and auxin have long been known to play positive roles in root-hair cell development (Grierson et al. 2002). Blocking ethylene synthesis and genetically knocking out ethylene-stabilized transcription factors reduce root hair densities (Tanimoto et al. 1995; Zhu et al. 2011), while roots treated with ethylene precursor and mutants with constitutive ethylene response produce ectopic root-hair cells in N positions (Duckett et al. 1994; Tanimoto et al. 1995). Recent studies showed that an ethylene-stabilized transcription factor EHTYLENE INSENSITIVE 3 (EIN3) associates with RHD6 and induces expression of a root hair promoting gene, *RHD6-LIKE 4* (*RSL4*) (Yi et al. 2010; Feng et al. 2017), suggesting that ethylene signaling pathway and RHD6

contribute to root-hair cell maturation cooperatively. Nevertheless, ethylene treatment still significantly reverses the dramatic root hair loss in *rhd6* mutant (Masucci et al. 1994), suggesting that RHD6 is not essential for ethylene signaling to promote root hair formation. Similar to ethylene, treatment of auxin also restores root hair formation in the *rhd6* mutant (Masucci et al. 1994), suggesting similar regulatory positions of these two hormone signaling pathways during root hair cell differentiation. This hypothesis was supported by later studies showing that auxin signaling up-regulates *RSL4* expression in an RHD6-independent manner (Yi et al. 2010).

Notably, *GL2* expression in roots is not altered by treatments with auxin/ethylene or by mutants affecting auxin/ethylene signaling (Masucci et al. 1996b), confirming that these two hormones promote root hair morphogenesis during late cell specification regardless of upstream regulation. In this way, auxin/ethylene-mediated root hair formation could provide a means to quickly adjust root hair densities without remodeling the upstream regulatory network. Indeed, both auxin and ethylene signaling pathways are responsive to nutrient availabilities (Visser et al. 2007; Mroue et al. 2018). Specifically, auxin/ethylene signaling pathways have been reported to increase root hair densities under iron and phosphate deprivation (Ma et al. 2001; Schikora et al. 2001; Schmidt et al. 2001).

Interestingly, detailed characterization of auxin/ethylene-induced roots revealed that sites of root hair emergence in root epidermal cells are shifted far from the root meristem end, while untreated roots have root hairs emerging at sites close to the root meristem end (Masucci et al. 1994). This observation implies that differences exist between auxin/ethylene-induced root hairs and naturally formed ones.

Abscisic acid (ABA) signaling is also involved in root hair formation because ABA treatment reverses the *rhd6* mutant phenotype (van Hengel et al. 2004). Meanwhile, both exogenous ABA treatment and mutants in ABA synthesis slightly alter *GL2* expression without significantly disrupting root hair patterning (van Hengel et al. 2004), indicating that ABA signaling pathway slightly impacts early-stage root epidermal cell specification.

Nutritional stresses remodel root epidermal cell specification

It is important to note that early studies of root epidermal cell fate regulation were conducted using complete-nutrient media that creates an optimized growth condition. Recent studies revealed that certain deficiencies in nutritional supplies markedly remodel root epidermal cell specification.

It has been long observed that phosphate deficiency (Pi-) has pleotropic effects on Arabidopsis root morphologies, including an increase in root hair densities and root hair lengths, which serve to increase root surface area (Bates et al. 1996; Ma et al. 2001; Muller et al. 2004). Detailed characterization of roots grown in Pi- conditions revealed that the higher root hair densities are due to: 1) arrested epidermal cell elongation; 2) increased numbers of cortical cells, which result in more H-position cell files per root; and 3) ectopic formation of root-hair cells in N positions (Ma et al. 2001; Schikora et al. 2001; Muller et al. 2004; Savage et al. 2013; Janes et al. 2018).

Under Pi- conditions, *GL2* expression in N-position cells is significantly reduced (Rishmawi et al. 2018), indicating disrupted non-hair cell specification. Several transcriptomic studies revealed that expression of *ETC1* is up-regulated in roots exposed to Pi- conditions (Misson et al. 2005; Savage et al. 2013). A combination of

transcriptional and translational reporters further illustrated that the *ETC1* transcription level is elevated in sub-epidermal tissues (mostly in root stele), and excessive ETC1 proteins migrate into the root epidermis (Rishmawi et al. 2018). Being functionally redundant with CPC, ETC1 is able to trigger ectopic root-hair cell formation when overexpressed (Victor Kirik et al. 2004), therefore suggesting that ETC1 accounts for the ectopic root-hair cell formation triggered by Pi-. Indeed, the *etc1* mutant depletes ectopic root hair production in response to Pi- (Savage et al. 2013).

The *cpc-1* mutant, which produces significantly less root-hair cells under full-nutrient conditions, exhibits markedly increased root-hair cell production in both H and N positions under Pi- conditions (Muller et al. 2004; Savage et al. 2013). Notably, the additional root hair production in H-position cells of *cpc-1* is also ETC1-dependent (Rishmawi et al. 2018), indicating that the Pi- triggered ETC1 effect is independent of cell positions. This is probably because stele-originated ETC1 proteins migrate into H- and N-position cells non-discriminatively. Interestingly, *etc1* also affects root hair elongation in response to Pi- (Chandrika et al. 2013), indicating a dual role of ETC1 in early and late stages of root-hair cell specification.

Iron deficiency (Fe-) has also been reported in numerous studies to affect root epidermal cell specification in Arabidopsis. Fe-deprived roots respond in a similar way as Pi-deprived ones, featuring longer root hairs and ectopic root hair production in N positions (Schmidt et al. 2001; Muller et al. 2004). Fe- is also able to induce additional root hairs in *cpc-1* mutant as Pi- (Muller et al. 2004), which suggests overlapped molecular mechanisms underlying these two nutritional stresses. However, the proportion of ectopic root-hair cells triggered by Fe- is less pronounced than that

19

triggered by Pi-, and root hair production in Fe- conditions show higher dependence on auxin/ethylene signaling pathways (described earlier) (Schikora et al. 2001; Schmidt et al. 2001). These findings implicate that Pi- probably triggers multiple responding pathways while Fe- only triggers a subset of these pathways.

Analogous regulation of other cell specification events in Arabidopsis

As central regulators for root epidermal specification, WER, GL3/EGL3 and TTG1 function through forming a MYB-bHLH-WD40 complex. This type of complex is known to regulate cell specification events in multiple plant tissues.

Hypocotyl stomata

The seedling hypocotyl is an embryo-originated stem structure connecting the cotyledon and root. The hypocotyl contains multiple cell layers including epidermis, cortex, endodermis and stele/vascular tissues that are arranged concentrically (Kim et al. 2017). Similar to roots, epidermal and cortical cell layers in hypocotyl both consist of longitudinal cell files, and the epidermis contains a larger number of cell files than cortex. Therefore, one epidermal cell file can be in contact with either one or two underlying cortical cell files (Pillitteri et al. 2013). As openings for gas exchange and water evaporation, stomatal cells are widely distributed in most aboveground epidermal tissues (Zeiger 1983). In hypocotyl, stomatal cells are formed only in cell files lying over two cortical cell files, or in the 'S' positions analogous to the H positions in root epidermis (Berger et al. 1998c; Hung et al. 1998).

The position-dependent stomata patterning in the hypocotyl epidermis strongly suggests a similar molecular basis to that underlying cell patterning in the root epidermis. Indeed, *wer-1*, *gl3 egl3*, *ttg1*, and *gl2-1* mutants all exhibit ectopic production

stomatal cells in hypocotyl (Berger et al. 1998c; Hung et al. 1998; Lee et al. 1999; Bernhardt et al. 2005), while *cpc-1* exhibits less stomata formation in S positions, which can be further enhanced by *try* (Serna 2008). Molecular analysis further confirmed that these regulator genes are regulated in a similar manner as in root epidermis. *GL2* and *CPC* are expressed preferentially in epidermal cell files touching single cortical cell files (analogous to the N positions in root epidermis) and are dependent on *WER*, *GL3/EGL3*, and *TTG1* (Berger et al. 1998c; Lee et al. 1999; Bernhardt et al. 2005). GFP-tagged CPC proteins are detected in both S and N positions, showing its capability of cell-to-cell movement (Serna 2008). Thus, hypocotyl stomata patterning likely depends on the same regulatory network as is used in root epidermis patterning.

Before emergence of stomatal cells, S- and N-position hypocotyl epidermal cells, just like in root epidermis, are distinguishable according to several morphological features. First, N-position cells show protruding cell shapes while S-position cells are non-protruding; second, total cell numbers of S-position cell files are larger than those of N-position cell files, which results from more rounds of cell divisions during embryogenesis (Gendreau et al. 1997; Pillitteri et al. 2013). These two features, however, are not altered by mutants of cell patterning regulators (i.e. *wer-1*, *gl3 egl3*, and *ttg1*) (Berger et al. 1998c; Hung et al. 1998). Therefore, these cell patterning regulators, unlike in root epidermis, are not involved during early hypocotyl epidermis development.

Notably, in hypocotyl epidermis, not all S-position cells develop into stomatal cells. Wild-type hypocotyls only contain an average of 1.5 stomatal cell units per cell file (Berger et al. 1998c). The S-position cells that don't develop into stomatal cells exhibit

no expression of *WER* or *GL2*, and stomatal cell number per cell file is not affected in mutants of these regulators (Hung et al. 1998; Lee et al. 1999). Therefore, additional regulatory factors exist within hypocotyl epidermis to space stomatal cells within hypocotyl epidermis files (Nadeau et al. 2002).

Leaf trichome

Trichomes are highly specialized, branch-forming epidermal cells in leaves. Arabidopsis trichome cells, distinct from regular leaf epidermal cells, undergo a sequential series of special developmental events including endoreplication/cell enlargement, surface outgrowth, and primary/secondary branching (Hulskamp et al. 1994; Hulskamp 2004). Genetic and molecular studies on trichome patterning have revealed a regulatory network closely related to that in the root epidermis. A MYB-bHLH-WD40 complex, consisting of GLABROUS 1 (GL1), GL3/EGL3, and TTG1, promotes trichome formation (Payne et al. 2000). This complex is believed to directly induce expression of *GL2*, which initiates trichome morphogenesis (Rerie et al. 1994; Szymanski et al. 1998; Morohashi et al. 2007; Wang et al. 2008). The *gl1*, *gl3 egl3*, and *ttg1* mutants produce no trichomes on leaves, and all leaf epidermal cells (except for stomatal cells) exhibit a universal cellular phenotype regarding cell sizes and polyploidy levels, indicating that these regulators operate at beginning stages of trichome development; by contrast, *gl2* mutant leaves exhibit reduced and aborted trichomes, suggesting a later role of GL2 protein during trichome development (Hulskamp et al. 1994; Rerie et al. 1994; F. Zhang et al. 2003).

Within the leaf epidermis, trichome cells are regularly spaced and seldom cluster, which is believed to result from a lateral-inhibition mechanism similar to that in root

epidermis (Hulskamp 2004). The CPC protein, expressed in trichome cells induced by GL1-GL3/EGL3-TTG1 complex, is capable of cell-to-cell movement (Zhao et al. 2008; Wester et al. 2009). CPC, TRY and ETC1 proteins function as negative regulators for trichome development with partially overlapping roles: *try* mutant leaves exhibit clustered trichomes adjacent to each other (Hulskamp et al. 1994); *cpc-1* mutant leaves exhibit increased numbers of trichomes but no clustering (Schellmann et al. 2002b; Victor Kirik et al. 2004); *cpc try* double mutant exhibit larger trichome clusters (Schellmann et al. 2002b); *cpc try etc1* mutant bear even larger trichome clusters expanding throughout leave areas (Victor Kirik et al. 2004).

Notably, trichomes in *try* mutant, apart from being clustered, display increased rounds of endoreplication and increased numbers of branches (Hulskamp et al. 1994), which is recognized as an enhancement of trichome specification. This observation suggests an interesting possibility that TRY also mediates cell-autonomous restrictions in trichome development, which is reminiscent of the inhibitory effects of TRY and CPC on WER function in N-position cells of the root epidermis (Simon et al. 2007) (described earlier).

As in the root epidermis, where MYB23 functions redundantly with WER, two R2R3-type MYB proteins, MYB23 and MYB82, are found to be functionally equivalent with GL1 for initiating trichome development (Kirik et al. 2005; Liang et al. 2014). Single mutants of these two genes, however, exhibited mild or no reduction in trichome density (Kirik et al. 2005; Liang et al. 2014). Additionally, MYB23 is involved in trichome branching during later development (Kirik et al. 2005; Kang et al. 2009).

Ribosome biogenesis and plant development

Ribosomes are housekeeping cellular components responsible for protein synthesis. As a ribonucleoprotein complex, one ribosome is composed of one large ribosomal subunit (LSU) and one small ribosomal subunit (SSU) (Ramakrishnan 2002). Based on sedimentation rates, eukaryotic ribosomes are designated as 80S (LSU as 60S and SSU as 40S) (S stands for the Svedberg coefficent unit). In plants, the 40S subunit contains 18S ribosomal RNA (rRNA) and approximately 33 ribosomal proteins (RPs), and the 60S subunit contains 25S, 5.8S, and 5S rRNAs together with approximately 47 RPs (Weis et al. 2015a; Saez-Vasquez et al. 2019). The biogenesis of ribosomes is a multi-step process, but can be roughly divided into rRNA biogenesis and RP assembly.

rDNA genes and rDNA transcription in Arabidopsis

The rRNAs are encoded by ribosomal DNA (rDNA) genes. Specifically, the 18S, 5.8S, and 25S rRNAs are encoded by polycistronic 45S rDNA genes, and the 5S rRNAs are encoded by 5S rDNA genes. Plant genomes possess hundreds to thousands of rDNA units, most of which are organized in arrays of tandem repeats interspersed by spacer sequences (Srivastava et al. 1991; Rosato et al. 2016). In Arabidopsis, the majority of 45S rDNA arrays are located at the tops of chromosomes 2 and 4 abutting the telomeres, termed as the nucleolus organizer regions 2 and 4 (NOR2 and NOR4) each containing 350~400 rDNA units (Copenhaver et al. 1995; Copenhaver et al. 1996). Under normal growth conditions, NOR2 is actively transcribed, while NOR4 is repressed due to silencing chromatin modifications (Pontvianne et al. 2013; Chandrasekhara et al. 2016). 5S rDNA arrays, on the other hand, are localized in the pericentromeric

heterochromatin regions of chromosomes 3, 4 and 5, although 5S rRNAs are mainly transcribed from chromosomes 4 and 5 (Murata et al. 1997; Cloix et al. 2000).

45S rDNA units are separated from their neighboring units by intergenic spacer regions, within which are the regulatory sequences necessary for rDNA gene transcription. 45S rDNA transcription is mediated by RNA polymerase I (Pol I) and requires a promoter region from -55 ~ -33 to +6 relative to the transcription initiation site (Doelling et al. 1995; Moss et al. 1995). One 45S rDNA unit contains 18S, 5.8S, and 25S rDNAs surrounded by the 5' and 3' external transcribed spacers (5' ETS and 3' ETS) and interspersed by the internal transcribed spacers 1 and 2 (ITS1 and ITS2) (Figure 1.6). 5' ETS region contains an $A_{123}B$ cluster conserved in Brassicaceae (Caparros-Ruiz et al. 1997; Saez-Vasquez et al. 2004a). Interestingly, early rRNA processing factors (see below) bind to the $A_{123}B$ clusters in both rDNA and rRNA (Caparros-Ruiz et al. 1997), which suggests the coordination between rDNA transcription and rRNA processing. Specifically in Arabidopsis, 5' ETS possesses a unique 1-kb insertion downstream of the $A_{123}B$ cluster with unknown function (Gruendler et al. 1991; Saez-Vasquez et al. 2019). Arabidopsis 3' ETS generally contains 3-5 repeat elements, and can be divided into four major types of variants (*VAR1-4*) according to the numbers of these elements and other sequence features (Pontvianne et al. 2010; Abou-Ellail et al. 2011; Weis et al. 2015a). *VAR1* is encoded by the silenced NOR2 and the rest variants are encoded by the activate NOR4 (Chandrasekhara et al. 2016). Notably, the 3' ETS sequence of *VAR1* rDNA does not contribute to the silencing of NOR2 (Mohannath et al. 2016). All types of 3' ETS variants contain particular sequences that can potentially recruit early rRNA processing factors that also bind to

25

the $A_{123}B$ cluster in 5' ETS (Abou-Ellail et al. 2011), thus leading to the thought that primary processing of 5' and 3' ETS could be coordinated (Weis et al. 2015a).

The 5S rDNAs are transcribed by RNA polymerase III (Pol III) that potentially recognizes promoter region from -30 to -1 relative to the transcription initiation site (Venkateswarlu et al. 1991; Cloix et al. 2003).

Arabidopsis rRNA processing

Following its transcription, the Arabidopsis 45S rRNA is cleaved at the B_0 site in 3' ETS, spliced to remove the 1-kb insertion in 5' ETS, and cleaved at the P site in 5' ETS, which eventually gives rise to 35S rRNA. The 7-kb 35S rRNA is the largest rRNA precursor (pre-rRNA) that is abundantly detected in Arabidopsis (Weis et al. 2015a; Saez-Vasquez et al. 2019), suggesting that its processing happens mostly after transcription.

The processing of 35S pre-rRNA follows two alternative pathways (Figure 1.6) (Weis et al. 2015a; Saez-Vasquez et al. 2019). The major pathway, termed as the ITS1-first pathway, first cleaves 35S pre-rRNA at the A_3 site within ITS1; the minor pathway, termed as the 5' ETS-first pathway, first cleaves 35S pre-rRNA at the P' and P_2 sites within 5' ETS and then cleaves at the A_2 site within ITS1. The resulting pre-rRNAs from both pathways then undergo stepwise trimming and cleavages to produce the 20S and 27SB$_{S/L}$ pre-rRNAs. Finally, 20S and 27SB$_{S/L}$ pre-rRNAs from both pathways generate mature 18S, 5.8S, and 25S rRNAs. In general, these two pre-rRNA processing pathways share the same set of cleavage/trimming sites (despite different temporal orders) except the alternative cleavages at the A_2 or A_3 sites, which defines separation of the SSU 18S rRNA from the LSU 5.8S/25S rRNAs. Curiously, a third and plant-

specific 35S pre-rRNA processing pathway has been recently identified, termed as the ITS2-first pathway (Palm et al. 2019; Saez-Vasquez et al. 2019). This pathway first cleaves 35S pre-rRNA at the C_2 site within ITS2 to separate 25S rRNA from 18S/5.8S rRNAs (Palm et al. 2019), which is distinct from the other two pathways that both first separate 18S rRNA from 5.8S/25S rRNAs.

Compared to 45S rRNA, the biogenesis of 5S rRNA is poorly understood in plants but could be predicted according to studies on other species. In yeast and drosophila, after transcription, the pre-rRNAs for 5S undergo 3' trimming mediated by several RNA 3' exonucleases (van Hoof et al. 2000; Ciganda et al. 2011; Gerstberger et al. 2017).

Ribosome biogenesis in eukaryotes

In yeast, shortly after transcription initiation, the nascent pre-rRNA recruits a large complex named as the SSU processome, or the 90S pre-ribosome (Grandi et al. 2002; Phipps et al. 2011). In general, 90S pre-ribosome contains pre-rRNAs, ribosome proteins (RPs) that compose the future ribosome, and multiple classes of proteins and RNAs that dynamically associate and dissociate to facilitate ribosome biogenesis (Grandi et al. 2002; Kornprobst et al. 2016). Along with pre-rRNA processing, 90S pre-ribosome undergoes stepwise maturation and eventually divides into the pre-40S and pre-60S ribosomes upon the A_2 cleavage that separates 18S rRNA from 5.8S/25S rRNAs (the A_2 cleavage is one step of the 5' ETS-first pathway, which is the major pre-rRNA processing pathway in yeast) (Schafer et al. 2003; Konikkat et al. 2017). After independent maturation and exportation processes, 40S and 60S ribosomes are assembled together in cytoplasm, where the final 3' maturation of 18S rRNA happens

27

(Garcia-Gomez et al. 2014). The exact time when 5S rRNAs participate during ribosome biogenesis is unknown, but yeast studies reveal that the 5S rRNAs are incorporated in 90S pre-ribosomes (Zhang et al. 2007; Henras et al. 2008).

In plants, a complex homologous to the yeast 90S pre-ribosome has been identified and named as the nuclear factor D (NF D) or the *Brassica oleracea* U3 snoRNP (BoU3) (Saez-Vasquez et al. 2004a; Saez-Vasquez et al. 2004b; Weis et al. 2015a). Prior to rRNA transcription, the BoU3 complex is recruited to the $A_{123}B$ cluster within the 5' ETS region in 45S rDNA (Saez-Vasquez et al. 2004a). After transcription starts, this complex binds to the $A_{123}B$ cluster in 45S rRNA and mediates cleavage at the P site (Saez-Vasquez et al. 2004a; Saez-Vasquez et al. 2004b). Later steps of plant ribosomal biogenesis is less well studied compared to yeast, but it has been considered that a similar procedure is adopted based on the fact that: 1) the majority of yeast 90S pre-ribosome components is conserved in Arabidopsis; and 2) common pre-rRNA intermediates exist in both yeast and Arabidopsis (Weis et al. 2015a; Saez-Vasquez et al. 2019).

In eukaryotic cells, major steps of ribosome biogenesis take place specifically at the nucleolus, a large and highly dynamic domain within the interphase nucleus (Olson et al. 2002; Lam et al. 2005). Although membrane-less, the nucleolus contains several distinct compartments. The dense fibrillar component (DFC) occupies the majority of nucleolar volume, serving as a matrix for the fibrillar centers (FCs) (Kalinina et al. 2018). DFC and FCs together form the nucleolonema that harbors active NOR4 while excluding silenced NOR2 (Chandrasekhara et al. 2016). Specifically, FCs contain rRNA transcription sites (Stepinski 2014), and DFC is considered to provide the environment

28

needed for transcription (Kalinina et al. 2018). In plant cells (soybean roots), the number

of FCs is proportional to rRNA transcription levels (Stepinski 2010). After transcription,

rRNA products are processed first in DFC then migrate to the peripheral granular

component (GC) where the final steps of rRNA processing as well as RP assembly

occur (Stepinski 2014; Kalinina et al. 2018).

Notably, plant cells contain a special cavity or vacuole at the center of nucleolus

(NoV). The function of this structure is largely unknown, but it is hypothesized that the

NoV serves as a sequestration or storage site of functional elements for ribosomal

biogenesis or other biological activities and potentially responds to developmental or

environmental signals (Mineur et al. 1998; Stępiński 2008; Stepinski 2014; Kalinina et al.

2018).

snoRNAs and ribosome biogenesis factors in eukaryotes

As a complicated biological process, ribosome biogenesis requires cooperation

of numerous non-ribosomal factors (Grandi et al. 2002; Weis et al. 2015a; Saez-

Vasquez et al. 2019). The snoRNAs are noncoding RNAs accumulating in nucleoli.

Based on sequence, snoRNAs can be divided into the box-C/D snoRNAs and the box-

H/ACA snoRNAs (Watkins et al. 2012). Different classes of snoRNAs associate with

specific and conserved sets of partner proteins to form functional snoRNPs that are

responsible for covalent modifications of rRNAs: box-C/D snoRNPs mediate 2'-*O*-ribose

methylation, and box-H/ACA snoRNPs mediate conversion of uridine to pseudouridine

(Brown et al. 2003; Thomson et al. 2013). In both cases, snoRNAs serve as the guiding

molecules through base pairing with target rRNAs (Brown et al. 2003; Watkins et al.

2012). Notably, 3D structure of yeast ribosomes revealed that these rRNA modification

sites, existing in both SSU and LSU, are prominently clustered around the A, P, and E sites of ribosome, which are critical reaction surfaces for charged tRNA entering, peptidyl tRNA formation, and discharged tRNA exiting (Decatur et al. 2002; Sloan et al. 2017). Compared to yeast and mammals, plants generally possess higher numbers of sites for methylation or pseudouridine conversion in mature rRNAs (approximately 2-fold of yeast and 1.2-fold of human for both types of modifications), which is roughly proportional to the increased numbers of detected snoRNA in their transcriptomes (Brown et al. 2003; Dieci et al. 2009; Sloan et al. 2017). This increase in rRNA modification sites might reflects more complicated regulations in ribosomal activities, as plants are more subject to environmental challenges due to their immobility.

The role of eukaryotic snoRNPs is not restricted to rRNA modifications: the U3 subgroup of box-C/D snoRNPs is the pioneering component of 90S pre-ribosome and is required for the co-transcriptional P-site cleavage (Hughes et al. 1991; Borovjagin et al. 1999; Saez-Vasquez et al. 2004b); the U14 box-C/D snoRNPs base-pairs with 18S rRNA and mediates cleavages in 5' ETS and ITS1 (Liang et al. 1995; Brown et al. 1998). Depletions or disruptions of these snoRNPs lead to abnormally accumulated pre-rRNAs (Li et al. 1990; Hughes et al. 1991). Additionally, an Arabidopsis box-C/D snoRNA *HIDDEN TREASURE 2* (*HID2*) was recently found to be involved in 27S pre-rRNA processing (Zhu et al. 2016).

It is of note that most functional studies of eukaryotic snoRNPs were conducted using yeast and mammalian cells, but formation and function of snoRNPs is considered conserved in plants, despite the existence of some species-specific snoRNAs subgroups and partner proteins (Brown et al. 1998; Brown et al. 2003).

Apart from snoRNPs, pre-ribosomes are decorated by numerous non-ribosomal proteins that are designated as ribosome biogenesis factors (RBFs) responsible for rRNA cleavages/modifications and RP assembly (Nazar 2004; Thomson et al. 2013). Depending on particular biochemical functions, RBFs fall into a spectrum of categories. Endonucleases (e.g. RNase III, RNase P-related, and RNase H-related, etc.) are required for pre-rRNA cleavage; exonucleases (e.g. 5'-3' XRN family and 3'-5' exosome, etc.) are required for pre-rRNA end trimming (Tomecki et al. 2017). Methyltransferases are responsible for rRNA methylations on purine and pyrimidine rings as well as the pseudouridine generated by snoRNPs; acetyltrasferases are responsible for rRNA acetylations on pyrimidine rings (Sloan et al. 2017; Sergiev et al. 2018). Just as the snoRNP-mediates rRNA modifications, these modification sites are also clustered around functional surfaces in ribosomes (Sloan et al. 2017; Sergiev et al. 2018). Additionally, pre-rRNA polyadenylation at the 3' terminal is mediated by exosome complexes most likely for pre-rRNA trimming or by-production degradation (Kuai et al. 2004; LaCava et al. 2005; Slomovic et al. 2006).

Given their distinct roles during ribosome biogenesis, different RBFs associate and dissociate the pre-ribosomes at different stages. In yeast the early-stage pre-90S ribosomes primarily precipitate with RBFs involved in SSU biogenesis (e.g. U3 snoRNP components) but show minor association with LSU biogenesis RBFs (Grandi et al. 2002), which is consistent with the fact that 18S rRNA, as a SSU component, is transcribed earlier than LSU components 5.8S and 25S rRNAs. LSU biogenesis RBFs mainly associate with the pre-60S ribosome after the A_2/A_3 cleavage separates pre-40S and pre-60S ribosomes (Fatica et al. 2002). Spatially, RBFs accumulate in different

cellular compartments depending on their specific roles. Most RBFs are prominently localized in nucleoli where the majority of ribosome biogenesis happens, while the Nob1p (yeast)/NOB1 (Arabidopsis) protein does not dissociate from pre-40S ribosome until after exportation to the cytosol in order to cleave 20S pre-rRNA at the D site (Figure 1.6) as the final step of 18S rRNA maturation (Fatica et al. 2003; Palm et al. 2018).

Studies on ribosomal biogenesis, which were conducted most thoroughly in yeast, identify approximately 250 RBFs, of which around 80% have homologous genes in plants (Ebersberger et al. 2014). Though only a small proportion of these RBFs have been experimentally characterized in plants, most of the tested proteins show conserved or similar functions as their yeast homologues (Weis et al. 2015a; Saez-Vasquez et al. 2019). Meanwhile, a batch of plant-specific RBFs has been identified to participate in pre-rRNA processing (Palm et al. 2019).

Regulation of ribosome biogenesis in plants

Ribosome biogenesis, as one essential cellular activity, should occur constitutively. Nevertheless, studies have shown that eukaryotic ribosome biogenesis is under cell-type-specific and developmental-stage-specific regulations (Sanchez et al. 2016; Kos-Braun et al. 2017; Chau et al. 2018).

In plants, ribosome biogenesis is regulated at multiple steps in response to developmental cues. In general, ribosome biogenesis is elevated in actively growing tissues such as embryos and meristems, where expression of RBF genes is upregulated (Saez-Vasquez et al. 2019). Consistently, the Target of Rapamycin (TOR) signaling pathway that regulates cell division and growth positively induces transcription

of rDNA and RP genes (Ren et al. 2012; Xiong et al. 2013). In Arabidopsis, NOR4 is actively transcribed while NOR2 is silenced (described above). In fact, NOR2 transcripts (*VAR1*) are detected during early embryonic development and early seedling development (Saez-Vasquez et al. 2019). After plants exit these early stages, NOR2 is then repressed via DNA methylation at cytosine and histone methylation at H3K9 in a chromosome-selective manner (Woo et al. 2008; Chandrasekhara et al. 2016; Mohannath et al. 2016). A possible rationale for this regulation is that the demand for ribosomes is higher in developing embryos and seedlings, thus leading to more rRNA production.

Arabidopsis processes pre-rRNA in three alternative pathways, the 5' ETS-first pathway (minor), the ITS-first pathway (major), and the additional ITS2-first pathway (described above). It is considered that having multiple pathways helps to secure sufficient rRNA production, which is supported by the discovery that the minor pathway is upregulated when the major pathway is impaired by specific RBF mutants (Weis et al. 2015a; Weis et al. 2015b). Moreover, the additional ITS2-first pathway is found to be upregulated in fast dividing tissues or upon auxin treatment (Palm et al. 2019).

Expression of RBF genes is coordinately upregulated under multiple environmental stresses including coldness, heat, and UV radiation (Saez-Vasquez et al. 2019). However, pre-rRNA processing is hampered by both heat and cold treatments (Weis et al. 2015a; Hang et al. 2018). These conflicting regulations might contribute to a tightly restricted level of ribosome production in order to meet the minimum survival requirement and in the meantime avoid wasting energy.

Phenotypes of ribosomal defective plants

In Arabidopsis, the necessity of ribosome in development has been indicated by the significant phenotypic abnormalities caused by ribosomal defects, which in general result from mutations of RBFs and RPs. Most of RBFs examined in Arabidopsis so far are rRNA processing factors and their mutants cause abnormal accumulation of rRNAs precursors and/or by-products (Lange et al. 2011; Missbach et al. 2013; Weis et al. 2014; Weis et al. 2015b). A few RBFs are ribosome assembly factors and their mutants show delayed productions of mature ribosome subunits (Schmidt et al. 2013). RPs are categorized as the large subunit proteins (RPLs) and the small subunit proteins (RPSs), and their mutants sometimes hamper productions of corresponding ribosome subunits (Creff et al. 2010). Interestingly, RBF and RP mutants in Arabidopsis exhibit highly overlapping phenotypes, suggesting that these mutants lead to similar ribosomal defects regardless of different molecular causes.

Ribosomal defects in plants usually have pleotropic effects in multiple tissues and organs. However, depending on the particular role of a RBF/RP, its mutant plant might exhibit different extents of 'severeness'. Mutants of essential RBFs/RPs usually result in embryo lethality/seed abortion (e.g. the *EMBRYO-DEFECTIVE* (*EMB*) RP/RBF group) and aborted female gametogenesis (e.g. the *SLOW WALKER* (*SWA*) RBF group) (Tzafrir et al. 2004; Shi et al. 2005; Byrne 2009; Weis et al. 2015a; Palm et al. 2019). Specifically, the *swa* mutants, together with several RBF mutants exhibiting defective male gametogenesis, primarily disable gametophyte progression during the mitotic cycles (Shi et al. 2005; N. Li et al. 2009; Missbach et al. 2013). A possible explanation is that mitosis has a higher demand for protein synthesis (and therefore ribosomes) for

chromosome duplication. This hypothesis is further supported by the fact that aborted embryo development and defective gametogenesis coincide in several RBF/RP mutants (Muralla et al. 2011; Weis et al. 2015a), and that some *emb* mutants surviving gametogenesis actually rely on the residual RP/RBFs from diploid mother cells (Muralla et al. 2011).

Plants carrying mutations of non-essential RBFs/RPs display a spectrum of developmental abnormalities. The most common phenotype is a smaller plant size due to reduced cell division, restricted cell growth and abnormal meristem development (Nishimura et al. 2005; Szakonyi et al. 2011; Ahn et al. 2016). Another recurring phenotype is reduced transmission through female or male, which potentially results from occasional failures during various stages of ovule or pollen development (Missbach et al. 2013; Zsogon et al. 2014; Hao et al. 2017).

The most unique phenotype of non-essential RBF/RP mutant plants is abnormal leaf development. In Arabidopsis, a considerable proportion of RBF/RP mutants identified so far cause pointed and narrow rosette leaves (e.g. the *DENTICULATA* (*DEN*) and *POINTED FIRST LEAF* (*PFL*) RP groups) (Van Lijsebettens et al. 1994; Berna et al. 1999; Horiguchi et al. 2011). In these mutant plants, rosette leaves are narrow and pointed with more marginal serrations, compared to the smooth and spatulate leaf shape in wild-type plants. Additionally, this phenotype usually coincides with disruptions in vascular patterning (which lead to abnormal leaf venations) and palisade mesophyll cell division (which lead to pale green leaf colors) (Byrne 2009; Horiguchi et al. 2012; Weis et al. 2015a). These observations suggest that ribosomal defects in these plants might affect certain regulatory pathways upstream of all these developmental events.

From this aspect, examinations of RP/RBF mutant plants revealed misregulation in auxin signaling pathway, including abnormal signal patterns of the auxin-responding reporter *DR5::GUS*, less sensitivity to auxin treatments, and impaired auxin transport (Petricka et al. 2007; Rosado et al. 2012; Zhao et al. 2015). Specifically, several RP mutant plants exhibited restricted *DR5::GUS* signals at leaf marginal serrations in contrast to the smooth and gradient signals at leaf margins of wild-type plants (Rosado et al. 2012). Therefore, mis-regulated auxin response caused by ribosomal defects could contribute to abnormal leaf development.

Some ribosomal defective plants exhibit special effects under particular mutant backgrounds. Mutants of some RP genes (e.g. the *PIGGY BACK* (*PGY*) RP group) cause ectopic adaxial outgrowth of leaf lamina in presence of the leaf-patterning mutant *asymmetric leaves 1* (*as1*) (Pinon et al. 2008; Horiguchi et al. 2011). Additionally, some RP/RBF mutant plants are not distinguishable from wild-type plants under normal growth conditions but exhibit hypersensitivity to challenging situations such as DNA damaging, high-salt stress, and high temperature (Revenkova et al. 1999; Ohbayashi et al. 2011; Palm et al. 2019).

Although it has been observed repeatedly that RP and RBF mutants tend to cause similar effects on plant growth and development, they are not necessarily equal regarding their effects on global ribosome function. The approximate number of RPs in a mature eukaryotic ribosome is 80 (Wilson et al. 2012; Weis et al. 2015a). In mammalian cells, 78 out of 80 RPs are encoded by single-copy genes; in yeast, 59 out of 79 RPs are encoded by two homologous genes (Planta et al. 1998; Uechi et al. 2001; Yoshihama et al. 2002). By contrast, in Arabidopsis, each RP gene family contains 2-7

members, which adds up to more than 200 RP genes in total (Barakat et al. 2001;

Hummel et al. 2015). Therefore, plants have the potential of a much higher level of

structural heterogeneity within their ribosomes (Giavalisco et al. 2005). It has been

hypothesized that in plants, ribosomes carrying different RP isoforms are

subfunctionalized according to different temporal or spatial cues (Horiguchi et al. 2012;

Weis et al. 2015a; Nicole Dalla Venezia et al. 2019). Regarding this, it is possible that a

RP mutant only disrupts a subgroup of ribosome pool, which leads to a tissue-specific

or developmental stage-specific phenotype. This type of RP mutant phenotype, if any, is

less likely to result from a RBF mutant (e.g. mutant of a pre-rRNA processing RBF),

which should have a universal impact of global ribosome population.

Translational regulation and upstream open reading frames

Developmental impacts of RP/RBF mutants in plants strongly suggest that

ribosomal defects cause misregulation of particular genes involved in developmental

events. One possible role of ribosomes in gene regulation is mediating translational

regulation.

In eukaryotes, classical translational regulation happens at translation initiation

step, and is mediated by a spectrum of *trans*-regulatory factors, e.g. the eukaryotic

initiation factors (eIFs) that is recruited by specific mRNA structures or sequences (*cis*-

elements) (Jackson et al. 2010; N. Dalla Venezia et al. 2019). In response to

physiological or environmental stimuli, eIFs are subject to phosphorylation or other

modifications that alter their functions, which leads to globally up- or down-regulation in

translation activities (Gallie et al. 1997; Sonenberg et al. 2009).

In addition to global translational regulation, a proportion of mRNAs are subject to gene-specific regulations due to the existence of one or several upstream open reading frames (uORFs) in their 5' UTRs (Young et al. 2016; Zhang et al. 2019). Comprehensive sequence analysis and ribosome profiling approaches have confirmed the existence as well as translational activities of uORFs in multiple species (Zhang et al. 2019). Specifically, more than 30% of Arabidopsis genes contain potential uORFs in their 5' UTRs, and around 90 uORFs are identified to encode highly conserved polypeptide sequences (Kim et al. 2007; Hsu et al. 2016).

In eukaryotes, mRNA translation starts with formation of the 43S pre-initiation complex (PIC) containing 40S SSU, the eIF2·GTP·Met-tRNA$_i^{Met}$ ternary complex (TC), eIFs 1, 1A, 3, and 5 (Aitken et al. 2012; Young et al. 2016). PIC binds to the 5' cap of mRNA and scans base by base from 5' to 3' until it encounters the first AUG, which triggers PIC dissociation and recruits 60S LSU (Aitken et al. 2012; Hinnebusch et al. 2012). If the first AUG is localized within a uORF, the common consequences are: 1) ribosome will 'stall' on 5'UTR and stop scanning for a second ORF; 2) the stop codon in uORF will trigger a nonsense-mediated decay process and lead to mRNA degradation; 3) ribosome subunits will dissociate from mRNA after uORF translation (Hinnebusch 1994; Morris et al. 2000; Zhang et al. 2019). In each case, translation of the downstream protein-coding ORF, or the main ORF (mORF), is inhibited. By contrast, some uORFs have been reported to have minor or even positive effects on mORF translation because they potentially allow for continuous scanning of 40S SSU and translation reinitiation (Hinnebusch 1994; Szamecz et al. 2008; Young et al. 2016). The determining factors for suppressing/non-suppressing effects of uORFs are case-specific,

given the studies showing that 5' and 3' flanking sequences and coding regions of uORFs all contribute to regulatory effects on mORFs (Grant et al. 1994; Szamecz et al. 2008; Lin et al. 2019).

It has been found that uORFs are associated with regulatory genes involved in development or stress reponses in yeast, human, and plants (Jorgensen et al. 2012; Sidrauski et al. 2015; Merchante et al. 2017; Zhang et al. 2019). The most commonly observed effect of uORFs on these regulatory genes is that they repress mORFs translation under normal conditions and this repression is attenuated upon negative growth signals, starvation, or pathogen attacks (Hinnebusch 1994; Y. Y. Lee et al. 2009; Pajerowska-Mukhtar et al. 2012). The potential biological rationale of having uORF-mediated regulation on these regulators is that translational regulation is an immediate and rapid effect compared to transcriptional regulation that involves production of nascent mRNAs (Xu et al. 2017b).

The regulatory effects of uORFs on mORFs involve ribosome assembly, therefore naturally relying on the integrity of ribosomes. From this perspective, uORFs can serve as a monitor for ribosomal health in cells and mediate gene-specific regulation in response to ribosomal defects. In Arabidopsis, the *AUXIN RESPONSE FACTOR 3* (*ARF3*) and *ARF5* genes, which encodes effector transcription factors of auxin signaling pathway, contain uORFs that show minor regulatory effects in wild-type plants but significantly inhibit ARFs production in several RP mutants (Rosado et al. 2012). The molecular mechanism of this ribosomal-defect-triggered uORF function is still unclear, but this regulation presumably helps to restrain plant growth to accommodate ribosomal shortage.

Ribosomal stress responses in plants

As stated above, ribosomal defects affect cellular responses to auxin signal pathway in a uORF-dependent manner. However, removal of the repressive uORFs fail to reverse growth defects in ribosomal defective mutants, including the reduced growth rates and the misshaped rosette leaves (Rosado et al. 2012), suggesting the existence of additional regulators responding to ribosomal defects.

As ribosomes participate in one of the most energy-consuming cellular activities in eukaryotes, ribosome biogenesis is linked to energy status in cells (Warner 1999; Strunk et al. 2009; Zhou et al. 2015). Accordingly, ribosome biogenesis is also subject to environmental disturbances including heat shock, hypoxia, nutrient starvation, and pathogen infections (Mayer et al. 2005; Ohbayashi et al. 2017b; Slomnicki et al. 2017; Xu et al. 2017a). In animal cells, these environmental stresses trigger 'ribosomal stress responses' via the Mdm2-p53 pathway (Mdm2 stands for Murine double minute 2; p53 is also known as Tumor protein 53) (Dez et al. 2004; Lior Golomb et al. 2014). In unstressed cells, p53 function is blocked by Mdm2 that functions as an E3 ubiquitin ligase (Haupt et al. 1997; Kubbutat et al. 1997). Defective ribosome biogenesis causes structural collapse of nucleoli, therefore releasing RPs into the nucleoplasm, where they bind to Mdm2 and stabilize p53 (Marechal et al. 1994; Y. Zhang et al. 2003; Zhang et al. 2009). Activation of p53 eventually leads to cell cycle arrest, senescence, and apoptosis (Levine 1997).

In plants, multiple RBF mutants exhibited enlarged and abnormal nucleoli (Abbasi et al. 2010; Ohbayashi et al. 2011), implying a similar nucleolar collapse as in animal cells. However, homologues of p53 and Mdm2 do not exist in plant genomes, so

for long it has been uncertain whether a similar cellular response pathway exists in plants. Recently, a mutant named *suppressor of root initiation defective two 1* (*sriw1*) was found in a genetic screen to 'rescue' the delayed growth and retarded tissue regeneration in plants carrying mutations in RBF genes *ROOT INITIATION DEFECTIVE 2* (*RID2*), *RID3*, and *RNA HELICASE 10* (*RH10*) (Ohbayashi et al. 2017a). These three RBFs are involved in pre-rRNA processing, and mutant of each gene leads to abnormal accumulation of particular pre-RNA intermediates (Ohbayashi et al. 2017a). Most interestingly, the 'rescued' *sriw1 rid2*, *sriw1 rid3*, and *sriw1 rh10* double mutants still exhibit a similar level of abnormally accumulated pre-rRNA intermediates (Ohbayashi et al. 2011). Therefore, it has been proposed that the mutated gene in *sriw1* mutant acts as a 'mediator' between defective ribosome biogenesis and reduced plant growth/cell division (Ohbayashi et al. 2011; Ohbayashi et al. 2017b; Salome 2017). Moreover, the fact that the *sriw1* mutation also markedly ameliorates the pointed leaf shapes of several RBF/RP mutants indicates that this 'mediator' responds to various ribosomal defects and operates on multiple developmental events (Ohbayashi et al. 2017a).

The *sriw1* mutant is a missense mutation in the *ANAC082* gene, which encodes a protein containing a plant specific NAC domain (NAM standing for NO APICAL MERISTEM, ATAF1/2 standing for ARABIDOPSIS THALIANA ACTIVATING FACTOR 1/2, and CUC2 standing for CUP-SHAPED COTYLEDON) (Ooka et al. 2003). The NAC domain possesses DNA-binding ability and ANAC082 shows transactivating activities in yeast one-hybrid and transient leave transfection (Lindemose et al. 2014; Ohbayashi et al. 2017a), suggesting its potential function as a transcription factor. Consistent with the dimerizing feature of NAC domains (Ernst et al. 2004), ANAC082 interacts with other

NAC family members *in vivo* (Yamaguchi et al. 2015), suggesting cooperation of multiple NAC proteins in RBF mutants. More functional characteristics of ANAC082, especially its *in vivo* target genes, are needed in the future.

The role of ANAC082 in plant RBF/RP mutants is reminiscent of p53 in animal cells upon ribosomal stress. However, the molecular basis for activation of ANAC082, though not yet defined, is most likely different from that of p53. As stated earlier, regulation of p53 activity relies on Mdm2. *ANAC082*, on the other hand, might be regulated translationally through an evolutionarily conserved uORF that potentially represses the translation of its mORF under normal conditions (Ebina et al. 2015; Ohbayashi et al. 2017b). This repressive effect is probably attenuated in RBF/RP mutants due to the harmed ribosomal integrity, thus allowing for ANAC082 production. Additionally, the abnormal nucleolar morphology in plant RBF mutants might not be the same as the nucleolar collapse in animal cells that triggers p53 activation, as it is fully reversed by *anac082-1* mutant (Ohbayashi et al. 2017a).

ANAC082 has been linked to several developmental abnormalities in RBF/RP plants, including reduced cell division, slower plant growth, and pointed leaf shape (Ohbayashi et al. 2017a). An appealing further direction to expand the role of ANAC082 in plant development would be to explore and test *anac082* mutants in ribosomal defective plants carrying varieties of phenotypes. Notably, the role of ANAC082 has primarily been tested in non-essential RBF/RP mutants, so it remains unclear whether the aborted embryo development and/or gametogenesis (described above) that occurs in essential RBF/RP mutants is a consequence of programmed cell death mediated by ANAC082.

Foreshadowing the thesis

Genetic approaches, including forward and reverse genetics, have been widely used to decipher biological processes in plants. In fact, several important cell fate regulator genes for root epidermal development, including *WER* (Lee et al. 1999), *SCM* (Kwak et al. 2005), and *CPC* (Wada et al. 1997), were discovered through forward genetics, which employed genetic screens to discover mutant lines displaying altered root epidermal cell patterns. In addition, redundant regulator genes, including *MYB23* (Kang et al. 2009), were discovered through reverse genetics according to their similarities with identified regulator genes. Given the establishment of a regulatory network model that effectively explains Arabidopsis root epidermal cell specification, an emerging question is whether there are still unknown players participating in this process.

A potential drawback of traditional genetic screens using wild-type plants is the difficulty to identify mutants carrying less striking root epidermis pattern alterations. Therefore, a modified screen, which eventually led to the two projects to be described in following chapters, was conducted using *cpc-1* as the genetic background. As the major mediator of lateral inhibition from N- to H-position cells, the CPC protein is critical for proper development of root-hair cells (Wada et al. 2002; Kurata et al. 2005). Theoretically, in the *cpc-1* mutant, less inhibition of WER in H-position cells significantly reduces the molecular distinctions between H and N positions. Therefore, in *cpc-1* plants, even those H-position cells that successfully adopt the root-hair cell fate should be more sensitive to subtle disturbances that are otherwise invisible under wild-type backgrounds. Additionally, the intermediate phenotype of the *cpc-1* mutant

(approximately 70% reduction of root-hair cells, (Wada et al. 1997)) enables

identification of both enhancing and suppressing mutants. Furthermore, in order to rule

out mutants that disrupts downstream root epidermis development, which can still alter

cpc-1 phenotype (e.g. *rhd6*), the *GL2::GUS* reporter was introduced into the *cpc-1*

mutant so that only mutants affecting early cell specification regulation (upstream of

GL2) could be selected.

This novel mutant screening, initiated and carried on by multiple previous

researchers, successfully identified a pool of mutants that significantly alter *cpc-1*

mutant phenotype. Two of these mutants, both characterized as 'enhancers' of *cpc-1*,

give rise to Chapter 2 and Chapter 3 of this dissertation thesis.
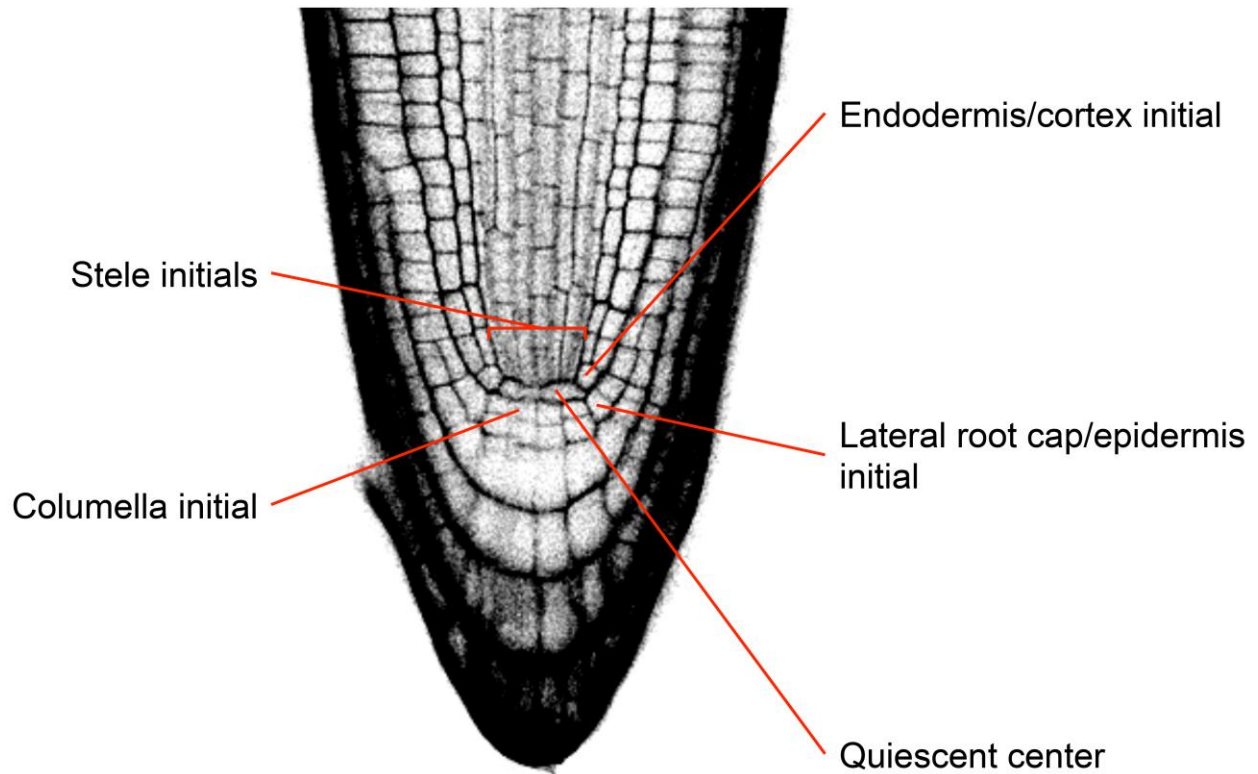
Figure 1.1 Structure of the root meristem in an Arabidopsis primary root.
Shown here is an inverted confocal image of an Arabidopsis root tip stained with the propidium iodide for cell wall visualization. In this picture, the 2 cells in the quiescent center are recognized by its unique position. The 2 endodermis/cortex initials are in direct contact with the quiescent center at the lateral side; the 4 columella initials are in direct contact with the quiescent center at the apical side; The 2 lateral root cap/epidermis initials are in direct contact with the columella initials at the lateral side.
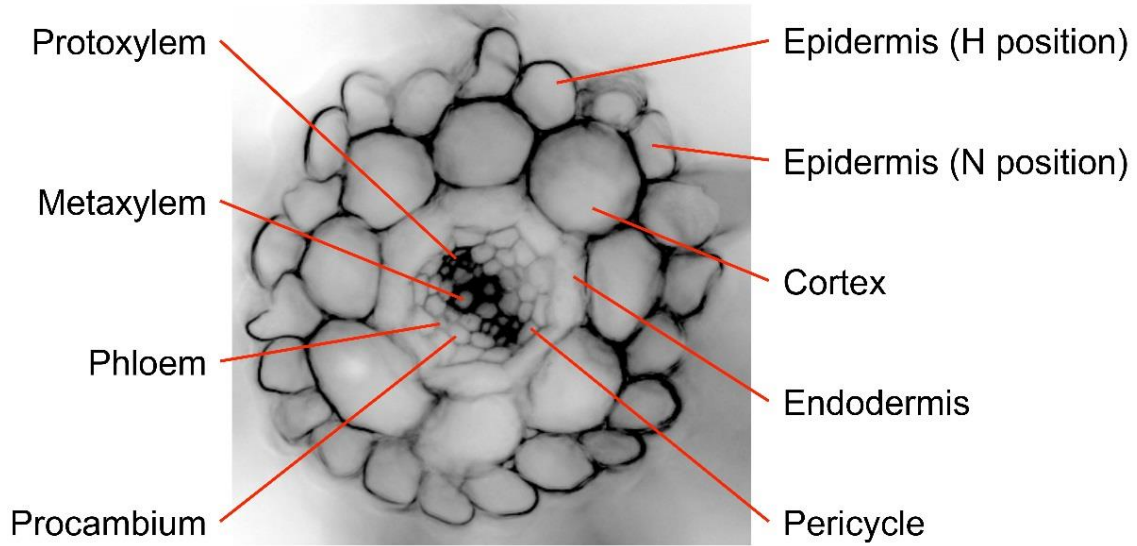
Figure 1.2 Spatial structure of an Arabidopsis primary root.
Shown here is an inverted fluorescent image of the cross-section an Arabidopsis primary root stained with the Fluorescent Brightener 28 for cell wall visualization. Different cell layers are marked. The xylems are featured with thickened cell walls.
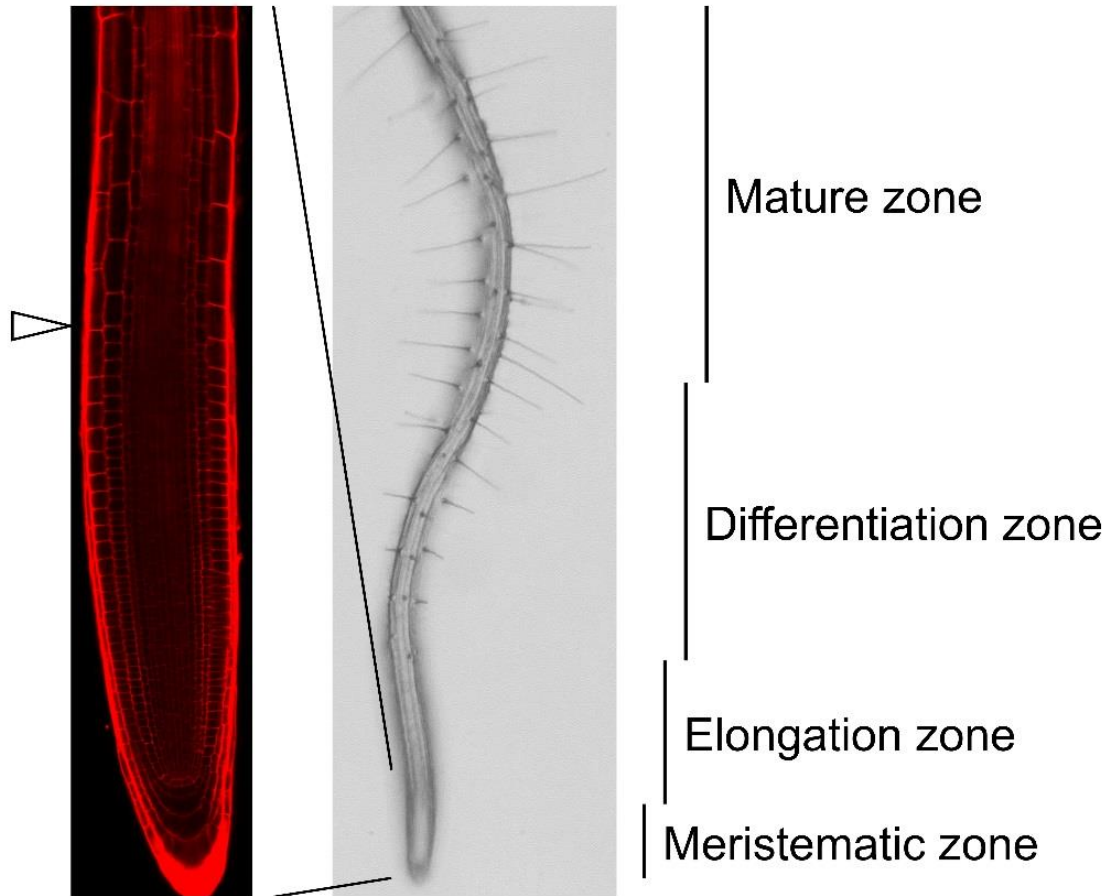
Figure 1.3 Temporal structure of an Arabidopsis primary root.
Left panel is a confocal picture of Arabidopsis root tip region stained with propidium iodide for cell wall visualization. The boundary between the meristematic and elongation zones, which is marked by the fast elongation of cortical cells, is indicated by the white arrow on the left. The right panel is a bright field picture of an Arabidopsis root. The boundary between the elongation and differentiation zones is marked by the emergence of the first root hair. The transition from the differentiation zone to the mature zone is recognized where the length of root hairs become comparable.
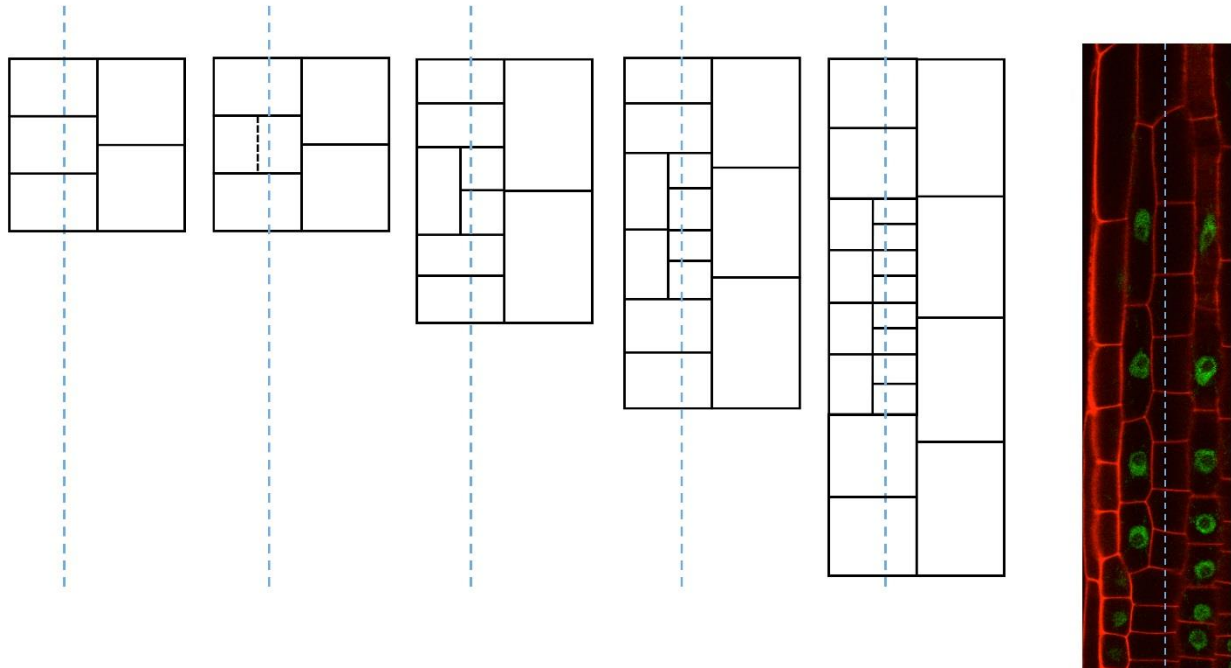
Figure 1.4 The formation of an epidermal clone in Arabidopsis primary root.
The schematic pictures illustrate the formation of an epidermal clone. The blue dashed
line indicates the position of the anticlinal cell wall boundary of the underlying cortical
cells. This clone originated from a H-position cell that undergoes anticlinal cell division
(indicated by the black dashed line). The two resulting daughter cells end up with
different cell positions, with the left one at the N position and the right one at the H
position. The two daughter cells then adopt diverging cell development, indicated by
their different cell division rate. The rightmost panel shows a confocal picture of an
epidermal clone. The red color represents the propidium iodide staining and the green
color represents the *GL2::GL2-GFP* reporter signals, which marks the N-position cell
fate establishment. The blue dashed line indicates the position of the anticlinal cell wall
boundary of the underlying cortical cells. The two cell files within the clone exhibit
different cell division rate as well as different marker expression
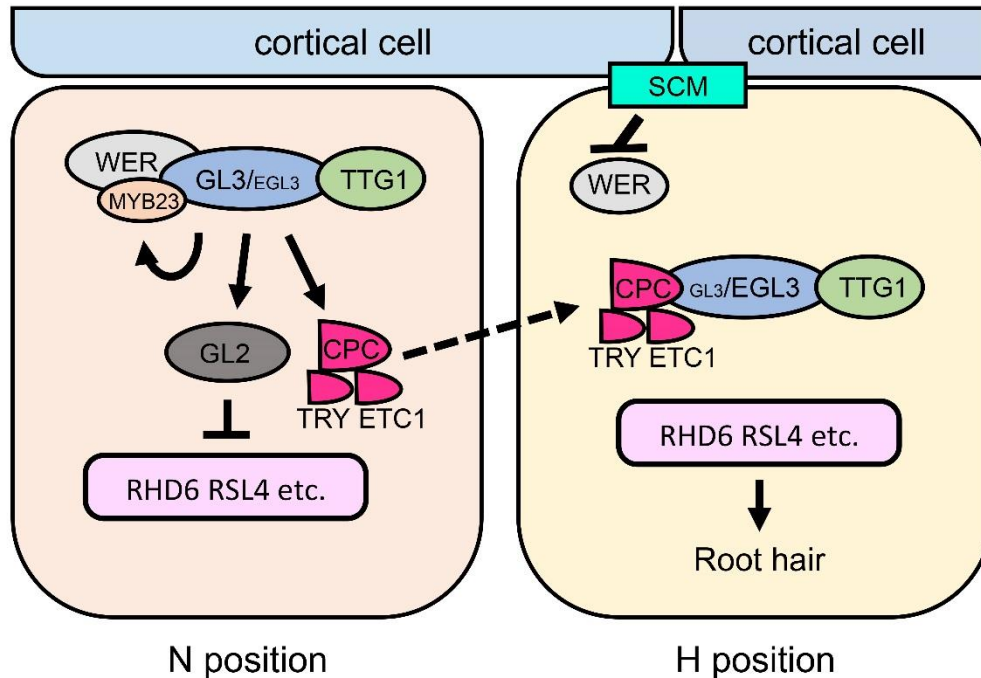
Figure 1.5 The model figure explaining the regulatory network of Arabidopsis root epidermal cell specification.

The black arrows represent transcriptional regulation and the dashed arrows represent protein translocalization. In N-position cell, the WER-GL3/EGL3-TTG1 is formed preferentially and positively regulates expression of MYB23, GL2 and R3-type MYB genes including CPC, TRY and ETC1. The MYB23 protein acts as a positive feedback for the complex and functions redundantly with WER. The GL2 protein acts as a transcriptional repressor for multiple root-hair-promoting genes including RHD6 and RSL4. The R3-type MYB proteins translocation to the adjacent H-position cell and inhibits the formation of WER-GL3/EGL3-TTG1 complex. In addition, the WER gene expression is inhibited by the SCM protein preferentially localized on the membrane of the H-position cell. Consequently, the root-hair-promoting genes are expressed the H-position cell and leads to root hair formation.
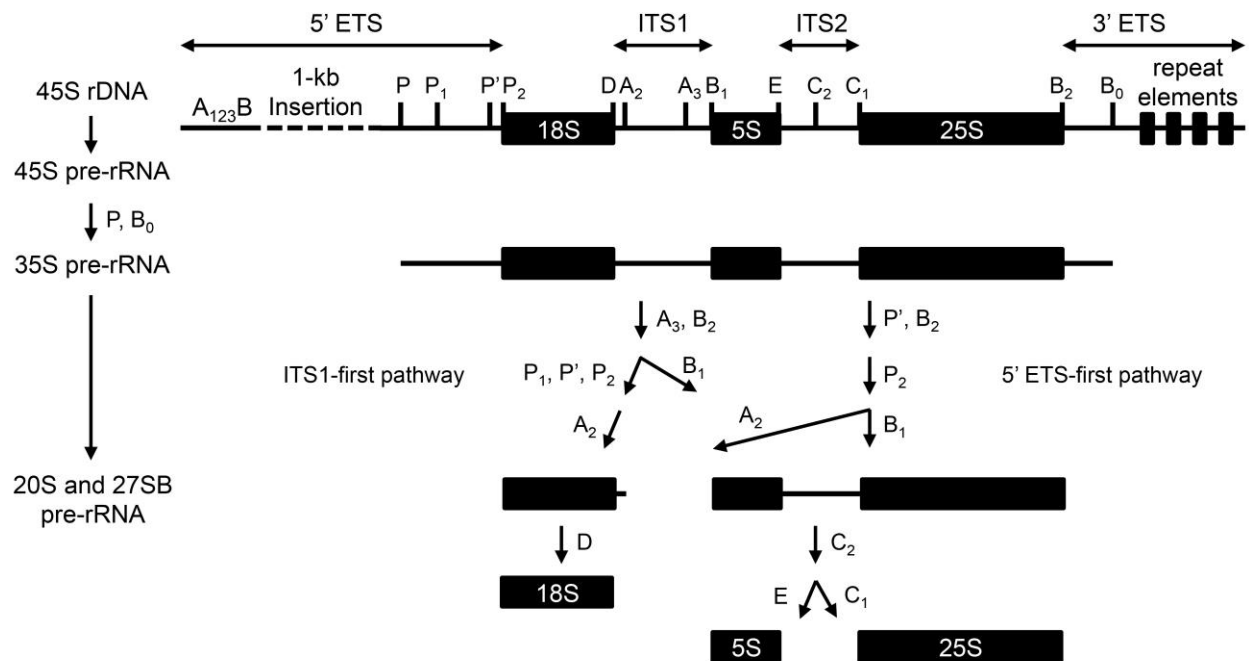
Figure 1.6 The schematic figure explaining pre-rRNA processing in Arabidopsis (according to (Weis et al. 2015a; Saez-Vasquez et al. 2019)).
The transcribed 45S pre-rRNA is cleaved at the B0 site, spliced at its 5' ETS to remove the 1-kb insertion, and then cleaved at the P site to generate 35S pre-rRNA. The 35S pre-rRNA undergoes two alternative processing pathways, the ITS1-first pathway and the 5' ETS-first pathway. Processing sites for each step is indicated, where either cleavage or trimming happens. So far it is regarded that cleavage happens at the P1, P', P2, D, A2, A3, B1, C1, and C2 sites, while trimming happens at the E and B2 sites.

Chapter 2

Cell-type Patterning in the Arabidopsis Root Epidermis Modulated by a Critical Residue in the WEREWOLF Regulatory Protein

The contents of this chapter were previously published in the scientific journal *Plant Physiology* (Wang et al. 2019). The positional mapping was conducted by Christa Barron. The yeast two-hybrid assays and the electrophoretic mobility shift assays were conducted by Dr. Kook Hui Ryu. I conducted all other experiments.

Abstract

The Arabidopsis root epidermis exhibits a position-dependent pattern of root-hair and non-hair cell types. A highly orchestrated network of gene regulatory interactions, including the R2R3-type MYB transcription factor WEREWOLF (WER), is responsible for generating this cell pattern during root development. In this study, we identified a novel *wer* mutant from a genetic enhancer screen, designated *wer-4*, which exhibits an abnormal pattern of root-hair and non-hair cells. We discovered that *wer-4* bears a single-residue substitution (D105N) in the DNA-binding R3 MYB repeat of WER, which differentially affects the transcription of WER target genes, including *GLABRA 2* (*GL2*), *CAPRICE* (*CPC*), *TRIPTYCHON* (*TRY*), and *ENHANCER OF TRY AND CPC 1* (*ETC1*) genes. This effectively rewires the gene regulatory network, leading to new levels and distributions of cell fate regulators in the differentiating epidermal cells that ultimately

generates the novel cell-type pattern. We also created several new WER variants with substitutions at the D105 position, and these exhibit a variety of gene expression and cell-type pattern alterations, further supporting the critical role of this residue. These findings provide new insights into WER protein function and its importance in generating the proper balance of downstream transcriptional factors in the gene regulatory network that establishes root epidermal cell fate.

Introduction

The Arabidopsis root epidermis has been used extensively as a simple model for studying cell fate regulation in plants (Duckett et al. 1994; Schiefelbein et al. 2014). Only two cell types, root-hair cells and non-hair cells, are present in the Arabidopsis root epidermis, and the fate of a newly formed root epidermal cell is dependent on its relative position to underlying cortical cells. An epidermal cell located outside a cleft between two cortical cells (the H position) differentiates into a root-hair cell, whereas an epidermal cell located outside one cortical cell (the N position) differentiates into a mature non-hair cell (Berger et al. 1998a). The obvious morphological differences between root-hair and non-hair cells, their consistent arrangement, and their early seedling phenotypes enable effective identification and characterization of mutant abnormalities. These features make the root epidermis a powerful system for studying cell specification using genetic and molecular tools.

A wealth of prior studies has uncovered a highly orchestrated network of transcriptional regulators responsible for establishing position-dependent gene expression leading to the two cell fates in the Arabidopsis root epidermis. The core

component of this network is a MYB-bHLH-WD40 protein complex that preferentially

accumulates in the N-position cells (Schiefelbein et al. 2014). In this complex, MYB is

an R2R3-type MYB protein encoded by *WEREWOLF* (*WER*), the bHLH proteins are

encoded by the functionally redundant *GLABRA 3* and *ENHANCER OF GLABRA 3*

(*GL3*/*EGL3*), and the WD40 protein is encoded by *TRANSPARENT TESTA GLABRA 1*

(*TTG1*) (Galway et al. 1994; Lee et al. 1999; Walker et al. 1999; Bernhardt et al. 2003;

Bernhardt et al. 2005). The WER-GL3/EGL3-TTG1 complex directly promotes

transcription of *GLABRA 2* (*GL2*), leading to preferential GL2 accumulation in the N-

position cells (Masucci et al. 1996a; Song et al. 2011). *GL2* encodes an HD-ZIP

transcription factor that inhibits the expression of root-hair promoting genes, thus

causing the N-position cells to adopt the non-hair cell fate (Rerie et al. 1994; Bruex et al.

2012; Lin et al. 2015). Accordingly, null mutants of *WER*, *GL3*/*EGL3*, *TTG1*, or *GL2*

yield plants lacking non-hair cells and exhibiting a hairy root phenotype.

In addition to promoting the non-hair cell fate, the WER-GL3/EGL3-TTG1

complex also influences root-hair cell fate through regulation of the single-repeat R3-

type MYB genes *CAPRICE* (*CPC*), *TRIPTYCHON* (*TRY*) and *ENHANCER OF TRY*

AND CPC 1 (*ETC1*) (Schellmann et al. 2002a; V. Kirik et al. 2004; Simon et al. 2007).

These three genes are preferentially expressed in the N-position cells, but the proteins

translocate to the adjacent H-position cells (Kurata et al. 2005), where they inhibit

formation of the WER-GL3/EGL3-TTG1 complex through competitive binding to

GL3/EGL3 (Wada et al. 2002; Song et al. 2011). As a consequence, the H-position cells

express relatively low levels of *GL2* and high levels of root-hair promoting genes (Bruex

et al. 2012; Lin et al. 2015). The CPC, TRY, and ETC1 proteins are largely functionally

redundant, although the *CPC* gene is expressed most abundantly and plays the major role (Simon et al. 2007).

In addition to the CPC/TRY/ETC1 proteins, another factor influencing the accumulation pattern of the WER-GL3/EGL3-TTG1 complex is the preferential expression of the *WER* gene in the N-position cells (Lee et al. 1999; Ryu et al. 2005), which is due to *WER* transcriptional repression in the H-position cells mediated by the receptor-like kinase SCRAMBLED (SCM) (Kwak et al. 2005). In addition, WER-GL3/EGL3-TTG1 accumulation is influenced by GL3 and EGL3, which participate in negative transcriptional feedback loops and exhibit differential accumulation and mobility between N- and H-position cells as well as affecting CPC accumulation (Bernhardt et al. 2005; Kang et al. 2013). Collectively, these components and interactions of the gene regulatory network ultimately establish stable cell-type specific gene expression in the H-position and N-position cells.

To gain further insights into the mechanisms controlling cell-type patterning in the Arabidopsis root epidermis, we sought to identify new mutants that alter the root-hair/non-hair cell distribution. Through an enhancer genetic screen using the *cpc-1* mutant, we identified a novel mutant allele of *WER* that disrupts the position-dependent pattern of root-hair and non-hair cells. The WER protein encoded by the mutated *WER* gene possesses a single residue substitution at position 105, which causes abnormal target gene transcription, disrupts the spatial distribution of cell fate regulators, and reduces the molecular distinction between H-position and N-position cells. We further generated WER variants with novel substitutions at the same position, which also exhibit abnormalities in root epidermis gene expression and patterning. These findings

highlight the critical role of WER transcriptional activity in root epidermal cell patterning, and they show how a gene regulatory network may be rewired to generate a new developmental phenotype.

Results

Identification of a novel *WER* mutant allele

To discover new mutants affecting root epidermis patterning, we conducted an enhancer genetic screen in the *cpc-1 GL2::GUS* mutant background. The *cpc-1* mutant produces fewer root-hair cells (approximately 40% of the wild-type number; Figure. 2.1, A and B) and exhibits a corresponding increase in ectopic *GL2::GUS* reporter expression in differentiating H-position cells (Figure 2.1C), providing a sensitized background suitable for detecting subtle disruptions of the patterning mechanism. We mutagenized the *cpc-1 GL2::GUS* line using ethyl methanesulfonate (EMS) and identified seedlings in subsequent generations exhibiting a more extreme reduced-hair phenotype. One of the resulting lines, ultimately designated as *cpc-1 wer-4* (see below), produced very few root-hair cells (approximately 7% of the wild-type number; Figure 2.1, A and B) and exhibited greater ectopic expression of *GL2::GUS* in differentiating H-position cells than *cpc-1* (Figure 2.1C), suggesting that the gene affected by this new enhancer mutation acts upstream of *GL2*. We separated the *wer-4* allele from *cpc-1* genetically, and discovered that the *wer-4* single mutant produces an abnormal spatial distribution of epidermal cell types, including 13% non-hair cells in the H position (ectopic non-hair cells) and 28% root-hair cells in the N position (ectopic root-hair cells) (Figure 2.1B). We also showed that plants heterozygous for this mutation (*wer-4/+*)

exhibited a normal root epidermis pattern (Figure 2.1B). Thus, the *wer-4* mutant

possesses a recessive allele that affects cell-type patterning at an early stage during

Arabidopsis root epidermis development.

To identify the mutated gene in *wer-4*, we performed genetic mapping with

molecular markers and narrowed its location to a region on chromosome 5 near the

marker nga151 ((Bell et al. 1994); see Materials and Methods). This region includes the

root epidermis regulatory gene *WER* (Lee et al. 1999). Upon sequencing the *WER* gene

in the *wer-4* mutant, we identified a single G to A substitution within the open reading

frame at position 4,764,045, which changes the aspartic acid encoded by the 105th

codon to asparagine (D105N) (Figure 2.1D).

To determine whether the identified *WER* mutation is responsible for the *wer-4*

phenotype, we introduced the *WER::WER-GFP* transgene (which encodes a functional

WER protein (Ryu et al. 2005)) into the *wer-4* mutant by crossing. The resulting

WER::WER-GFP wer-4 plants exhibited a root epidermal cell-type pattern comparable

to the *WER::WER-GFP* plants (Figure 2.1B). This indicates that the single nucleotide

change in the *WER* gene in the *wer-4* line is the cause of its abnormal cell-type pattern.

The *wer-4* mutant alters expression of *WER* target genes

The *wer-4* mutant phenotype is distinct from previously described *wer* mutants,

which all exhibit a strong "hairy" root phenotype due to the loss of non-hair cells (Lee et

al. 1999). The D105 residue affected by the *wer-4* mutation is located at the beginning

of the third α-helix of the R3 domain, which is involved in DNA recognition (Ogata et al.

1994; Jia et al. 2004) (Figure 2.1C). Given this, we hypothesized that the *wer-4*

mutation causes abnormal regulation of WER target genes.

To investigate this possibility, we analyzed WER target gene expression in the

wer-4 mutant. We observed strong effects of *wer-4* on *TRY* and *ETC1* gene expression.

Using quantitative real-time PCR (qPCR), we found that both two genes exhibited a

dramatic decrease of transcript amounts in *wer-4* roots that is comparable with or even

lower than the null *wer-1* mutant (Figure 2.2A). Consistently, the *wer-4* mutant exhibited

largely depleted *ETC1::GUS* signals in the root epidermis (Figure 2.2B). These results

suggest that the mutated WER protein in *wer-4* is essentially unable to induce

expression of *ETC1* and *TRY*. The *TRY* and *ETC1* genes encode CPC-like R3-type

MYB proteins that are partially functionally redundant with *CPC*, and both *etc1* and *try*

mutants enhance the *cpc-1* phenotype (V. Kirik et al. 2004; Simon et al. 2007).

Considering this, the loss of *TRY* and *ETC1* expression in *wer-4* help to explain its

ability to enhance the *cpc-1* mutant phenotype (Figure 2.1, A and B).

Although the *try* and *etc1* mutants enhance *cpc-1*, by themselves the *try*, *etc1*,

and *try etc1* mutants do not substantially alter root epidermis development (V. Kirik et al.

2004). Thus, the abnormal cell-type pattern in the *wer-4* mutant is not solely due to its

effects on *TRY* and *ETC1*, implying that additional WER targets are affected in *wer-4*.

Therefore, we studied expression of the two major players in root epidermal

development that are known to be direct WER transcriptional targets: *GL2* and *CPC*

(Ryu et al. 2005; Song et al. 2011).

For *GL2,* we made use of the *GL2::GUS* and *GL2::GFP* transcriptional reporters

and discovered that both reporters exhibited increased overall expression in developing

wer-4 root epidermal cells, including some ectopic expression in H-position cells (Figure

2.2C). To evaluate expression from individual cells, we quantified the fluorescence

signals from differentiating epidermal cells in the N and H positions of the *GL2::GFP* line

and plotted the signal distribution from both wild-type and *wer-4* roots (Figure 2.2E).

Consistent with the visual phenotypes (Figure 2.2C), a large proportion of the *wer-4*

cells exhibited greater GFP levels than wild-type cells in both the N and H positions

(Figure 2.2E). Further, the *wer-4* mutant possessed a wider distribution of GFP signal

levels within cells in both the N and H positions, relative to the wild type (Figure 2.2E).

These results indicate that the *wer-4* mutation leads to greater but more variable *GL2*

transcription in the developing root epidermis. However, the amount of *GL2* transcripts

in *wer-4* roots is only around 70% of that in the wild type roots (Figure 2.2A), implying

that *GL2* is also down-regulated post-transcriptionally in *wer-4.*

To examine *CPC* gene expression, we used a *CPC::GUS* transcriptional reporter

and discovered an overall decrease in the GUS staining level as well as greater cell-cell

variation in the *wer-4* root epidermis as compared to wild type (Figure 2.2D). By

analyzing GUS signal levels from individual cells, we confirmed the greater cell-cell

variation and the general reduction of GUS levels in the N-position cells as well as the

greater variation of GUS levels in the H-position cells of *wer-4* (Figure 2.2F). This shows

that the *wer-4* mutant causes a general decrease in *CPC* transcription and reduced

establishment of distinct *CPC* expression within and between cells in the H and N

positions. Consistently, the amount of *CPC* transcripts in *wer-4* is significantly lower

than the wild type but still higher than *wer-1* (Figure 2.2A), indicating that the *CPC*

transcript amount is largely determined by its transcription level.

It is reported that *ETC1*, *TRY*, *GL2*, and *CPC* are also expressed in the leaf

trichome cells under the regulation of a parallel MYB-bHLH-WD40 protein complex

containing the GLABROUS 1 (GL1) MYB protein instead (Pattanaik et al. 2014). To

confirm that the effects of *wer-4* on *ETC1*, *TRY*, *GL2*, and *CPC* are root-specific, we

examined the expression of these genes in leaves. Indeed, the *ETC1::GUS*, *GL2::GUS*,

and *CPC::GUS* reporters exhibited comparable signals in the trichome cells of both

wild-type and *wer-4* leaves (Figure 2.3A). Additionally, the *ETC1*, *TRY*, *GL2*, and *CPC*

transcript levels in leaves are not significantly affected by *wer-4* (Figure 2.3B).

The abnormal distributions and the various levels of *GL2* and *CPC* transcription

in *wer-4* root epidermis led us to examine whether *wer-4* might disrupt the coordinated

transcriptional regulation between *GL2* and *CPC*. To simultaneously analyze expression

of both genes in individual cells, we generated wild-type and *wer-4* plants bearing both

the *GL2::GFP* and *CPC::GUS* reporters. In wild-type roots, *GL2* and *CPC* are known to

be coordinately regulated with preferential transcription of both genes in the N-position

cells ((Lee et al. 2002); Figure 2.4, A and B). In the *wer-4* mutant, we also observed a

general correlation in expression between the *GL2::GFP* and *CPC::GUS* reporters in

both H- and N-position cells (Figure 2.4, A and B). Thus, despite the abnormal relative

levels and lack of H/N cell specificity for *GL2* and *CPC* expression in the *wer-4* mutant,

they largely remain under coordinated transcriptional regulation. Given that coordinated

regulation is maintained but the relative promoter activity of *GL2* and *CPC* is altered

(comparing the GFP vs. GUS reporter levels in WT and *wer-4* in Figure 2.2, E and F)),

we conclude that the *wer-4* mutant alters the ratio of *GL2* transcription to *CPC*

transcription within individual cells, relative to the wild type.

To find out the reason for the effects of *wer-4* on WER target gene transcription,

we examined the function of WER protein carrying the *wer-4* mutation. As one

component of the MYB-bHLH-WD40 complex, WER is reported to directly associate

with GL3/EGL3 (Bernhardt et al. 2003). Using the yeast two-hybrid assay, we observed

that both the wild-type WER protein and the *wer-4* mutant protein (hereafter designated

as WER[D105N]) exhibited significantly stronger association with GL3 compared to the

empty vector (Figure 2.5, A and B). Notably, WER[D105N] showed even stronger

association with GL3 compared to WER (Figure 2.5, A and B). Therefore, the D105N

substitution caused by the *wer-4* mutant does not harm the association between WER

and GL3. Considering this, we conclude that the depleted expression of *TRY* and *ETC1*

as well as the decreased *CPC/GL2* transcription ratio in *wer-4* are not due to defective

formation of the WER-GL3/EGL3-TTG1 complex.

We then analyzed the affinities of WER and WER[D105N] proteins to their target

gene promoters. Previous studies have defined two *in vivo* WER binding sites within the

GL2 promoter (elements GWBSI and GWBSII) and the *CPC* promoter (elements WBSI

and WBSII) (Figure 2.6A) (Ryu et al. 2005; Song et al. 2011). Using the electrophoretic

mobility shift assay (EMSA), we observed that both WER and WER[D105N] exhibited

detectable binding to three of these four promoter elements (Figure 2.7). To compare

the relative binding of WER and WER[D105N] to the *GL2* and *CPC* promoter elements, we

performed competition EMSA assays using the *CPC* promoter element WBSI as an

unlabeled competitor against the labeled *GL2* promoter element GWBSI. We

discovered that WER[D105N] remained bound to GWBSI at higher competitor

concentrations than WER and resulted in a much higher IC50 value (Figure 2.6, B and

C), indicating that WER[D105N] has a lower affinity to the *CPC* promoter element than to

the *GL2* promoter element, compared to wild-type WER protein. This result was

endorsed by a reciprocal EMSA assay using GWBSI as an unlabeled competitor against the labeled WBSI, where WER[D105N] showed less resistance to the competitor than WER (Figure 2.6, B and C). Interestingly, WER[D105N] also exhibited greater relative binding to the GWBSI than to GWBSII compared to WER (Figure 2.8), implying that the GWBSI element may be primarily responsible for the differential effect of WER[D105N]. Together, these results indicate that the D105N substitution in the WER protein alters its relative affinity for its *GL2* and *CPC* promoter binding sites and therefore decreases the *CPC*/*GL2* transcription ratio in the *wer-4* root epidermal cells.

Effect of *wer-4* on the cell-type pattern

Next, we sought to understand how the altered regulation of WER target genes ultimately leads to the abnormal cell-type pattern in the *wer-4* mutant. In the established model for epidermal cell patterning, the specification of root-hair/non-hair cell fates is the result of differential accumulation of the WER-GL3/EGL3-TTG1 complex in the H- and N-position cells (Schiefelbein et al. 2009; Schiefelbein et al. 2014). To determine whether this is altered in *wer-4*, we analyzed GL3 protein accumulation using the *GL3::GL3-YFP* reporter (Bernhardt et al., 2005). In contrast to the wild-type roots where the GL3-YFP proteins exhibited preferential accumulation in the nuclei of N-position cells, the *wer-4* roots showed relatively lower GL3-YFP nuclear signals in both H- and N-position cells (Figure 2.9A). Consistently, quantification of YFP signals revealed that the signal level difference between N-position and H-position cells in *wer-4* mutant is much less significant than wild type (Figure 2.9E). Notably, GL3-YFP accumulation in the root apical meristem remained unchanged in the *wer-4* mutant (Figure 2.9A), indicating that the impact of *wer-4* is specific in the root epidermis. GL3 serves as an

important component of the WER-GL3/EGL3-TTG1 component (Bernhardt et al. 2003; Bernhardt et al. 2005). Therefore, the abnormal GL3 accumulation in *wer-4* reflects that the *wer-4* mutant is unable to establish differential accumulation of the WER-GL3/EGL3-TTG1 complex between H and N positions.

The CPC-mediated lateral inhibition pathway helps to generate the proper accumulation pattern of the WER-GL3/EGL3-TTG1 complex (Bernhardt et al. 2005; Schiefelbein et al. 2014). Therefore, it is likely that the reduced transcription of *CPC* in *wer-4* (Figure 2.2, D and F) is, at least in part, responsible for its altered WER-GL3/EGL3-TTG accumulation. To further address whether reduced *CPC* transcription leads to less CPC protein production, we made use of the *CPC::CPC-GFP* reporter (Kurata et al. 2005). It has been reported that the GFP tag affects the mobility of CPC and traps CPC within the N-position cells (Kurata et al. 2005). Indeed, we observed the CPC-GFP signals in the nuclei of both H- and N-position cells in wild-type and *wer-4* roots (Figure 2.9B). Specifically, the *wer-4* mutant exhibited much lower nuclear GFP signals compared to wild type (Figure 2.9B), and GFP quantification revealed a significant decrease of average signal level in *wer-4* (Figure 2.9D). Meanwhile, the CPC-GFP signals within the stele tissue showed no decrease in the *wer-4* mutant (Figure 2.9B), indicating that the impact of *wer-4* is specific in the root epidermis. These results indicate that the *wer-4* mutant produces less CPC in the root epidermis.

In addition to CPC, the SCM-mediated signaling pathway is also involved in establishing the position-dependent accumulation of the WER-GL3/EGL3-TTG1 complex (Kwak et al. 2005; Kwak et al. 2007). To test the possible contribution of SCM to the *wer-4* phenotype, we generated the *scm-2 wer-4* double mutant and discovered

that it exhibited more extreme disruption of the cell-type pattern than *wer-4* single

mutant (Figure 2.9C). This additive genetic effect implies that *wer-4* does not generate

its abnormal cell-type pattern through altering SCM (e.g. hypothetical feedback

regulation of *wer-4* on SCM). Thus, the negative effect of *wer-4* on CPC is the more

likely explanation for the misregulated accumulation of the WER-GL3/EGL3-TTG1

complex.

In wild-type roots, the differential accumulation of the WER-GL3/EGL3-TTG1

complex causes preferential *GL2* gene expression and GL2 protein accumulation in N-

position cells, which generates the non-hair cell fate (Galway et al. 1994; Masucci et al.

1996a; Lee et al. 1999; Bernhardt et al. 2003; Lin et al. 2015). Thus, we analyzed

whether GL2 protein accumulation is altered in the *wer-4* mutant. Using a *GL2::GL2-

GFP* translational fusion line, we found that *wer-4* exhibited variable GL2-GFP

accumulation in N-position cells as well as many H-position cells (i.e., ectopic GL2

accumulating cells) (Figure 2.10A). To examine the relationship between *GL2* promoter

activity and GL2 protein accumulation within individual cells, we created wild-type and

wer-4 lines bearing both the *GL2::GUS* and *GL2::GL2-GFP* reporters. We observed a

strong correlation of the cell-to-cell signal variations between *GL2::GUS* and *GL2::GL2-

GFP* in both wild-type and *wer-4*, indicating that *GL2* promoter activity largely

determines relative GL2 protein accumulation (Figure 2.10C). We also quantified GL2-

GFP levels in H-position and N-position cells from wild type and *wer-4* bearing the

GL2::GL2-GFP reporter and discovered that cells in both positions exhibited higher

signal variations in *wer-4* than in the wild type (Figure 2.10B). Specifically, 25% of the

N-position cells in *wer-4* exhibited weaker GFP signals than the N-position cells in wild

63

type (marked with red stars in Figure 2.10B upper panel), which roughly matches the

percentage (28%) of root-hair cells in the N position of *wer-4* (Figure 2.1B);

approximately 20% of the H-position cells in *wer-4* cells exhibited GFP signals that are

comparable or higher than the GFP signals in wild-type N-position cells (marked with

red stars in Figure 2.10B lower panel), which is comparable to the fraction (13%) of non-

hair cells produced in the H position of *wer-4* (Figure 2.1B). These results suggest that

epidermal cell fates in the *wer-4* mutant are correlated with GL2 protein levels. To

further address this possibility, we analyzed older epidermal cells (within the early

maturation zone) in wild-type and *wer-4* roots bearing *GL2::GFP*, which enabled us to

assess both *GL2* transcription (which is proportional to GL2 protein levels) and cell fate

(i.e. whether or not root hair is produced) in individual cells. We discovered that root-hair

cells in the N position of *wer-4* exhibited lower GFP signals than the adjacent non-hair

cells in the same cell file, and non-hair cells in the H position of the *wer-4* mutant

showed higher GFP signals relative to their H-position neighbors and comparable to

non-hair cells in the N position (Figure 2.10D). These results support the hypothesis that

in *wer-4,* ectopic cell fates in the H and N positions are the result of abnormal GL2

protein accumulation.

     Finally, we examined the possible effect of *wer-4* on the ability of root epidermal

cells to differentiate properly. In particular, we hypothesized that the ectopic root-hair

cells that arise in N position may not fully differentiate like authentic root hair cells, due

to the lower but significant amounts of GL2 protein they produce (Figure 2.10B). Indeed,

we discovered that the length of root hairs formed by the N-position cells of the *wer-4*

mutant are much shorter than these formed by the H-position cells of wild-type or *wer-4*

(Figure 2.11). This difference was also apparent from visual observation of the *wer-4* mutant roots (Figure 2.1A).

In summary, the *wer-4* mutation alters cell fate patterning as well as cell differentiation, likely due to inappropriate establishment of cell-type specific accumulation of the WER-GL3/EGL3-TTG1 complex, which leads to variable levels of GL2 protein accumulation.

WER protein function is altered by manipulating its D105 residue

Our analysis of the *wer-4* mutant reveals that the D105 residue is important for proper WER protein function, and a substitution from aspartic acid to asparagine alters its transcriptional regulatory activity. To further analyze this residue and its importance in root epidermal patterning, we engineered additional substitutions at this position, including glutamic acid (E), with an R group similar to aspartic acid, glutamine (Q), the amide derivative of asparagine, and alanine (A), with the smallest and uncharged R group. We constructed each transgene using an identical *WER* genomic DNA fragment, including 4-kb 5' flanking sequence and 1-kb 3' flanking sequence, each differing only in nucleotides affecting codon 105 (Figure 2.12A). As controls, transgenes encoding WER and WER^{D105N} were also constructed. To monitor the effect of each *WER* transgene on target gene transcription, we transformed each construct into *wer-1 GL2::GUS* or *wer-1 CPC::GUS* plants. At least three independent homozygous single-insertion T3 lines were analyzed for each transformation experiment.

The *wer-1* plants carrying the *WER::WER* transgene exhibited a wild-type cell-type pattern and preferential expression of both *GL2::GUS* and *CPC::GUS* reporters in N-position cells (Figure 2.12, B to D). The *wer-1* plants bearing the *WER::WER^{D105N}*

transgene exhibited a phenotype similar to *wer-4*, including a distorted cell-type pattern, overall elevated and ectopic *GL2::GUS* expression, and abnormal *CPC::GUS* expression (Figure 2.12, B to D). Thus, the control transgenes successfully replicate the *WER* functions in wild-type and *wer-4* plants.

Each of the three new substitutions of the D105 residue alters WER protein function in a different way. The *WER::WER^D105E* transgene exhibited the least recovery of WER function. In these lines, only 10% of N-position cells were able to differentiate as non-hair cells (Figure 2.12D). Consistently, the expression of the *GL2::GUS* and *CPC::GUS* reporters occurred in a small fraction of the differentiating epidermal cells (Figure 2.12, B and C). These results indicate that the D105E substitution substantially impairs WER's ability to induce *GL2* and *CPC* transcription, and ultimately, non-hair cell specification.

The *WER::WER^D105A* transgene largely restored the wild-type root epidermal cell pattern to the *wer-1* mutant with a minor increase of ectopic root-hair cells (around 6%) in two of the three independent transgenic lines (Figure 2.12D). The preferential expression of both *GL2::GUS* and *CPC::GUS* reporters in N-position cells is also restored, but both reporters were expressed at higher overall levels than in wild type (Figure 2.12, B and C), suggesting that the D105A residue substitution enhances WER's ability to promote transcription from the *GL2* and *CPC* promoters without significantly disrupting the cell fate network.

The *WER::WER^D105Q* *wer-1* plants produced approximately 20% ectopic root-hair cells in the N position (Figure 2.12D). The numbers of cells expressing *GL2::GUS* and *CPC::GUS* in the N positions were both reduced (Figure 2.12, B and C), and

66

interestingly, the overall expression level of each reporter was increased compared to the *WER::WER wer-1* lines. These results indicate that the D105Q substitution enhances WER's ability to promote *GL2* and *CPC* transcription, but the balance of these and/or other regulators within the cell fate network is disrupted to cause abnormal cell specification.

To compare different WER variants with the wild-type WER, we crossed the homozygous single-insertion T3 plants carrying various *WER::WER* transgenes with the wild-type plants and analyzed the F1 plants. For each transgene, 3 independent T3 lines were used for crosses.

The F1 plants from the *WER::WER^D105N* ✗ WT crosses exhibited the wild-type *GL2::GUS/CPC::GUS* expression and root epidermis pattern (Figure 2.13, A to C), which is consistent with our analysis on the *wer-4*/+ plants (Figure 2.1B). The F1 plants from the *WER::WER^D105E* ✗ WT crosses fully restored wild-type *GL2::GUS/CPC::GUS* expression and root epidermis pattern (Figure 2.13, A to C). Thus, a single copy of the wild-type WER is sufficient to complement the defective WER^D105E function. The F1 plants from the *WER::WER^D105A* ✗ WT crosses exhibited wild-type *GL2::GUS/CPC::GUS* expression patterns and root epidermis pattern (Figure 2.13, A to C), which is predictable given the phenotypes of the *WER::WER^D105A* T3s (Figure 2.12, B to D). Interestingly, the F1 plants showed higher *CPC::GUS* expression levels compared to the control F1s from the *WER::WER* ✗ WT crosses (Figure 2.13B), suggesting that WER^D105A outcompetes WER in regulating *CPC*. The F1 plants from the *WER::WER^D105Q* ✗ WT crosses also showed significantly increased *CPC::GUS* expression (Figure 2.13B). Moreover, two of the three F1 populations exhibited about

67

10% of ectopic root-hair cells (Figure 2.13C), and the *GL2::GUS/CPC::GUS* signals also showed occasional down-regulation in N-position cells in several F1 populations (#1 and #3 for *GL2::GUS*, #1 and #2 for *CPC::GUS*) (Figure 2.13, A and B). Therefore, WER^{D105Q} outcompetes WER in regulating *CPC* and disrupts non-hair cell fate establishment in the presence of WER.

In summary, the D105E, D105A, and D105Q substitutions alter WER's ability to properly regulate the *GL2* and *CPC* genes. The D105E substitution leads to defective WER function that can be rescued by wild-type WER; the D105A and D105Q substitutions enhance WER's ability to regulate *GL2* and *CPC*, but both with relatively stronger impacts on the *CPC* gene. In the case of the D105E substitution, this impact is significant enough to disrupt non-hair cell fate establishment.

Discussion

In this report, we demonstrated the significance of a specific residue (D105) in the WER transcription factor for appropriate regulation of root epidermal patterning. It is particularly interesting that substitutions of this residue did not abolish WER function, but rather they altered the ability of WER to properly regulate downstream genes and caused a variety of cell-type pattern phenotypes. The importance of this residue was first recognized through the identification and characterization of the *wer-4* mutant, which exhibited a novel cell-type pattern in the root epidermis. We showed that the D105N substitution in *wer-4* caused differential effects on WER target promoter binding, generated an imbalance in the levels of downstream gene expression, and reduced the molecular distinctions that normally exist between differentiating H-position and N-

68

position epidermal cells. We also created three new WER variants with substitutions at D105 and each exhibited abnormalities in WER function and/or cell-type pattern. Altogether, these results reinforce the central role of WER in defining the epidermal cell type pattern, and they reveal the specific importance of the D105 residue for the transcriptional regulatory activity of WER.

Role of D105 Residue for WER Protein Function

Plant R2R3-type MYB proteins are defined by their similarities to the mammalian c-Myb protein, of which the R2 and R3 repeats comprise the minimum DNA binding domains (Paz-Ares et al. 1987; Sakura et al. 1989; Kanei-Ishii et al. 1990). The solution structure of the mouse c-Myb R2 and R3 domains revealed that each domain consists of 3 α-helices with a tryptophan-formed hydrophobic core, and the third helices of each domain are DNA recognition helices containing several amino acids that directly associate with DNA bases (Ogata et al. 1994). The R2 and R3 repeats of the WER protein resemble those in the mammalian c-Myb protein (Jin et al. 1999), with each repeat containing 3 α-helices with appropriately spaced tryptophan residues and the same DNA-associating amino acids at the same relative positions (Tombuloglu et al. 2013; Wang et al. 2015) (Figure 2.1D). Furthermore, the previously defined *in vivo* DNA binding sites of WER show substantial similarity to the DNA binding consensus sequence for the mammalian c-Myb (Ryu et al. 2005; Kang et al. 2009; Song et al. 2011). Thus, it is likely that WER recognizes DNA in a comparable manner with its well-studied mammalian homologue, although WER itself has not been analyzed biochemically in the same detail as c-Myb (Saikumar et al. 1990; Gabrielsen et al. 1991).

The D105 residue in the WER protein is conserved in more than 90% of all R2R3-type MYB proteins in Arabidopsis as well as in the mammalian c-Myb (Ogata et al. 1994; Lin-Wang et al. 2010). Although this residue is not one of the c-Myb residues shown to directly associate with DNA, it is located near these residues and within the same DNA-recognizing helix of the R3 domain (Figure 2.1D). Intriguingly, the solution structure of mouse c-Myb suggests that this aspartic acid residue may be involved in formation of a salt bridge that aids interaction between the R2 and R3 domains, which is essential for DNA binding (Ogata et al. 1994). However, to our knowledge, no studies have directly analyzed the functional importance of this amino acid.

In our study, we discovered that substitutions of the D105 residue affected WER's ability to promote transcription of its target genes. Specifically, the *wer-4* mutant (encoding the WER^{D105N} protein) exhibited a dramatic reduction in *TRY* and *ETC1* gene expression, a mild reduction in *CPC* gene expression, and a slightly elevated level of *GL2* gene expression in the developing root epidermis (Figure 2.2). In addition, our EMSA experiments showed that the WER^{D105N} protein has an altered relative affinity for its target promoters, with a greater preference for the *GL2* promoter over the *CPC* promoter, compared to the wild-type WER (Figure 2.6). Given that the D105 residue is located in the putative DNA recognition helix, we conclude that the role of the D105 residue is to aid DNA recognition, and the abnormal transcriptional regulation of WER target genes in *wer-4* is due to the differential effect of the D105N substitution on WER's affinity for individual target gene promoters.

We also made use of the yeast-two hybrid assays to show that the D105N substitution in WER does not harm but even enhances the interaction between WER

70

and GL3 (Figure 2.5). Interestingly, the D105 residue is not located within the conserved bHLH-binding motif of WER ((Zimmermann et al. 2004), Figure 2.1D), suggesting that the conserved bHLH-binding motif of R2R3-type MYB proteins requires particular neighboring residues for a proper function. On the other hand, the potentially enhanced association between WER[D105N] and GL3 is less likely to be the reason for the differential effects of *wer-4* on various target gene transcription. This is because this change should have a universal impact among all WER target genes since the MYB-bHLH association is essential for all transcriptional regulations.

In addition to the *wer-4* mutant, we substituted the D105 residue in WER with more variants and observed distinct effects of these new substitutions (Figure 2.12, 2.13). The D105E substitution essentially depletes WER protein function and results in the 'hairy' phenotypes resembling the *wer-1* null mutant. The heterozygote analysis then showed that the impaired WER function is not through a dominant-negative effect. The D105A and D105Q substitutions show similar effects of enhancing the regulatory function of WER. However, the D105Q substitution causes greater and semi-dominant disruptions on non-hair cell fate establishment. A possible explanation for this phenotype is that both D105A and D105Q substitutions leads to excessive CPC production, but this effect is stronger in the case of D105Q, which not only mediates lateral inhibition in the H position, but also disturbs WER function in the N position. Meanwhile, it is of special interest that both D105A and D105Q substitutions cause stronger impacts on *CPC* expression than on *GL2*, according to the heterozygote analyses. This result, together with our studies on *wer-4* that the D105N substitution affects the relative affinities of WER to *GL2* and *CPC* promoters, suggest that the D105

71

residue is involved in balancing the activity of WER among its various target gene promoter regions.

A Model for the Abnormal Pattern Formation in the *wer-4* Mutant

The *wer-4* mutant exhibits a novel cell-type distribution in the root epidermis, with root-hair cells and non-hair cells produced in both the H and N positions rather than strictly position-dependent cell fate specification. Based on our results, we propose the following explanation for this abnormal pattern (Figure 2.14). The WER^{D105N} protein encoded by *wer-4* has altered relative affinities for various WER target gene promoters, including relatively weak affinity for the *CPC* promoter and very weak affinity for the *TRY* and *ETC1* promoters. This results in lower production of R3-type MYB competitors (CPC, TRY, and ETC1) in the developing root epidermis (Figure 2.2, 2.9), which allows for abnormal accumulation of the WER-GL3/EGL3-TTG1 complex in the H-position cells. As a result, CPC are ectopically produced in the H-position cells and this leads to abnormal movement of H-cell-produced CPC to N-position cells. Thus, rather than mediating unidirectional lateral inhibition (from N-position cells to H-position cells) as in wild-type roots, CPC in *wer-4* tends to mediate mutual disruptions of the WER-GL3/EGL3-TTG complex between H- and N-position cells. This weakens the position-dependent accumulation of the WER-GL3/EGL3-TTG1 complex that normally occurs in N-position cells, although the intact SCM signaling pathway in *wer-4* (Figure 2.9C) ensures that N-position cells still tend to accumulate higher complex levels than H-position cells. Variable amounts of the WER-GL3/EGL3-TTG complex in both H- and N-position cells (Figure 2.9, A and E) directly leads to variable and ectopic expression of *GL2* (Figure 2.2C) and GL2 protein productions (Figure 2.10, A and B). The final fate of

each individual cell depends on its GL2 protein level; epidermal cells that accumulate no, or low levels of, GL2 protein differentiate into root-hair cells, whereas cells that accumulate higher GL2 protein differentiate into non-hair cells (Figure 2.10, B and D). Thus, the abnormal WER target gene expression in *wer-4* ultimately leads to a mixture of both root-hair and non-hair cell types in the H- and N-position cells.

In addition to an effect on cell fate specification, we have shown that *wer-4* also affects root hair morphogenesis. Specifically, many of the ectopic root-hair cells in *wer-4* produced shorter root hairs than wild type (Figure 2.11), suggesting that the small yet significant amounts of GL2 present in these N-position cells (Figure 2.10B) is able to partially inhibit root hair growth though insufficient to induce the non-hair cell fate. This suggests that GL2, as a well-known positive regulator of non-hair genes and negative regulator of root-hair genes (Lin et al. 2015), functions in a concentration-dependent manner in root-hair cell differentiation.

Notably, our study revealed a discrepancy between the relative levels of *GL2* gene transcription and GL2 proteins in *wer-4*. Although *wer-4* has an elevated level of *GL2::GFP* transcriptional reporter expression relative to the wild type (Figure 2.2E), the overall level of its *GL2::GL2-GFP* translational fusion reporter signal is comparable to wild type (Figure 2.10B). Given that these two reporter constructs contain the same 5'-*GL2* promoter region (2-kb fragment, see Materials and Methods), this discrepancy suggests the existence of a post-transcriptional mechanism regulating GL2 protein accumulation. This hypothesis is also consistent with our qPCR result that *GL2* transcript level is not increased but slight decreased in the *wer-4* mutant (Figure 2.2A). These observations, together with the report that overexpressing *GL2* with the

73

CaMV35S promoter induces GL2 self-inhibition and perhaps cell toxicity (Ohashi et al. 2002), are indicative of a unknown mechanism that monitors and restricts GL2 production.

Evolutionary Implications of the WER D105 Substitutions

A central issue in evolutionary developmental biology is to understand how transcriptional regulatory networks might evolve to generate new developmental phenotypes (Nocedal et al. 2015). Our study of the effects of altering a single residue in the WER protein on the root epidermal network provides some insight into this issue. We found that WER transcriptional activity is affected in different ways by substitutions of the D105 residue. In particular, our data shows that the D105N substitution modifies the affinities of WER for its target gene promoters, implying that this residue is important for modulating the relative activity of WER on its targets. From an evolutionary view, this opens the possibility that substitutions of this residue may provide a way to rewire the network and generate new phenotypic variations. Indeed, it may be argued that WER^{D105N}, WER^{D105Q} and WER^{D105E} represent examples of network rewiring, because these changes in WER altered the spatial distribution of gene expression programs and yielded new root epidermal cell-type patterns.

Further, it is notable that two of the D105 substitutions of WER that we generated and analyzed in our study, D105A and D105E, occur naturally in some members of the R2R3-type MYB protein family of Arabidopsis (Figure 2.1D, (Stracke et al. 2001)). Among the 125 R2R3-type MYB proteins (Stracke et al. 2001), almost 95% possess an aspartic acid residue (D) in the corresponding position of D105 in WER (i.e. D-type), while five members have alanine (A-type) and four members have glutamic acid (E-type)

(Lin-Wang et al. 2010). Interestingly, four of the A-type MYB proteins (MYB75, MYB90, MYB113, MYB114) are involved in anthocyanin biosynthesis (Gonzalez et al. 2008; Lin-Wang et al. 2010); two of the E-type MYB proteins (MYB115 and MYB118) are involved in glucosinolate and omega-7 biosynthesis (Y. Zhang et al. 2015; Troncoso-Ponce et al. 2016); and another two E-type MYB proteins (MYB64 and MYB119) are involved in female gametogenesis (Rabiger et al. 2013). Thus, groups of R2R3-type MYB proteins carrying variations of WER D105 tend to participate in particular biological processes. This implies that changes in this residue may help R2R3-type MYBs to evolve new target gene specificities permitting the MYBs and their associated regulatory gene networks to generate new phenotypes.

Materials and methods

Plant materials and growth conditions

Most of the mutant and transgenic lines have been previously described: *cpc-1* (Wada et al. 1997), *wer-1* (Lee et al. 1999), *GL2::GUS* (Masucci et al. 1996a), *GL2::GFP* (Lin et al. 2001), *CPC::GUS* (Wada et al. 2002), *ETC1::GUS* (V. Kirik et al. 2004), *GL3::GL3-YFP* (Bernhardt et al. 2005), *CPC::CPC-GFP* (Kurata et al. 2005). The *GL2::GL2-GFP* transgenic line was a kind gift from Dr. Lijun An and Dr. Fei Yu (Northwest Agriculture and Forestry University, China). The *GL2::GUS* reporter includes a 4kb-long promoter region of *GL2* gene upstream of translational start site (ATG). The *GL2::GFP* and *GL2::GL2-GFP* reporters both include a 2kb-long promoter region of *GL2* gene.

Arabidopsis seeds were surface sterilized with 30% bleach and 0.02% Triton-X.

Seeds were sown on mineral nutrient mix media solidified with 0.3% Gelrite

(Schiefelbein et al. 1990). Plates were then incubated at 23°C under continuous light

and 4-day-old seedlings were used for experiments. Mature plants were generated by

transplanting seedlings to soil and grown in growth chambers under long-day light cycle

at 23°C (daytime) to 18°C (nighttime).

Genetic screening and positional mapping

Mutagenesis of the *cpc-1 GL2::GUS* line (Wassilewskija [Ws] ecotype) with ethyl

methanesulfonate (EMS) was performed as previously reported (Estelle et al. 1987).

The *cpc-1 wer-4* mutant was identified from the M2 population through a visual screen

for root hair density with a dissection microscope. The F2 and F3 offspring from a cross

between *cpc-1 wer-4* and a Columbia wild-type plant were analyzed using multiple

simple sequence length polymorphism (SSLP) markers (Bell et al. 1994), and strong

linkage was identified with marker nga151 (position 4.67 Mb on chromosome 5), near

the *WER* gene (position 4.76 Mb on chromosome 5).

The Derived Cleaved Amplified Polymorphic Sequences (dCAPS; (Neff et al.

2002)) technique was used for *wer-4* genotyping, using primers listed in Table 2.1.

Transgene construction and plant transformation

The *WER* genomic segment including 4-kb 5' promoter sequence, 1-kb genomic

sequence and 1-kb 3' terminal sequence was cloned using Phusion (NEB) and

integrated into the pCB302 binary vector (digested with SpeI and BamHI; (Xiang et al.

1999)) using the HiFi assembly system (NEB). For *WER::WER* transgenes carrying

different substitutions of D105, the same 6-kb *WER* genomic segment was cloned into

two pieces separated at the mutation site using primers carrying corresponding

nucleotide changes. The two *WER* genomic sequence fragments (4.7-kb and 1.3-kb)

bearing the preferred mutations were then combined into the pCB302 vector using the

HiFi assembly system. Cloning primers are listed in Table 2.1. Verified constructs were

then transformed into *wer-1* plants carrying either the *CPC::GUS* or *GL2::GUS* reporter

through floral dipping as described (Clough et al. 1998).

After plant transformation, T_0 plants were grown and T_1 seeds were harvested

and subjected to glufosinate-ammonium (PESTANAL®, Sigma-Aldrich) selection.

Resistant T_1 seedlings were then grown for T_2 seeds, and the segregation rate of

individual T_2 populations for resistance and root-hair pattern was used to identify single-

insertion lines. For each transformation experiment, homozygous T_3 populations from

at least 3 independent single-insertion lines were used for further experiments.

Microscopy and image analysis

The quantification of root epidermal cell types was performed using a bright field

compound microscope, following brief staining with toluidine blue. Cell positions were

determined according to underlying cortical cells and hair cells were scored by visible

protrusion as root hairs regardless of root hair length. For each genotype, three

independent replicates were performed. For each replicate, up to 10 seedlings were

used and 10 cells in both H and N positions were scored in each seedling (total of 100

cells).

Histochemical analysis of GUS fusion reporter lines was performed as described

(Masucci et al. 1996a). Specifically, 10 µl/mL of X-Gluc (Gold Biotechnology) substrates

were used for *GL2::GUS* (20min at 37°C); 20 µl/mL of X-Gluc substrates were used for

CPC::GUS (90min at 37°C) and *ETC1::GUS* (3hrs at 37°C). GUS signal quantification

was performed using ImageJ as described (Beziat et al. 2017). To generate histograms

for *CPC::GUS* signal distribution, wild-type and *wer-4* roots were stained and

photographed under the same conditions. For each root, 10 continuous cells in one file

were analyzed from the oldest cell prior to rapid elongation (i.e. the cell's length

exceeds its width) down toward the root tip. For all cells, the GUS signal was measured

using the same region of interest (ROI) frame and the mean values were plotted into

histograms.

To analyze GUS fusion reporters expression in leaves, the first pairs of true

leaves from 14-day old plants were collected and incubated in staining buffer containing

20 μl/mL of X-Gluc substrates at 37°C for 2 hours (for *GL2::GUS*) or 4 hours (for

ETC1::GUS and *CPC::GUS*). The stained leaves were then cleared with ethanol:acetic

acid mixtures as described (Beziat et al. 2017) to remove chlorophyll before imaging.

Fluorescence imaging was performed using a TCS SP5 DM6000B broadband

confocal microscope (Leica) with 20× or 40× dry lens. Seedling roots were briefly

stained in propidium iodide (PI) for cell wall visualization. Default excitement and

emission settings for GFP, YFP, and PI signals were used for imaging. To generate

histograms for *GL2::GFP* signal distribution, wild-type and *wer-4* root images were

captured using the same settings. Care was taken to ensure each root was imaged on

similar Z-axis positions marked by the maximum nucleus size. GFP quantification was

performed using ImageJ under RGB separate channels and only green channels were

quantified. Ten continuous cells in each H- and N-position cell files were quantified

using similar criteria as for GUS quantification. The GFP signals for the entire cells were

measured using free-shape ROIs and the mean values were plotted into histograms. Similarly, for *GL2::GL2-GFP* and *GL3::GL3-YFP* signal histograms, 10 continuous cells in each H- and N-position cell files were analyzed from wild-type and *wer-4* roots. For each root, GFP signals in the nuclei were specifically collected using round-shape ROIs and the mean values from each cell were used for plotting histograms. For *CPC::CPC-GFP* signal analysis, total signal levels in all cells within the meristematic zone (from the first measurable cell to the last cell before rapid elongation) from both H and N positions in each root are measured with free-shape ROIs and then divided by the number of measured cell to generate an average GFP signals for each root. For each genotype, 20 roots were used.

To examine the expression of fluorescence reporters and GUS reporters within the same root, seedling roots were first imaged with a confocal microscope, and then the roots were removed from the microscope slides and stained for GUS signals. The stained roots were then imaged under the bright-field microscope. Special care was taken to ensure that the roots were placed in a similar posture on the slide as for the confocal imaging according to the cotyledons, and the same groups of cells were chosen for imaging based on the landmarks of the root epidermis. For *GL2::GUS* signal quantification, due to the significant difference in signal levels between wild-type and *wer-4* roots, staining time was set differently for wild type and *wer-4* to ensure signals from both genotypes were within measurable ranges.

To measure root hair length, photos of root hairs were obtained using a light compound microscope, and measurement was performed using ImageJ. For each wild-type root, 10 root hairs on cells located in the H position were measured in the fully

maturation zone, which is approximately 3~5mm from root tips and marked by an overall stable length of root hairs. For each *wer-4* root, 10 root hairs on cells located in H and N positions were measured separately within the fully maturation zone.

RNA extraction and quantitative real-time PCR (qPCR)

Total RNA was extracted from root tips (including meristematic zone, elongation zone and early maturation zone) as described (Huang et al. 2015) (RNeasy Plant Mini kit, QIAGEN). To analyze transcript levels in leaves, the first pairs of true leaves from 14-day old plants were collected and RNA was extracted using the same method. RNA was treated with the RQ1 DNase (Promega). cDNA was synthesized with the SuperScript First-Strand Synthesis System (Invitrogen). Quantitative PCR was set up using the Radiant Green Hi-ROX qPCR Kit (Alkali Scientific Inc.) and conducted using the StepOnePlus real-time PCR system (Applied Biosystems). The Delta-Delta-Ct method (Livak et al. 2001) was used to determine the relative transcript amounts. The *GAPCP2* gene (*AT1G16300*, encoding a GAPDH isoform) was used as the internal reference gene. Primers used for qPCR are listed in Table 2.1.

Yeast two-hybrid assays

The yeast two-hybrid assays were conducted as previously described (Lee et al. 1999; Bernhardt et al. 2003). The pGBT9 construct containing the BD-GL3 fusion and the pGAD424 construct containing the AD-WER fusion were the same as previously used (Bernhardt et al. 2003). The AD-WER^{D105N} construct was generated through replacing the wild-type *WER* coding sequence with the *wer-4 WER* coding sequence. After transformation into the HF7c yeast strain, the β–galactosidase assays were conducted

using at least three individual transformants for each AD/BD combination and analysis of each transformants were repeated three times.

Electrophoretic mobility shift assay (EMSA)

The EMSA was performed as described (Ryu et al. 2005) with purified WER and WER^{D105N} proteins. For EMSA experiments with GWBSI/II or WBSI/II, and competition EMSA experiment between GWBSI and GWBSII, probe labeling was carried out with T4 polynucleotide kinase and [γ-^{32}P]ATP (Ryu et al. 2005). For competition EMSA experiment between GWBSI and WBSI, commercial hot probes with infrared labeling was used (Integrated DNA Technologies). Each EMSA experiment was repeated at least three times. Probe sequences are listed in Table 2.1. The EMSA binding signals were quantified using ImageJ and used for non-linear regression. Given the different affinities of WER and WER^{D105N} to GWBSI and WBSI, in both competition assays, the relative amounts of WER and WER^{D105N} were adjusted to make sure binding signals for both proteins are within measurable ranges.

Accession numbers

Sequence data from this chapter can be found in the GenBank/EMBL data libraries under the following accession numbers: *WER* (AT5G14750), *MYB23* (AT5G40330), *GL1* (AT3G27920), *MYB113* (AT1G66370), *MYB115* (AT5G40360), *GL2* (AT1G79840), *CPC* (AT2G46410), *ETC1* (AT1G01380), *TRY* (AT5G53200), *GL3* (AT5G41315), *SCM* (AT1G11130).

A

WT cpc-1 cpc-1 wer-4 wer-4

B

Ectopic non-hair cells
Ectopic root-hair cells

Percentage

cpc-1 cpc-1 wer-4 WT wer-4 wer-4/+ WWGFP WWGFP in wer-4

C

WT
GL2::GUS

cpc-1
GL2::GUS

cpc-1 wer-4
GL2::GUS

D

```
WER     YKKGLWTVEEDKILMDYVKAHGKGHWNRIAKKTGLKRCGKSCRLRWMNYLSPN
MYB23   YKKGLWTVEEDKILMDYVRTHGOGHWNRIAKKTGLKRCGKSCRLRWMNYLSPN
GL1     YKKGLWTVEEDNILMDYVLNHGTGQWNRIKVRTGLKRCGKSCRLRWMNYLSPN      R2
MYB113  LRKGTWTTEEDILLRQCIDKYGEGKWHRVPLRTGLNRCRKSCRLRWLNYLKPS
MYB115  IGKGQWTPTEDELLVRMVKSKGTKNWTSIAKMFQ-GRVGKQCRERWHNHLRPN
                α1              α2              α3

WER     VKRGNFTEQEEDLIIRLHKLLGNRWSLIAKRVPGRTDNQVKNYWNTHLSKKL
MYB23   VNRGNFTDQEEDLIIRLHKLLGNRWSLIAKRVPGRTDNQVKNYWNTHLSKKL
GL1     VNKGNFTEQEEDLIIRLHKLLGNRWSLIAKRVPGRTDNQVKNYWNTHLSKKL      R3
MYB113  IKRGKLCSDEVDVLVLRHKLLGNRWSLIAGRVPGRTANDVKNYWNTHLSKKH
MYB115  IKKNDWSEEEDQILIEVHKIVGNKWTEIAKRVPGRSENIVKNHWNATKRRLH
              α1          α2          α3
```

82

Figure 2.1 The *wer-4* mutant allele enhances the *cpc-1* phenotype and possesses a missense mutation in the *WER* gene.
(A) Seedling roots of wild type, *cpc-1*, *cpc-1 wer-4*, and *wer-4* displaying their root-hair phenotypes. The arrows point to significantly shorter root hairs in the *wer-4* root. Bar=200µm. (B) Quantifications of root epidermis specification in seedling roots of various genetic backgrounds. *WWGFP* represents the *WER::WER-GFP* reporter. Error bars represent standard deviations from three replicates. Statistical significance is determined by two-way ANOVA. *** represents p<0.001, ns represents not significant. (C) *GL2::GUS* reporter expression in seedling root tips of wild type, *cpc-1*, and *cpc-1 wer-4*. Stars indicate H-position cell files. For each genotype, the left and right panels show the same root under different magnifications. Bar=50µm. (D) Alignment of the R2R3 domains of multiple Arabidopsis MYB proteins. The red arrow marks the position of the D105N residue substitution in the *wer-4* mutant. The black lines indicate the three α-helices in each repeat. Stars indicate conserved tryptophan residues. Diamonds indicate conserved residues that directly associate with DNA bases in mammalian c-Myb. The green dotted frame indicates the conserved bHLH interaction domain.
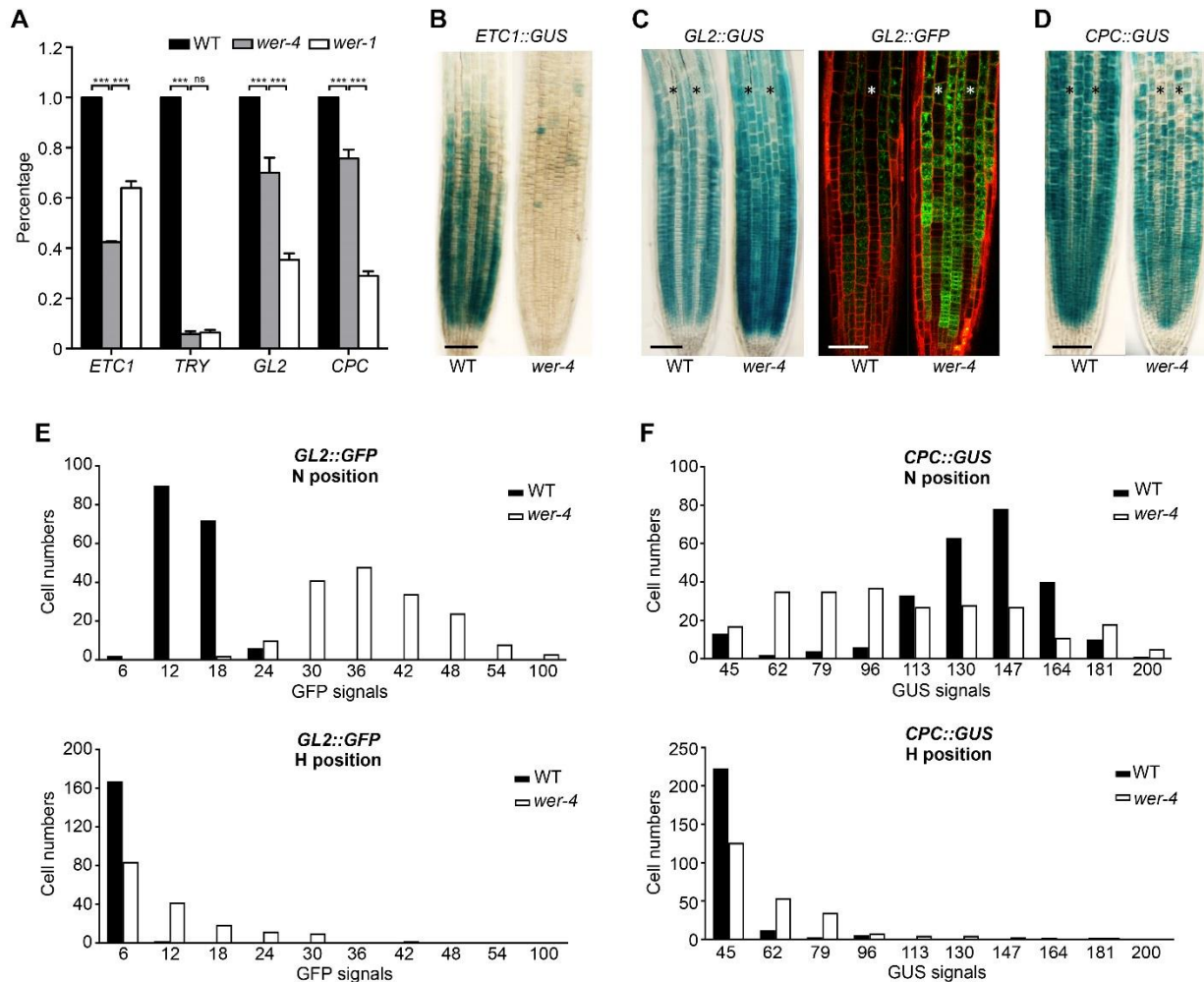
Figure 2.2 The *wer-4* mutant affects expression of WER target genes.
Relative amounts of *ETC1*, *TRY*, *GL2*, *CPC* transcripts in seedling root tips of wild type,
wer-4 and *wer-1*, determined with quantitative real-time PCR. Error bars represent
standard deviations from three replicates. Statistical significance is determined with
one-way ANOVA. *** indicates $p<0.001$ and n.s. indicates not significant. (B)
ETC1::GUS transcriptional reporter expression in seedling root tips of wild type and
wer-4. Bar=50µm. (C) Expression of *GL2::GUS* and *GL2::GFP* transcriptional reporters
in wild-type and *wer-4* seedling root tips. Stars indicate H-position cell files. Bar=50µm.
In the fluorescence image, the red color represents propidium iodide and the green
color represents GFP. (D) Expression of *CPC::GUS* transcriptional reporter in wild-type
and *wer-4* seedling root tips. Stars indicate H-position cell files. Bar=50µm. (E)
Histograms of *GL2::GFP* signal levels in N-position and H-position epidermal cells of
wild-type and *wer-4* seedling root tips (n=170). Ten cells in H and N positions were
analyzed per root and 17 roots were analyzed for each genotype. (F) Histograms of
CPC::GUS signal levels in N-position and H-position epidermal cells of wild-type and
wer-4 seedlings root tips (n=240). Ten cells in H and N positions were analyzed per root
and 24 roots were used for each genotype.

84
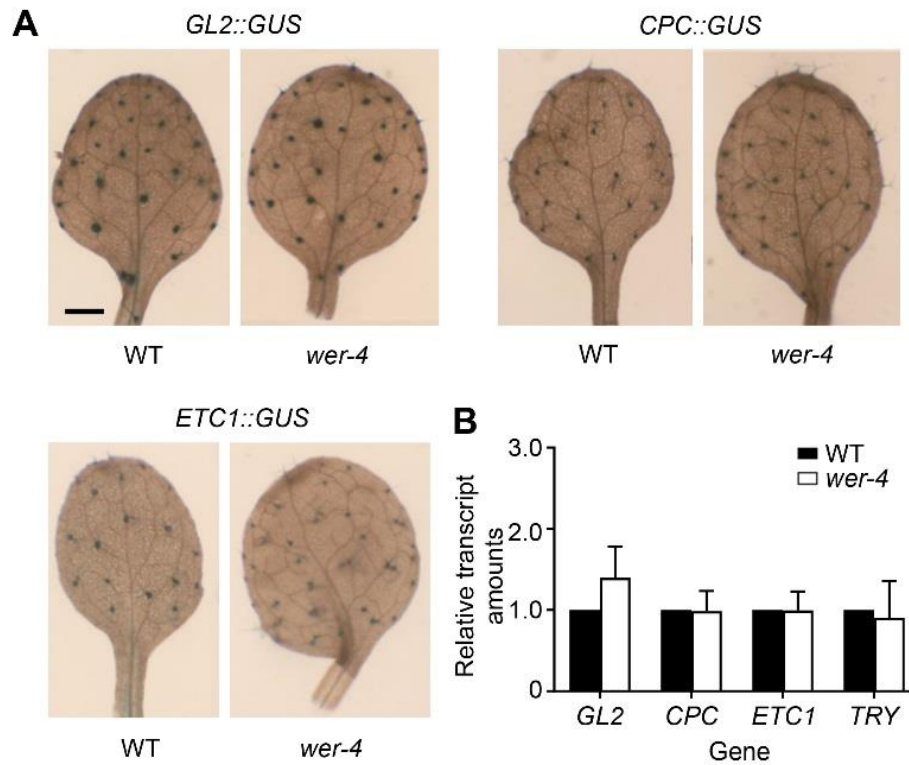
Figure 2.3 Expression of WER target genes in leaves is not affected by *wer-4*.
(A) Expression of the *GL2::GUS*, *CPC::GUS*, and *ETC1::GUS* reporters in wild-type
(WT) and *wer-4* leaves. For all experiments, the first pair of true leaves are used.
Bar=0.5mm. (B) Relative transcript amounts of *GL2*, *CPC*, *ETC1*, and *TRY* in the first
pair of true leaves of WT and *wer-4* mutant are determined by RT-qPCR. Error bars
indicate standard deviations from three replicates. Two-way ANOVA analysis revealed
no significant differences between wild type and *wer-4* ($p > 0.05$).
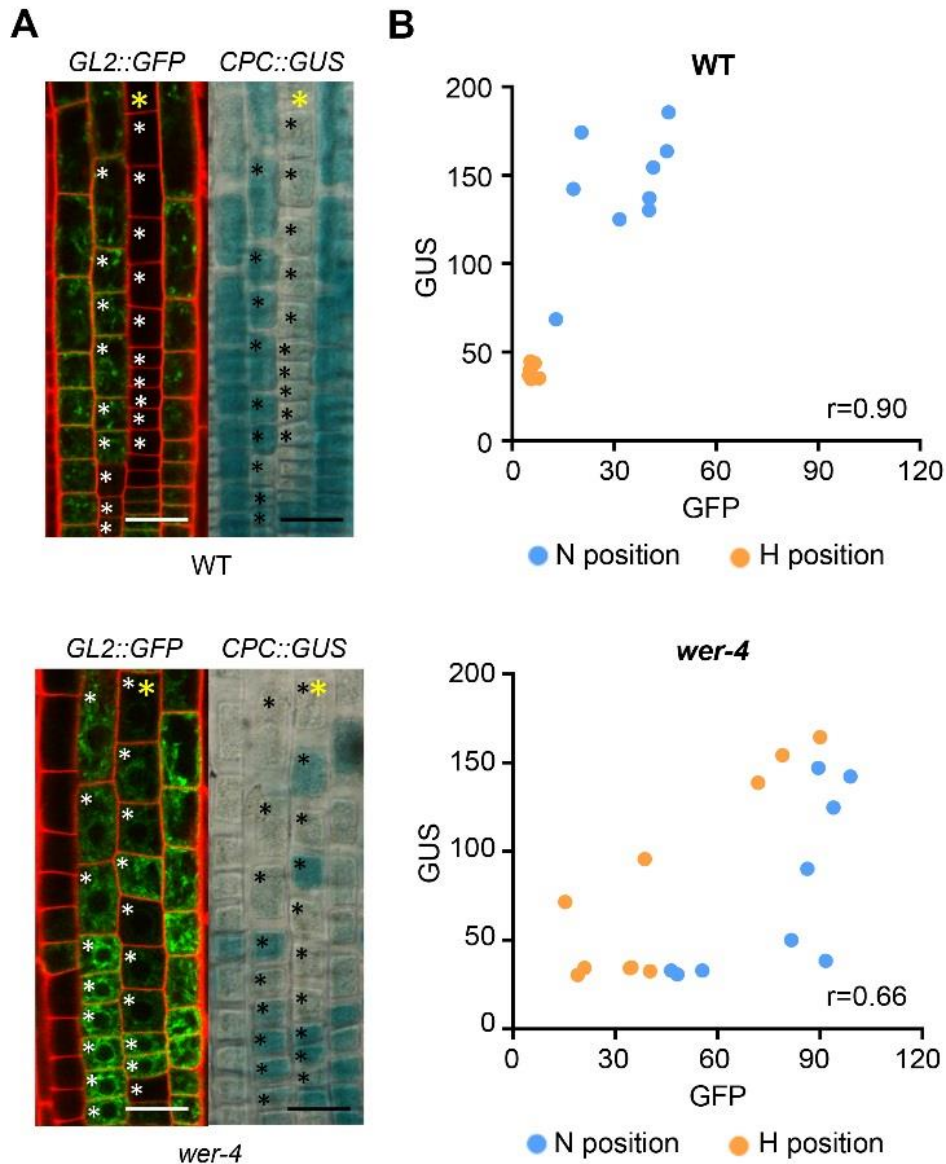
Figure 2.4 Expression of the *GL2* and *CPC* genes is coordinated in *wer-4* root epidermal cells.

(A) Expression of the *GL2::GFP* and *CPC::GUS* reporters within one single root of wild-type and *wer-4* seedlings. The yellow stars indicate H-position cell files. In the fluorescence images, the red color represents propidium iodide and green color represents GFP. Bar=25µm. (B) Scatter plots of GFP and GUS signal levels in root epidermal cells of wild type and *wer-4* roots. Each data point represents one cell marked with black/white stars in (A). r represents the Pearson correlation coefficient determined with all data points from both H and N positions in each plot.

A

2
1 3
6 4
5

B

1.pGAD+pGBD 4.pGAD+pGBD-GL3

2.pGAD-WER+pGBD 5.pGAD-WER+pGBD-GL3

3.pGAD-WER^{D105N}+pGBD 6.pGAD-WER^{D105N}+pGBD-GL3
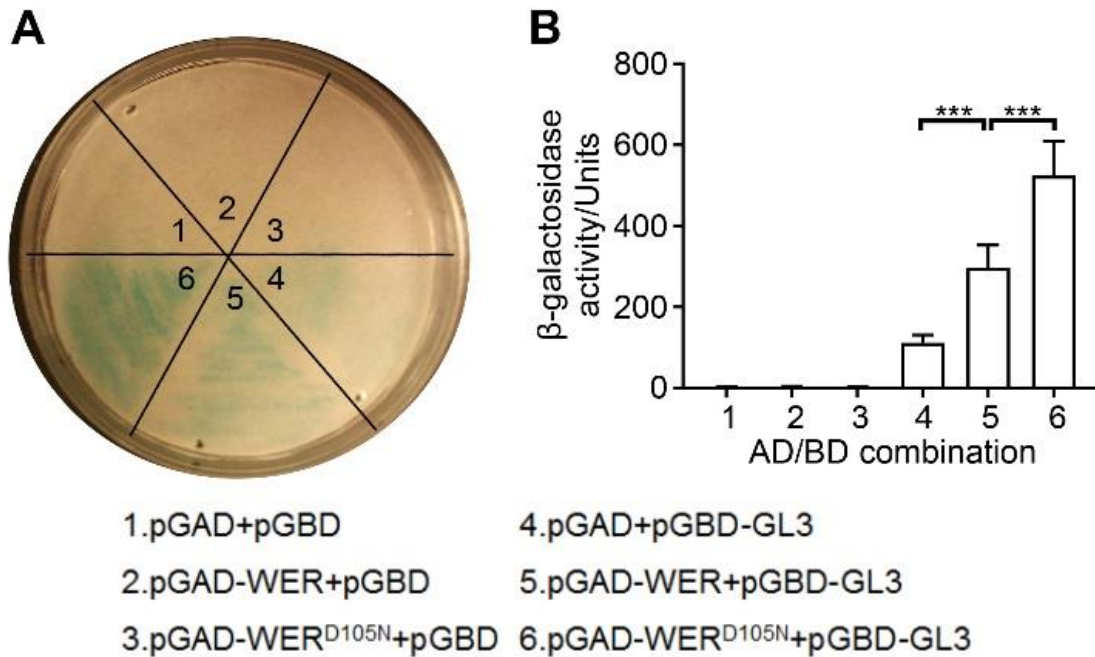
Figure 2.5 The WER^{D105N} protein is able to associate with GL3.
(A) Yeast two-hybrid filter assays showing the β-galactocidase activities in yeast cultures expressing GL3 together with WER or WER^{D105N}. (B) Yeast two-hybrid liquid assays confirming the interaction between GL3 and WER or WER^{D105N}. Error bars represent standard deviations from three replicates. Statistical significance is determined by one-way ANOVA. *** represents $p<0.001$.

87

A

GWBSI   GAAAA**T**GCG**GTT**GGAGAATT
GWBSII   TGTTAAAA**GTT**A**GTT**GAGTC

WBSI   TTTAAAATA**A**GTA**GTT**ATGG
WBSII   TATTTCTC**CAAC**TGTCTGTA

B
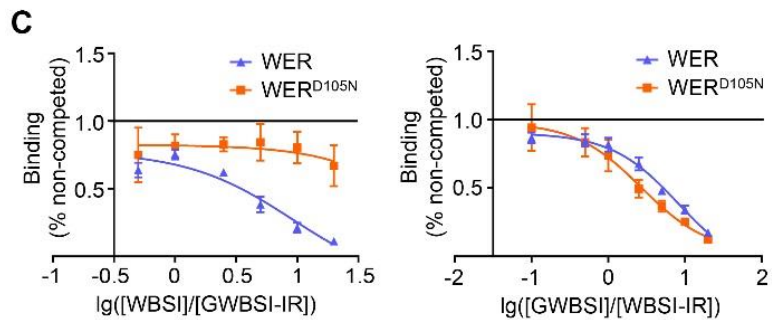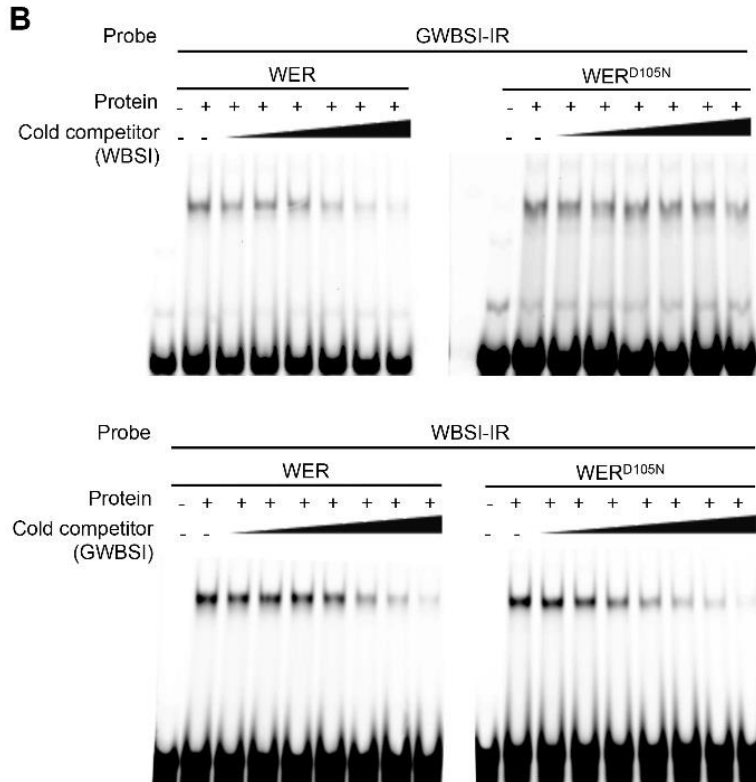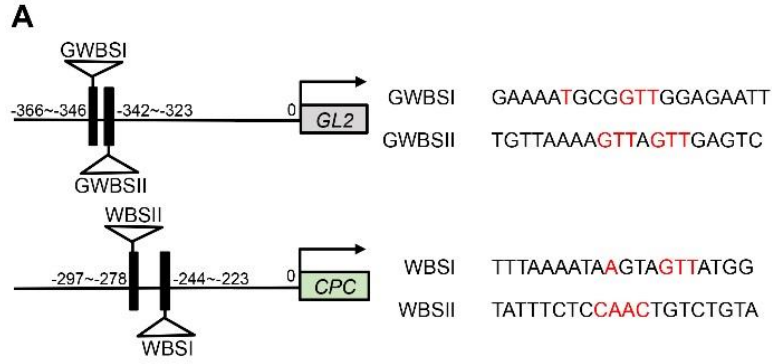
	GWBSI-IR + WBSI	WBSI-IR + GWBSI
WER	9.182	8.139
WER^D105N	>40000	2.712

Figure 2.6 The WER^{D105N} protein exhibits altered affinities for WER binding sites in the *GL2* and *CPC* promoters.

(A) Schematic diagrams of previously identified WER binding sites in the *GL2* and *CPC* promoters. Numbers indicate relative distance of each binding site from the transcription start site (TSS). On the right are the sequences of WER binding sites. The nucleotides reported to be essential for WER recognition are colored in red. (B) Competition EMSA assays between GWBSI and WBSI. The upper panel shows the result using GWBSI as the hot probe (labeled with infrared dye) and WBSI as the cold competitor. The concentrations of the unlabeled competitor are 0.5x, 1x, 2.5x, 5x, 10x, and 20x compared to the labeled probe in Lane 3-8 of the WER and WER^{D105N} experiments. The lower panel shows the result using WBSI as the hot probe and GWBSI as the unlabeled competitor. The concentrations of the unlabeled competitor are 0.1x, 0.5x, 1x, 2.5x, 5x, 10x, and 20x compared to the labeled probe in Lane 3-9 of the WER and WER^{D105N} experiments. (C) Semilog plots of the competition EMSA results shown in (B). Error bars indicate standard deviations from 3 replicates. The one-site competitive binding curve model was used for nonlinear regression of each competition experiment. The calculated IC50 values (cold competitor/hot probe molar ratio) are listed in the table at the bottom.
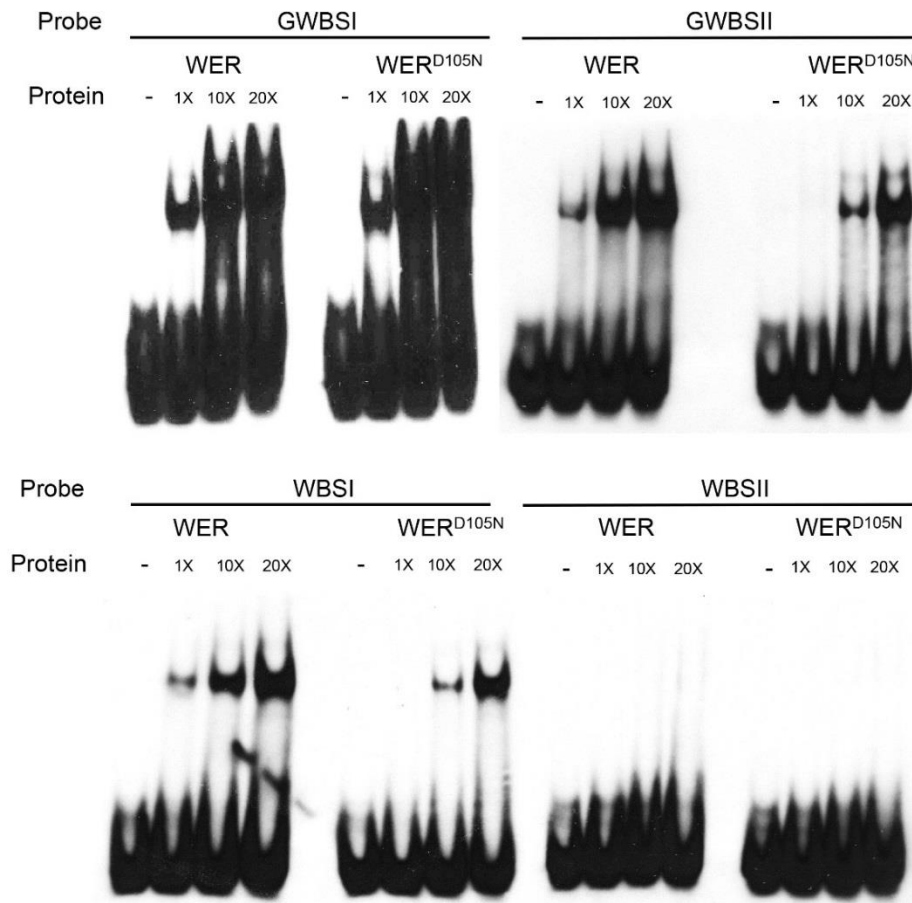
Figure 2.7 The WER and WER[D105N] proteins are able to bind to *GL2* and *CPC* promoter regions.
The EMSA assays were performed using purified WER and WER[D105N] proteins and GWBSI, GWBSII, WBSI, WBSII hot probes, 20bp long each. The sequences of all probes are listed in Table 2.1.
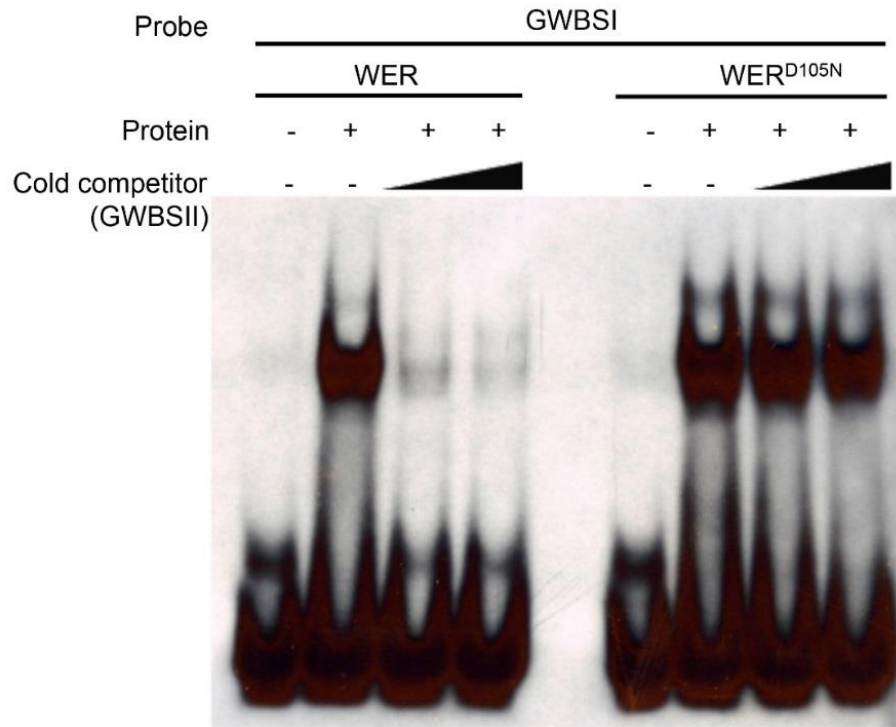
Figure 2.8 The WER^D105N protein exhibits unbalanced affinities between binding sites in *GL2* promoter regions compared to WER.

Competition EMSA assays using GWBSI as the hot probe and GWBSII as the cold competitor. The amounts of cold competitors are 5× and 10× compared to the hot probe in lane 3 and 4 of both WER and WER^D105N experiments.
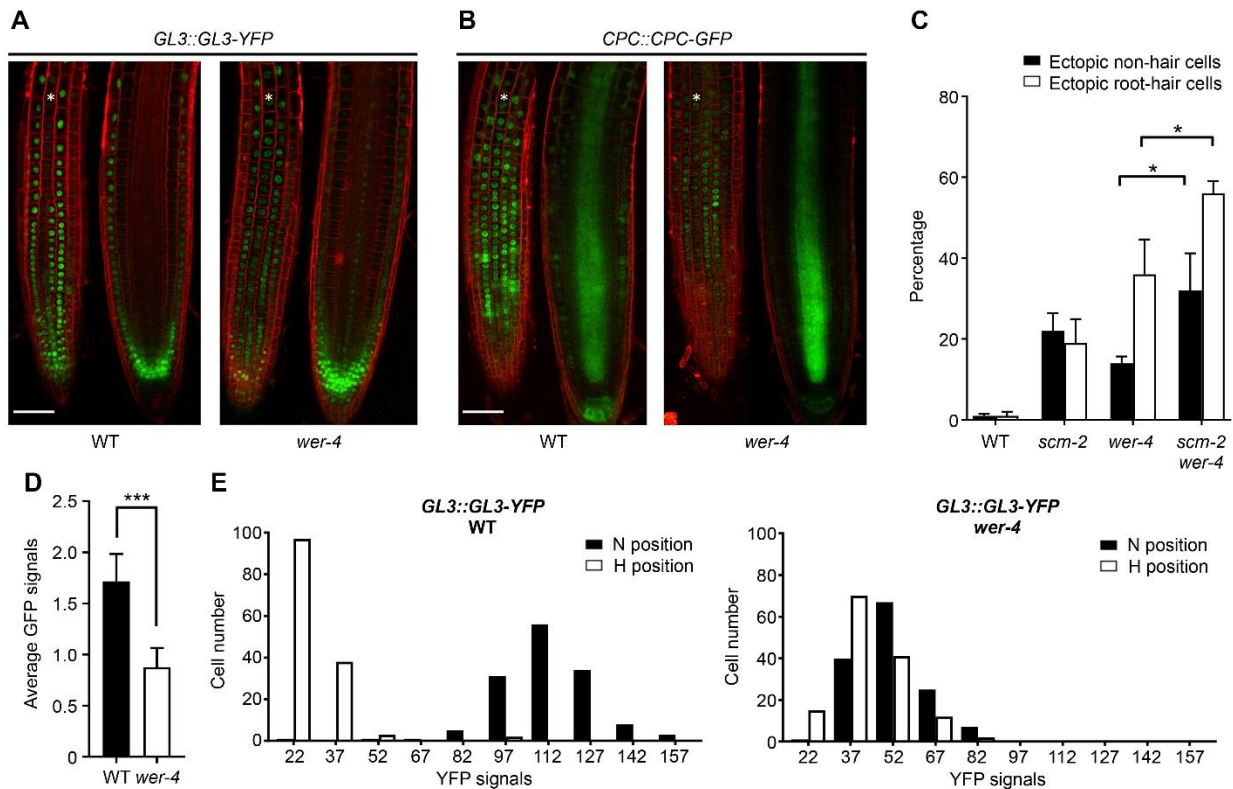
Figure 2.9 The *wer-4* mutant disrupts root epidermal cell fate establishment.
(A) Accumulation of the GL3-YFP fusion protein in wild-type and *wer-4* seedling roots
bearing the GL3::GL3-YFP transgene. White stars mark the H-position cell files. The red
color represents propidium iodide and the green color represents YFP. Bar=50μm. For
each genotype, the left and right panels show the same root focused on the epidermal
and stele layers. (B) Accumulation of the CPC-GFP fusion protein in wild-type and *wer-
4* seedling roots bearing the CPC::CPC-GFP transgene. White stars mark the H-
position cell files. The red color represents propidium iodide and the green color
represents GFP. Bar=50μm. For each genotype, the left and right panels show the
same root focused on the epidermal and stele layers. (C) Quantifications of root
epidermis specification in seedling roots of wild type, *scm-2*, *wer-4*, and *scm-2 wer-4*.
The error bars represent the standard deviations from three replicates. Statistical
significance is determined by two-way ANOVA. * represents $p < 0.05$. (D) Quantifications
of the CPC-GFP signals in root epidermis of wild-type and *wer-4* roots. For each root,
the GFP signals within all measurable epidermal cells are measured and results are
plotted using the average GFP signals per cell. A total of 20 roots are measured for
each genotype. Statistical significance is determined with the t-test. (E) Histograms of
GL3::GL3-YFP signal levels in N-position and H-position cells of wild-type and *wer-4*
seedling root tips (n=150). Ten cells in each position were analyzed per root and 15
roots were used for each genotype.

92
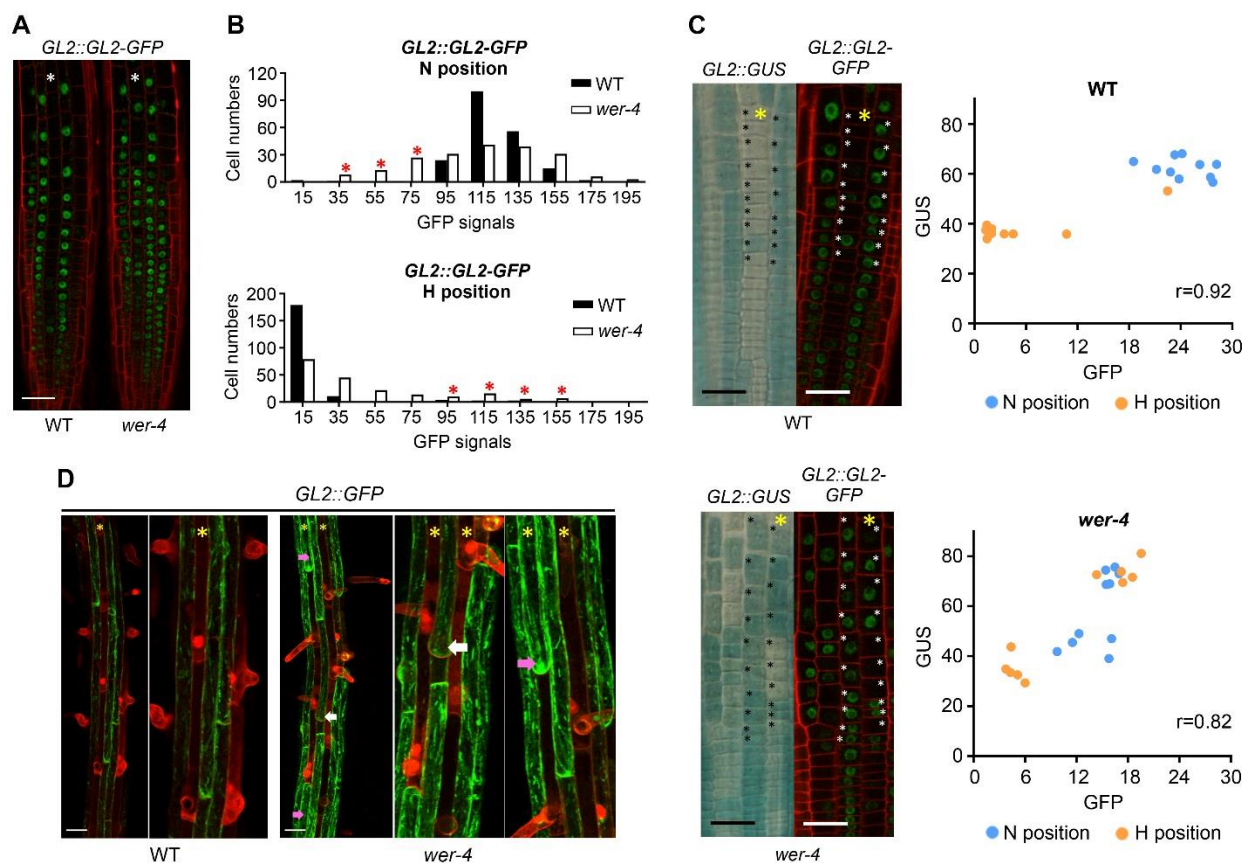
Figure 2.10 Ectopic cell fates in the *wer-4* mutant are associated with abnormal GL2 protein accumulation.

(A) Accumulation of GL2-GFP fusion protein in the root epidermis of wild type and *wer-4* seedlings carrying the *GL2::GL2-GFP* reporter. Red color indicates propidium iodide and green color indicates GFP. Stars indicate H-position cell files. Bar=50µm. (B) Histograms of quantified *GL2::GL2-GFP* signals in wild-type and *wer-4* roots (n=200). Ten cells from H and N positions in each root are measured and 20 roots are used for each genotype. Red stars in the N-position panel indicate groups of *wer-4* N-position cells with GFP signals lower than wild-type N-position cells. Red stars in H-position panel indicate groups of *wer-4* H-position cells with GFP signals comparable or higher than wild-type N-position cells. (C) Expression of *GL2::GUS* and *GL2::GL2-GFP* reporters in one single root of wild type and *wer-4*. The yellow stars indicate H-position cell files. Bar=25µm. The scatter plots on the right show the GFP and GUS signal levels of cells marked with black/white stars in wild type and *wer-4* images. r represents the Pearson correlation coefficient determined with all data points from both H and N positions from each plot. (D) Expression of *GL2::GFP* in the differentiation zone (where root hairs are visible) of wild-type and *wer-4* seedling roots. Stars indicate H-position cell files. For both wild type and *wer-4* images, particular regions are zoomed in on the right. White arrows point to ectopic root-hair cells in N-cell positions and pink arrows point to ectopic non-hair cells in H-cell positions in *wer-4*. Bar=50µm.

93
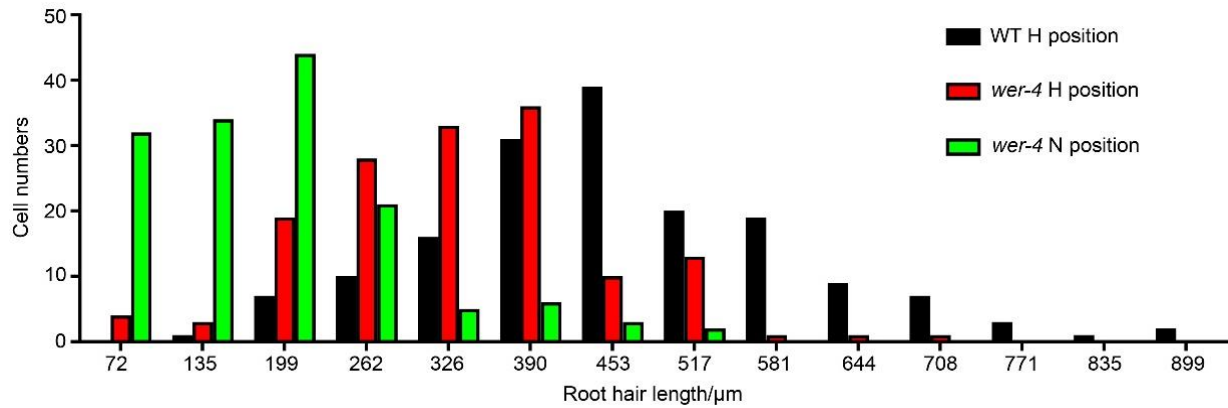
Figure 2.11 Histograms of root hair length from wild-type and *wer-4* root epidermal cells (n=150).
For wild-type roots, only root hairs from H-position cells were measured. For *wer-4* roots, root hairs from cells in the H and N positions were measured separately. For each genotype and position, 15 roots were analyzed. For each root, 10 root hairs from fully mature cells were measured.
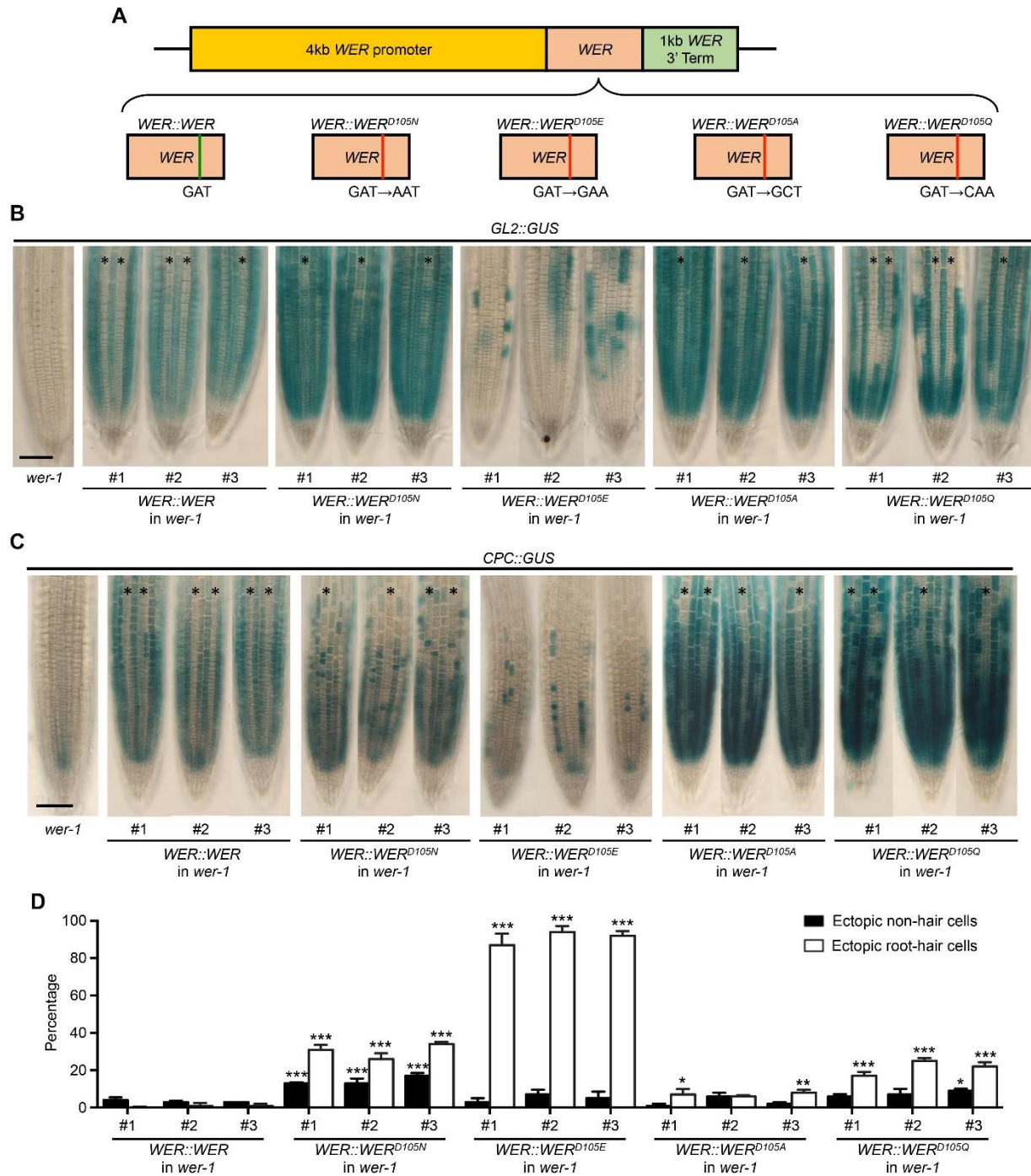
Figure 2.12 Substitutions of WER D105 residue alter root epidermal cell-type pattern. (A) Schematic drawings illustrate *WER::WER* transgenes with different residue substitutions at position 105. (B) Expression of the *GL2::GUS* transcriptional reporter in the *wer-1* mutant and *wer-1* mutants bearing different *WER::WER* transgenes. For each transgene, representative roots from 3 independent single-insertion lines are shown. Stars indicate H-position cell files. Bar=50μm. (C) Expression of the *CPC::GUS* reporter in the *wer-1* mutant and *wer-1* mutants bearing different *WER::WER* transgenes. For each transgene, representative roots from 3 independent single-insertion lines are

shown. Stars indicate H-position cell files. Bar=50μm. (D) Quantifications of root epidermis specification in the *wer-1* mutants bearing different *WER::WER* transgenes. Error bars represent standard deviations from three replicates. Two-way ANOVA is used to determine the differences among different transgenic lines using the #1 line of the *WER::WER* transgene as the control. All transgenic lines showing significant differences in H and/or N positions from the control are marked. *** represents $p < 0.001$, ** represents $p < 0.01$, * represents $p < 0.05$.
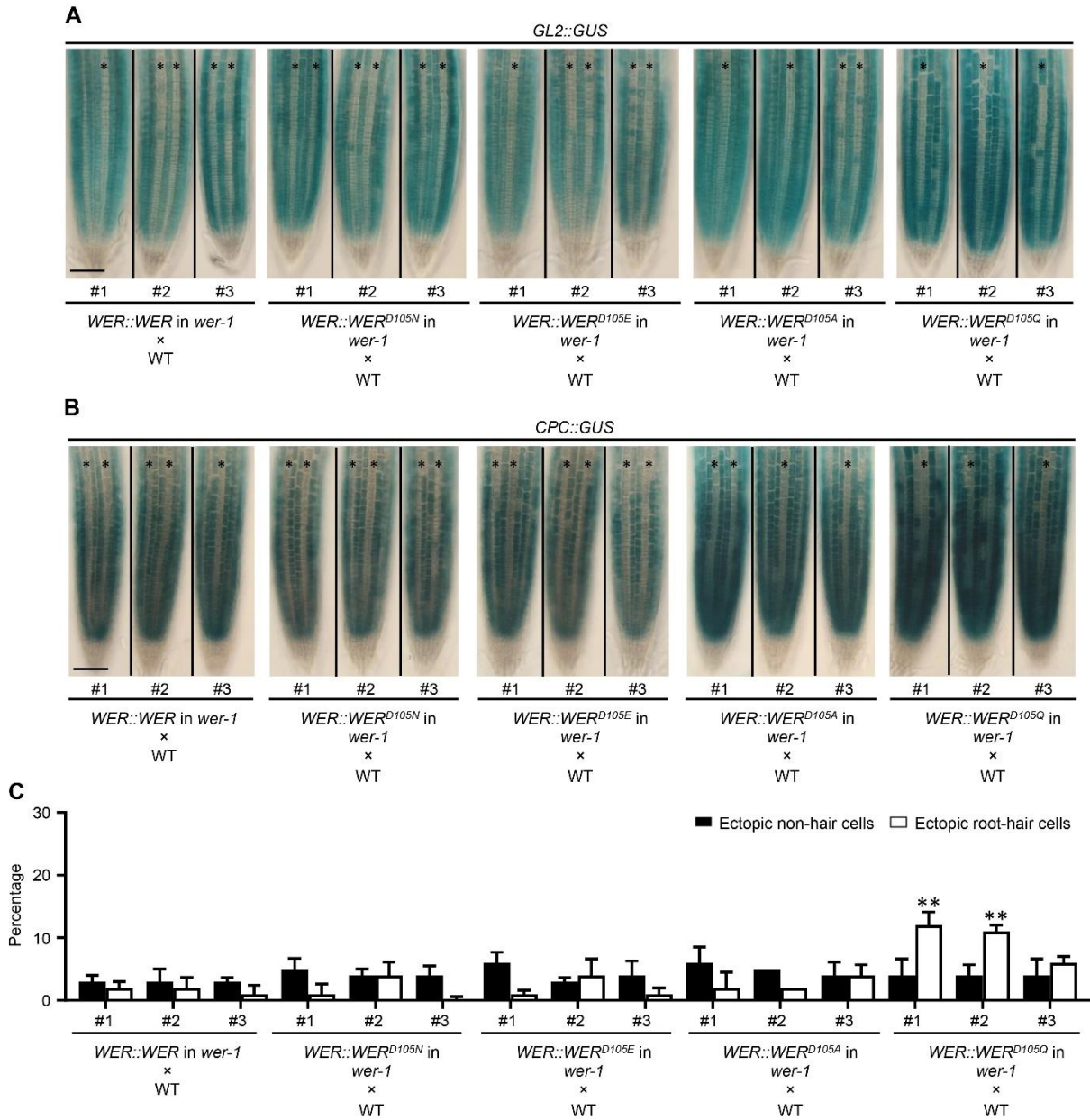
Figure 2.13 Functional comparison between WER and WER variants.
(A) Expression of the *GL2::GUS* transcriptional reporter in the F1 seedling roots from crosses between wild-type plants and *wer-1* mutants bearing different *WER::WER* transgenes. For each transgene, representative F1 roots from crosses using 3 independent single-insertion lines are shown. Stars indicate H-position cell files. Bar=50µm. (B) Expression of the *CPC::GUS* transcriptional reporter in the F1 seedling roots from crosses between wild-type plants and *wer-1* mutants bearing different WER::WER transgenes. For each transgene, representative F1 roots from crosses using 3 independent single-insertion lines are shown. Stars indicate H-position cell files. Bar=50µm. (C) Quantifications of root epidermis specification in the F1 seedling roots from crosses between wild-type plants and *wer-1* mutants bearing different *WER::WER* transgenes. Error bars represent standard deviations from three replicates. Two-way

ANOVA is used to determine the differences among different transgenic lines using the #1 F1 population of the WER::WER transgene as the control. All F1 populations showing significant differences in H and/or N positions from the control are marked. ** represents p<0.01.
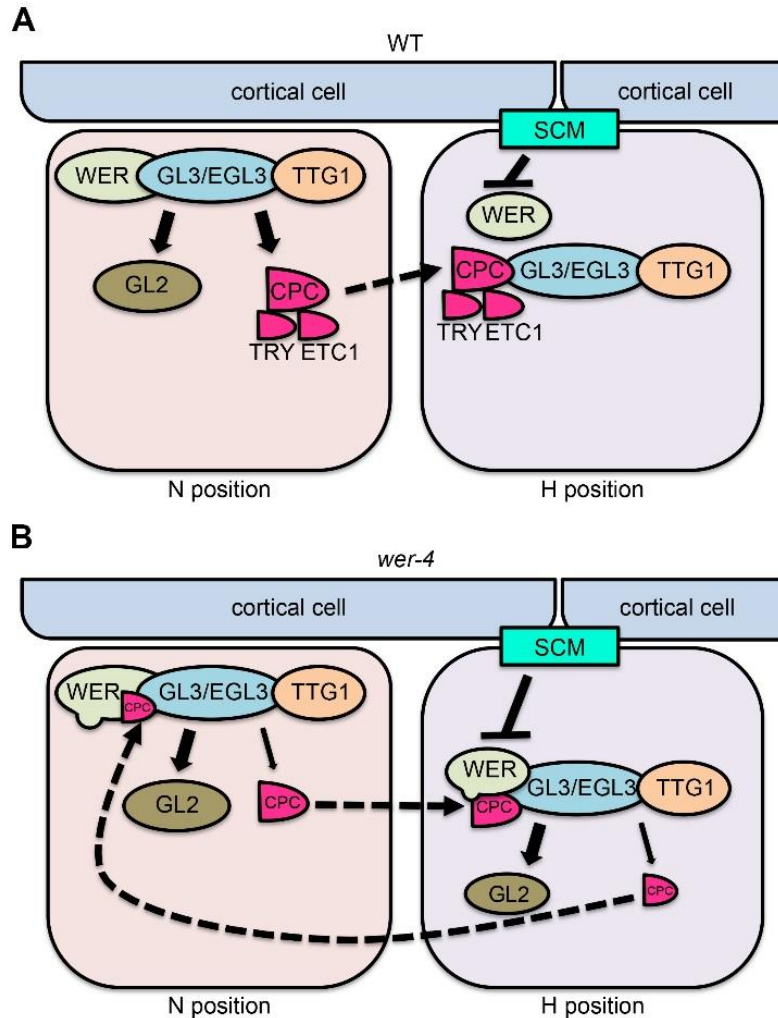
Figure 2.14 Models for epidermal cell fate regulation in wild-type and *wer-4* roots. The solid arrows (sharp or blunt) indicate transcriptional regulation. The dashed arrows indicate protein movement. (A) In the wild-type root epidermis, the WER-GL3/EGL3-TTG1 complex preferentially accumulates in N-position cells and promotes expression of *GL2*, *CPC*, *TRY* and *ETC1*. The GL2 protein remains in N-position cells and inhibits root hair formation. The CPC, TRY and ETC1 proteins move to adjacent H-position cells and compete with WER for GL3/EGL3 binding, allowing root hair formation. (B) In the *wer-4* mutant, the D105N residue substitution disrupts WER target gene transcription, largely abolishing *TRY* and *ETC1* expression and reducing the expression of *CPC* relative to *GL2*. As a consequence, there is reduced competition for GL3/EGL3 binding and enhanced formation of the WER-GL3/EGL3-TTG1 complex in H-position cells. This triggers abnormal expression of *GL2* and *CPC* in the H-position cells, leading to inappropriate CPC movement and accumulation in N-position cells, as well as reduction of the WER-GL3/EGL3-TTG1 complex. Therefore, in the *wer-4* mutant epidermis, the WER-GL3/EGL3-TTG1 complex accumulates abnormally in both H and N positions, leading to misspecification of cells in both positions.

Table 2.1 Primers used in genotyping, cloning, qPCR and electrophoretic mobility shift assays (EMSA).

Experiment	Name	Forward primer	Reverse primer
Genotyping	*wer-4*_dCAPS_HinfI	GGCTCCACAAGTTGCTTGGTAA	GTGTTCCAATAGTTCTTCACTTGATGAT
Cloning	pWER::WER_frag	CCGCGGTGGCGGCCGCTCTAGAAGGAGCTCTCTGATCTAAGCAC	TCGGGAATTCCTGCAGCCCGGGGGATATCGTTTTGCTGAAGTTGCTTTG
	pWER::WER^{D105N}_frag	CCGGGTCGAACGAATAATCAAGTGAAG	CTTCACTTGATTATTCGTTCGACCCGG
	pWER::WER^{D105A}_frag	CCGGGTCGAACGGCTAATCAAGTGAAG	CTTCACTTGATTAGCCGTTCGACCCGG
	pWER::WER^{D105E}_frag	CCGGGTCGAACGGAAAATCAAGTGAAG	CTTCACTTGATTTTCCGTTCGACCCGG
	pWER::WER^{D105Q}_frag_1	CCGGGTCGAACGCAAAATCAAGTGAAG	CTTCACTTGATTTTGCGTTCGACCCGG
	pWER::WER-YFP_frag_1	CCGCGGTGGCGGCCGCTCTAGAAGGAGCTCTCTGATCTAAGCAC	AGCTCCACCTCCACCTCCAAAACAGTGTCCATCTATAAAGTCCATC
	pWER::WER-YFP_frag_2	GGAGGTGGAGGTGGAGCTATGGTGAGCAAGGGCG	AGCAGAAAACACATCAGTTATCTACTTGTACAGCTCGTCCATG
	pWER::WER-YFP_frag_3	CAAGTAGATAACTGATGTGTTTTCTGCTTTTGTTATTTTAGTATTCGTTTATG	TCGGGAATTCCTGCAGCCCGGGGGATATCGTTTTGCTGAAGTTGCTTTG
RT-qPCR	GL2_q	GAGGAAGAAGTATCATCGTCAC	CTCTTTGAATAGCGCTTCCATG
	CPC_q	ATAAACGACGACGGAGACAG	GATACTACTCACCTCTTCGGAA
	ETC1_q	CAGCGTAAGTCGAAGCATCTTA	TCTTCCTGAGCCATTGCTATTT
	TRY_q	GTCGCCGTCGTAAGCAAC	CTGCTCACTTCTTCAGAGTC
	GAPDH_q	TTGGTGACAACAGGTCAAGCA	AAACTTGTCGCTCAATGCAATC
EMSA	GWBSI	GAAAATGCGGTTGGAGAATT	AATTCTCCAACCGCATTTTC
	GWBSII	TGTTAAAAGTTAGTTGAGTC	GACTCAACTAACTTTTAACA
	WBSI	TTTAAAATAAGTAGTTATGG	CCATAACTACTTATTTTAAA
	WBSII	TATTTCTCCAACTGTCTGTA	TACAGACAGTTGGAGAAATA

100

Chapter 3

Molecular Basis for a Cell Fate Switch in Response to Impaired Ribosome Biogenesis in the Arabidopsis Root Epidermis

The contents of this chapter were submitted for consideration to be published as a research article. Christa Barron performed the positional cloning. Dr. Angela Bruex generated the *APUM23::APUM23-GFP* transgenic line. I conducted all the other experiments.

Abstract

The Arabidopsis root epidermis consists of a position-dependent pattern of root-hair cells and non-hair cells. Underlying this cell-type patterning is a network of transcription factors including a central MYB-bHLH-WD40 complex containing WEREWOLF (WER), GLABRA 3/ENHANCER OF GLABRA 3 (GL3/EGL3), and TRANSPARENT TESTA GLABRA 1 (TTG1). In this study, we used a genetic enhancer screen to identify *apum23-4*, a mutant allele of the ribosome biogenesis factor (RBF) gene *PUMILIO 23* (*APUM23*), which caused prospective root-hair cells to develop into non-hair cells. We discovered that this cell fate switch relied on MYB23, a MYB protein encoded by a WER target gene and acting redundantly with WER. In the *apum23-4* mutant, *MYB23* exhibited ectopic expression that was WER-independent and instead required ANAC082, a recently identified ribosomal stress response mediator.

Furthermore, we examined additional RBF mutants that produced ectopic non-hair cells and determined that this cell fate switch is generally linked to defects in ribosome biogenesis. Taken together, our study provides a molecular explanation for root epidermal cell fate switch in response to ribosomal defects and, more generally, it demonstrates a novel regulatory connection between ribosome biogenesis and cell fate control in plants.

Introduction

The development of multicellular organisms relies on the appropriate specification of distinct cell types. In the Arabidopsis root epidermis, the root-hair and non-hair cell types are specified in a position-dependent manner (Duckett et al. 1994; Clowes 2000): epidermal cells adjacent to two underlying cortical cells (in the "H" position) adopt the root-hair cell fate, while those adjacent to only one underlying cortical cell (in the "N" position) adopt the non-hair cell fate. This simple patterning system has been used as a model to uncover the molecular basis for cell fate specification in plants (Masucci et al. 1996a; Lee et al. 1999).

Previous genetic and molecular studies have revealed a network of transcription factors underlying this cell patterning process. In N-position cells, WEREWOLF (WER), GLABRA 3/ENHANCER OF GLABRA 3 (GL3/EGL3), and TRANSPARENT TESTA GLABRA 1 (TTG1) form a MYB-bHLH-WD40 complex (Galway et al. 1994; Lee et al. 1999; Bernhardt et al. 2003; Bernhardt et al. 2005). This complex directly promotes transcription of *GLABRA 2* (*GL2*), encoding an HD-ZIP transcription factor, and *CAPRICE* (*CPC*), encoding an R3-type MYB protein (Ryu et al. 2005; Song et al. 2011). The GL2 protein accumulates in the N-position cells and directly suppresses expression

of downstream root-hair-promoting genes (Masucci et al. 1996a; Bruex et al. 2012; Lin et al. 2015). The CPC protein is able to translocate to the adjacent H-position cells and bind to GL3/EGL3 in competition with WER (Wada et al. 2002; Kurata et al. 2005; Song et al. 2011). In addition, a receptor-like kinase, SCRAMBLED (SCM), preferentially accumulates in H-position cells and further reduces WER-GL3/EGL3-TTG1 complex formation through suppressing *WER* expression (Kwak et al. 2005; Kwak et al. 2008). As a consequence, *GL2* expression is relatively weak in H-position cells, allowing for transcription of root-hair-promoting genes and resulting in root-hair cell differentiation (Cvrckova et al. 2010; Bruex et al. 2012; Huang et al. 2017).

The preferential accumulation of the WER-GL3/EGL3-TTG1 complex in N-position cells is reinforced by multiple feedback mechanisms (Schiefelbein et al. 2014). One of these feedback mechanisms involves MYB23, a close relative of WER (Stracke et al. 2001; Kang et al. 2009). The WER-GL3/EGL3-TTG1 complex directly promotes *MYB23* transcription in N-position cells, and the MYB23 protein is functionally redundant with WER (Kang et al. 2009). Thus, MYB23 acts in a positive feedback loop to ensure sufficient levels of the WER/MYB23 proteins for the MYB-bHLH-WD40 complex in N-position cells.

The proper differentiation of the root-hair and non-hair cells, like essentially all developmental processes, relies on the production and function of ribosomes. Ribosome biogenesis, including precursor ribosomal RNA (pre-rRNA) processing and ribosomal protein (RP) assembly, involves the organized cooperation of numerous ribosome biogenesis factors (RBFs) (Thomson et al. 2013; Weis et al. 2015a; Saez-Vasquez et al. 2019). In Arabidopsis, mutants of RBF genes have significant

103

developmental impacts, including embryo lethality, aborted gametophyte development, and tissue regeneration defects (Harscoet et al. 2010; Ohbayashi et al. 2011; Missbach et al. 2013), as well as milder phenotypes like retarded plant growth, merged or triple cotyledons, and narrow and pointed rosette leaves (Lange et al. 2011; Weis et al. 2014; Weis et al. 2015b). Interestingly, several characteristic phenotypes, such as the misshaped rosette leaves, are shared by mutants of functionally unrelated RBFs (Weis et al. 2015a), suggesting a common regulatory mechanism that responds to a variety of ribosome biogenesis defects and modulates plant development.

Recently, the *anac082-1* mutant, a missense mutation of the NAC family gene *ANAC082*, was reported to 'rescue' the regeneration defects and the pointed-leaf phenotypes of several RBF mutants (Ohbayashi et al. 2017a). Interestingly, the 'rescued' double mutants still exhibit impaired pre-rRNA processing similar to the corresponding RBF single mutants (Ohbayashi et al. 2017a), which implies that these developmental phenotypes are not directly caused by defective ribosome biogenesis. Therefore, ANAC082 is considered to be a key component of a regulatory pathway in plants that connects ribosomal status with specific developmental events (Ohbayashi et al. 2017a; Ohbayashi et al. 2017b; Salome 2017; Saez-Vasquez et al. 2019).

A linkage between root epidermal cell specification and ribosome biogenesis was first discovered through analysis of the RBF gene *ADENOSINE DIMETHYL TRANSFERASE 1A* (*DIM1A*) (Wieckowski et al. 2012). The DIM1A protein participates in N-6 dimethylation of the A1785 and A1786 bases in 18S rRNA (Wieckowski et al. 2012). The *dim1a* mutant exhibits approximately 20% reduction of root-hair cells due to an early cell fate switch that leads to ectopic non-hair cell formation (Wieckowski et al.

2012). However, the molecular mechanism underlying this cell fate switch was not determined.

In this study, we identified a nonsense allele of the RBF gene *ARABIDOPSIS PUMILIO 23* (*APUM23*), designated as *apum23-4*. We discovered a significant reduction in root hair formation in *apum23-4* resulted from a cell fate switch mediated by the abnormal upregulation of *MYB23*. Interestingly, we found that the increased *MYB23* expression in the *apum23-4* root epidermis was independent of the WER-GL3/EGL3-TTG1 complex, but instead required ANAC082. We also found that other RBF mutants, including *dim1a*, exhibited MYB23- and/or ANAC082-dependent root epidermal cell fate switch. Altogether, this study provides evidence for a novel regulatory pathway responsible for altering root epidermal cell fate in response to ribosomal defects.

Results

Identification of the *apum23-4* mutant

The *cpc-1* mutant produces approximately 30% of the normal number of root-hair cells, due to 70% of H-position cells adopting the non-hair cell fate (Figure 3.1, A and B). We took advantage of this intermediate phenotype and performed a *cpc-1* enhancer screen to identify genes involved in root epidermis specification. One of the resulting lines, later designated as *cpc-1 apum23-4*, exhibited an enhanced phenotype relative to *cpc-1*, producing almost hairless roots (Figure 3.1, A and B). We isolated plants homozygous for the *apum23-4* single mutant, and observed several growth abnormalities including delayed seed germination and shorter root hairs (Figure 3.1A, Figure 3.2). Furthermore, quantification of root epidermal cell specification in *apum23-4*

105

showed that 17% of the H-position cells lacked root hairs (i.e., 17% ectopic non-hair cells), a proportion significantly greater than that in the wild type (Figure 3.1B).

To identify the mutated gene in the *apum23-4* line, we performed map-based cloning and discovered a C to T single-nucleotide substitution within the first exon of the *AT1G72320* gene, which changes the 80th codon from CAG (glutamine) to TAG (stop codon) (Figure 3.3A). The *AT1G72320* gene is named *ARABIDOPSIS PUMILIO 23* (*APUM23*) and encodes an RNA-binding protein from the Pumilio family (Murata et al. 1995). Pumilio proteins are found in all eukaryotes and defined by the presence of tandem arranged, RNA-recognizing PUF repeats (Zamore et al. 1997; Edwards et al. 2001), which number from 2 to 11 in members of the Arabidopsis Pumilio family (Francischini et al. 2009; Tam et al. 2010). Distinct from the canonical Pumilio proteins that mediate translational regulation largely through binding to the 3'UTR of mRNAs (Wickens et al. 2002; Szostak et al. 2013; Wang et al. 2018), APUM23, like its well-studied yeast orthologue NOP9 (Thomson et al. 2007; Zhang et al. 2016), binds to rRNAs and contributes to pre-rRNA processing (Abbasi et al. 2010; C. Zhang et al. 2015).

Given that three mutant alleles of *APUM23* have been reported (Abbasi et al. 2010; Huang et al. 2014), the allele identified in our study was designated as *apum23-4.* Other *APUM23* mutants were reported to exhibit delayed germination and slower growth (Abbasi et al. 2010; Huang et al. 2014), but no root epidermis analyses were performed. To determine whether the abnormal root epidermal cell specification in *apum23-4* was due to the *APUM23* mutation, we examined *apum23-2* mutant roots and discovered a comparable proportion of ectopic non-hair cells as in *apum23-4* (Figure

3.3, A to C). We also generated an *APUM23::APUM23-GFP* transgene containing the

APUM23 genomic sequence (including the native promoter) with an in-frame C-terminal

GFP tag and introduced this into *apum23-4* plants. The resulting transformed plants

exhibited fully restored wild-type root-hair length and root epidermal cell pattern (Figure

3.3, B and C). These results confirm that the abnormal root epidermal phenotypes in

apum23-4 are due to the mutation in the *APUM23* gene.

We also performed an *APUM23* overexpression analysis by transforming

apum23-4 plants with a *35S::APUM23-YFP* transgene. We observed wild-type root hair

length and root epidermal cell pattern in these transformed plants (Figure 3.3, B and C),

suggesting that a particular level or cellular distribution of the APUM23 protein are not

critical for its role in root epidermal cell specification.

APUM23 localizes in the nucleoli of multiple root tissues

To study the accumulation pattern of APUM23, we analyzed the

APUM23::APUM23-GFP transgenic plants and discovered APUM23-GFP accumulation

in multiple tissues of the developing root (Figure 3.4A). In the root epidermis, the

APUM23-GFP protein accumulated in both H- and N-position cells (Figure 3.4C).

To study the subcellular localization of APUM23, we first generated control

transgenic plants bearing the mcherry-tagged FIBRILLARIN 1 (FIB1) driven by its native

promoter (*FIB1::FIB1-mcherry*). FIB1 is a known nucleolar protein participating in pre-

rRNA and small nucleolar RNA (snoRNA) processing (Pih et al. 2000; Pontvianne et al.

2010; Kalinina et al. 2018). Using DAPI staining to distinguish the nucleolus from the

nucleoplasm, we verified the nucleolar localization of FIB1-mcherry in root epidermal

cells (Figure 3.4B). We then generated plants bearing both the *APUM23::APUM23-GFP*

and *FIB1::FIB1-mcherry* transgenes, and we observed colocalization of the APUM23-GFP and FIB1-mcherry signals within individual root epidermal cells, indicating the nucleolar localization of APUM23 (Figure 3.4C).

Detailed examination of the APUM23-GFP and FIB1-mcherry accumulation revealed notable features of nucleoli in the developing root epidermis. First, the relative nucleolar size in N-position cells appeared to decrease as cells aged. N-position nucleoli were of similar size to H-position nucleoli in early meristematic cells but their relative size decreased in older elongating cells (Figure 3.4C, right panels). Second, the ratio between the APUM23-GFP and FIB1-mcherry proteins appeared to decrease in N-position cells compared to H-position cells as they aged. The GFP/mcherry signal ratios were comparable between H- and N-position cells in the meristematic region but diverged in the elongation region (Figure 3.4C, right panels). These observations suggest distinct nucleolar activities between root-hair cells and non-hair cells during root epidermis development.

MYB23 mediates ectopic non-hair cell specification in *apum23-4*

To uncover the mechanisms underlying ectopic non-hair cell formation in the *apum23-4* mutant, we first made use of the *GL2::GUS* transcriptional reporter, a marker for early non-hair cell fate establishment (Masucci et al. 1996a). In wild-type roots, *GL2::GUS* exhibited strong preferential expression in N-position cells, while in *apum23-4* roots, ectopic *GL2* expression was observed in some H-position cells (Figure 3.5A). Specifically, approximately 15% of H-position cells expressed *GL2::GUS* signals in *apum23-4* (Figure 3.5E), a proportion comparable to that of the ectopic non-hair cells in *apum23-4* (Figure 3.1B). Additionally, the ectopic non-hair cell formation in *apum23-4* is

GL2-dependent, given that the *gl2-1 apum23-4* double mutant lacked all non-hair cells in both H and N positions (Figure 3.5B). Therefore, the ectopic non-hair cells in *apum23-4* result from an early *GL2*-dependent switch during epidermal cell fate specification in the H position.

GL2 expression in the root epidermis is controlled by a MYB-bHLH-WD40 complex consisting of WER, GL3/EGL3, and TTG1, and the absence of any of these three components leads to loss of both *GL2* expression and non-hair cells (Galway et al. 1994; Lee et al. 2002; Bernhardt et al. 2003) (Figures 3.5, A and B). To analyze the role of these components for the ectopic *GL2* expression in *apum23-4,* we separately introduced *wer-1*, *gl3 egl3,* and *ttg1* mutations into the *apum23-4 GL2::GUS* line. The *gl3 egl3 apum23-4* and *ttg1 apum23-4* mutants lacked significant *GL2::GUS* expression in the developing root epidermis (Figure 3.5A) and produced nearly 100% root-hair cells in both H and N positions (Figure 3.5B). However, the *wer-1 apum23-4* double mutant exhibited considerable *GL2::GUS* expression that greatly exceeded the *wer-1* single mutant (Figure 3.5A). Interestingly, the *GL2::GUS* signals in *wer-1 apum23-4* lacked N-position specificity (approximately 20% of H-position cells and 31% of N-position cells expressed *GL2::GUS*; Figure 3.6) and initiated accumulation in older cells (relative to WT; Figure 3.5A). Consistent with its *GL2::GUS* expression pattern, the *wer-1 apum23-4* mutant produced approximately 20% and 35% non-hair cells in the H and N positions, respectively (Figure 3.5B).

The above results suggest that GL3/EGL3 and TTG1 are required, while WER is not required, for the ectopic non-hair cell formation in *apum23-4*. Therefore, we hypothesized that (an)other MYB protein(s) function in place of WER in the *apum23-4*

background to form a MYB-bHLH-WD40 complex and induce *GL2* expression to generate non-hair cells. MYB23 was a candidate for this role given its known root epidermis expression and close functional relationship to WER, although the *myb23-1* single mutant had no significant defects in root epidermal cell patterning (Kang et al. 2009). We introduced the *myb23-1* mutation into the *wer-1 apum23-4* background and discovered that the resulting triple mutant lacked *GL2::GUS* expression and essentially lacked non-hair cells (Figure 3.5, A and B). Furthermore, we generated the *apum23-4 myb23-1* double mutant and observed a significantly reduced proportion of ectopic non-hair cells and ectopic *GL2::GUS*-expressing cells, relative to the *apum23-1* single mutant (both reduced to <5%; Figure 3.5, C to E). Therefore, MYB23 is required for the ectopic *GL2* expression and non-hair cell fate specification in the *apum23-4* mutant.

Abnormal MYB23 expression in *apum23-4*

In wild-type roots, *MYB23* is preferentially expressed in the N-position cells of the developing root epidermis (Kang et al. 2009). To examine its expression in *apum23-4*, we used the *MYB23::GUS* reporter (Kang et al. 2009) and observed considerable ectopic GUS expression in the H-position cells compared to wild type (Figure 3.7A). Specifically, 13% of the H-position cells in *apum23-4* showed detectable GUS signals (Figure 3.8), a proportion comparable to that of ectopic non-hair cells in *apum23-4* (Figure 3.1B).

In the wild-type root epidermis, *MYB23* transcription is directly induced by the WER-GL3/EGL3-TTG1 complex, and loss of *WER* gene function eliminates *MYB23* expression (Kang et al. 2009) (Figure 3.7A). However, we observed substantial *MYB23::GUS* expression in *wer-1 apum23-4* and these *GUS* signals lacked N-position

specificity (Figure 3.7A), which resembled the expression of *GL2::GUS* in *wer-1 apum23-4* (Figure 3.5A).

To test whether the observed ectopic *MYB23* expression leads to ectopic MYB23 protein accumulation, we made use of a *MYB23::MYB23-GFP* translational reporter (Kang et al. 2009). We discovered that MYB23-GFP protein accumulated ectopically in the nuclei of H-position cells of *apum23-4* as well as in both H- and N-position cells of *wer-1 apum23-4* (Figure 3.7B), which was consistent with the *MYB23::GUS* results (Figure 3.7A). Next, to determine whether these MYB23-GFP-accumulating cells are also expressing *GL2,* we examined the roots of *apum23-4* and *wer-1 apum23-4* plants bearing both the *MYB23::MYB23-GFP* and *GL2::GUS* reporters. In both the *apum23-4* and *wer-1 apum23-4* lines, we observed a correlation between MYB23-GFP accumulation and *GL2::GUS* expression within individual root epidermal cells (Figure 3.7C). Additionally, we generated *apum23-4* plants bearing both the *GL3::GL3-YFP* (Bernhardt et al. 2005) and *GL2::GUS* reporters, and we found a similar correlation between these two reporter signals in root epidermal cells (Figure 3.7D), supporting the notion that MYB23 induces *GL2* expression through its association with GL3.

In summary, we demonstrated a spatial correlation between MYB23 accumulation and *GL2* expression in *apum23-4*, suggesting that *MYB23* upregulation in *apum23-4* causes abnormal spatial expression of *GL2* and, ultimately, ectopic non-hair cells. More importantly, our finding that ectopic *MYB23* expression in *apum23-4* is WER independent suggests a novel mechanism for up-regulating *MYB23* in the *apum23-4* background.

ANAC082 is required for MYB23-mediated ectopic non-hair cell specification in *apum23-4*

Recently, the NAC family member ANAC082 was identified as a plant-specific mediator of ribosomal stress responses, given that the *anac082-1* mutant markedly reversed several developmental abnormalities in RBF mutants (Ohbayashi et al. 2017a). Therefore, we sought to test whether the ectopic non-hair cells in *apum23-4* are ANAC082 dependent.

First, we generated the *anac082-1 apum23-4* double mutant and observed substantial recovery of the seed germination and growth rate compared to *apum23-4* (Figure 3.2), indicating that these phenotypes are ANAC082 dependent. Further, *anac082-1 apum23-4* produced <3% ectopic non-hair cells, which is comparable to wild type (Figure 3.9B). This result was confirmed using a different *anac082* mutant (a T-DNA insertion mutation, *GABI_282H08*), which also reversed the *apum23-4* root hair pattern (Figure 3.10A). Consistent with these observations, <3% of the H-position cells in *anac082-1 apum23-4* expressed the *GL2::GUS* reporter (Figure 3.9A, Figure 3.10B). In addition, we found that the *anac082-1 wer-1 apum23-4* triple mutant restored the *wer-1* mutant phenotype, essentially lacking *GL2::GUS* expression in the root epidermis and producing >95% root-hair cells in both H and N epidermis positions (Figure 3.9, A and B). Notably, we observed no effect of the *anac082-1* or *GABI_282H08* mutant alone on root epidermis development; each single mutant exhibited a wild-type pattern of root epidermal cell types and *GL2::GUS* expression (Figure 3.9, A and B; Figure 3.10A). Therefore, ANAC082 has no significant role in root epidermal cell patterning under

normal ribosome biogenesis conditions, but mediates ectopic non-hair cell specification

in the *apum23-4* background.

Given that both ANAC082 and MYB23 are required for ectopic *GL2* expression

and ectopic non-hair cell production in *apum23-4*, we examined the possible regulatory

relationship between MYB23 and ANAC082. First, we examined *MYB23::GUS*

expression in *anac082-1 apum23-4* and discovered that the ectopic *MYB23* expression

in the H-position cells of *apum23-4* is ANAC082 dependent (Figure 3.9C, Figure 3.10C).

Similarly, the substantial *MYB23::GUS* expression in the *wer-1 apum23-4* mutant was

found to be *anac082-1* dependent (Figure 3.9C). Consistent with these results, the

ectopic *MYB23::MYB23-GFP* signals in *apum23-4* and *wer-1 apum23-4* were depleted

by the *anac082-1* mutation (Figure 3.9D). Notably, the *anac082-1* single mutant

exhibited no effect on *MYB23* expression (Figure 3.9C). Taken together, these results

suggest that ANAC082 induces *MYB23* expression to cause ectopic *GL2* expression

and switch epidermal cell fate in the *apum23-4* mutant.

Multiple RBF mutants exhibit ectopic non-hair cells

The *apum23-4* mutant phenotype analyzed in this study is reminiscent of *dim1a*,

a previously reported RBF mutant exhibiting ectopic *GL2::GUS* expression (Figure

3.11A, (Wieckowski et al. 2012)). Further, like *wer-1 apum23-4*, the *wer-1 dim1a* double

mutant exhibited significant *GL2::GUS* expression and non-hair cells in both H and N

cell positions (Wieckowski et al. 2012) (Figure 3.11, A and B; Figure 3.6). To test

whether MYB23 plays the same role in the *dim1a* phenotype as it does in *apum23-4*, we

generated the *wer-1 myb23-1 dim1a* and *myb23-1 dim1a* mutants. The *wer-1 myb23-1*

dim1a triple mutant exhibited no significant *GL2::GUS* signals and ≥95% root-hair cells

in both H and N positions (Figure 3.11, A and B), and the *myb23-1 dim1a* double mutant

exhibited a significantly decreased proportion of ectopic non-hair cells compared to

dim1a (Figure 3.11C). This shows that MYB23 is required for the ectopic non-hair cell

formation in *dim1a*.

We also incorporated the *MYB23::GUS* reporter into the *dim1a* mutant and

observed ectopic GUS signals in H-position cells at a frequency comparable to *apum23-

4* (Figure 3.12A, Figure 3.8). Further, the *wer-1 dim1a* double mutant exhibited

substantial *MYB23::GUS* signals (Figure 3.12A), indicating WER-independent *MYB23*

up-regulation similar to the *apum23-4* mutant.

Next, we tested the effect of ANAC082 on the *dim1a* phenotype. We introduced

the *anac082-1* mutation into *dim1a* mutant lines carrying *MYB23::GUS* or *GL2::GUS*

reporters and found that each reporter exhibited a wild-type expression pattern in the

dim1a anac082-1 background (Figure 3.12, A and B; Figure 3.10, B and C).

Consistently, both *dim1a anac082-1* and *dim1a GABI_282H08* mutants restored wild-

type root epidermal cell patterning (Figure 3.12C, Figure 3.10A). In addition, *anac082-1*

eliminated expression of the *MYB23::GUS* and *GL2::GUS* reporters, as well as non-hair

cell production, in the *wer-1 dim1a* double mutant (Figure 3.12, A to C). Taken together,

these results show that ANAC082 plays a similar role of inducing MYB23-dependent

GL2 expression and cell fate switching in both the *dim1a* and *apum23-4* mutants.

Although the *apum23* and *dim1a* mutants exhibit similar root epidermis

phenotypes, the APUM23 and DIM1A proteins have distinct biochemical functions in

ribosome biogenesis. Accordingly, we hypothesized that the ectopic production of non-

hair cells may be a general response to defective ribosome biogenesis. To test this, we

examined a collection of previously defined RBF mutants (Weis et al. 2015a) (Table 3.1). Among these, we discovered that mutations of the *PROTEIN ARGININE METHYLTRANSFERASE 3* (*PRMT3*) gene, *prmt3-1* and *prmt3-2*, exhibited ectopic non-hair cells similar to *apum23-4* and *dim1a* (Figure 3.11B). The *prmt3-1* mutant also exhibited delayed germination (Figure 3.2). During rRNA biogenesis, PRMT3 influences the balance between two alternative pre-rRNA processing pathways (Hang et al. 2014).

To study the cause for the ectopic non-hair cells in *prmt3-1*, we introduced the *GL2::GUS* reporter and found approximately 20% of the H-position cells exhibited ectopic *GL2::GUS* expression (Figure 3.11A, Figure 3.13). Further, the *wer-1 prmt3-1* double mutant exhibited substantial *GL2::GUS* expression and produced non-hair cells in both H and N positions, demonstrating a WER-independent effect (Figure 3.11, A and B; Figure 3.6). A role for MYB23 in the *prmt3-1* phenotype was shown by the elimination of *GL2::GUS* expression and non-hair cell production in the *wer-1 myb23-1 prmt3-1* plants, relative to the *wer-1 prmt3-1* double mutant (Figure 3.11, A and B), and the significant decrease in ectopic non-hair cells in the *prmt3-1 myb23-1* double mutant compared to *prmt3-1* (Figure 3.11C). Finally, the *prmt-1* mutant exhibited a comparable proportion of H-position cells expressing *MYB23::GUS* as the *apum23-4* and *dim1a* (Figure 3.12A, Figure 3.8). Therefore, like *apum23-4* and *dim1a*, the ectopic non-hair cell specification in *prmt3-1* is mediated by MYB23.

In summary, we identified two additional RBF mutants (*dim1a* and *prmt3-1*) exhibiting ectopic non-hair cells likely resulting from similar misregulation of epidermal cell fate as in *apum23-4*. These findings support the hypothesis that epidermal cell fate

switching is a general response to ribosomal defects rather than a particular RBF deficiency.

Cycloheximide treatment induces WER-independent *GL2* expression

In addition to genetic disturbances in RBF genes, drug-induced ribosomal defects can also trigger ectopic establishment of non-hair cell fates. Cycloheximide (CHX), widely used as a translation inhibitor, disrupts pre-rRNA processing in yeast and mammals (de Kloet 1966; Stoyanova et al. 1979). CHX was reported to induce ectopic *GL2* expression in the root epidermis (Wieckowski et al. 2012), similar to the RBF mutants. We further analyzed the effect of CHX treatment on root epidermis development by monitoring *GL2::GUS* expression in the *wer-1* mutant. Using a series of CHX concentrations, we found that *GL2::GUS* expression was induced in a *WER*-independent manner in both H and N position cells (Figure 3.14). Notably, the *wer-1 myb23-1* and *wer-1 anac082-1* double mutants exhibited no *GL2::GUS* up-regulation in response to CHX treatments (Figure 3.14), implying that the effect of CHX also relies on the ANAC082-MYB23 regulatory module that operates in the RBF mutants.

The *apum24-2* mutant is a distinct type of RBF mutant with ectopic non-hair cells

Another Arabidopsis Pumilio protein, APUM24, has been identified as a RBF required for pre-rRNA processing (Shanmugam et al. 2017; Maekawa et al. 2018). As *APUM24* knockout mutants were reported to exhibit seed abortion due to defective female gametogenesis and embryogenesis, we analyzed the *APUM24* knockdown mutant *apum24-2* (Shanmugam et al. 2017; Maekawa et al. 2018). We discovered that *apum24-2* mutant roots exhibited shorter root hairs resembling other examined RBF mutants (Figure 3.15A). Furthermore, the *apum24-2* mutant produced a significant

116

proportion of ectopic non-hair cells (Figure 3.15D) and ectopic *GL2::GUS* signals in the H position (Figure 3.15B, Figure 3.13). Therefore, like *APUM23*, knockdown of the *APUM24* gene function leads to ectopic non-hair cell specification.

Structural studies of the APUM23 yeast orthologue Nop9 and the APUM24 human orthologue Puf-A revealed that the two proteins, though both containing 11 PUF repeats, possess divergent protein structures and nucleotide binding characteristics (Qiu et al. 2014; Zhang et al. 2016). To test the functional relationship between the Arabidopsis APUM23 and APUM24 proteins, we created an *APUM23::APUM24* transgene and transformed it into the *apum23-4* mutant, and reciprocally, we created an *APUM24::APUM23* transgene and transformed it into the *apum24-2* mutant. In each case, the resulting transgenic plants exhibited the abnormal root epidermis phenotypes of the original mutant backgrounds (Figure 3.15D), indicating that APUM23 and APUM24 are functionally distinct.

We then studied the cause for the ectopic non-hair cells in *apum24-2*. The *wer-1 apum24-2* double mutant exhibited no significant non-hair cells in the H position but a considerable proportion of non-hair cells (>30%) in the N position, and the *wer-1 myb23-1 apum24-2* mutant showed no significant reduction in the proportion of these non-hair cells (Figure 3.15E). Further, the *apum24-2 myb23-1* mutant produced >10% ectopic non-hair cells, which is not significantly different from *apum24-2* (Figure 3.15D). In addition, the *MYB23::GUS* reporter showed dramatically decreased expression in the *apum24-2* root epidermis (Figure 3.15C). These results indicate that, unlike *apum23-4*, the ectopic non-hair cells in *apum24-2* are MYB23-independent. Consistent with this, the *apum23-4 apum24-2* double mutant produced an additive increase of ectopic non-

117

hair cells compared to each of the two single mutants (Figure 3.15D), suggesting that ectopic non-hair cell production in *apum23-4* and *apum24-2* is due to separate pathways. Notably, the *gl3 egl3 apum24-2* mutant still efficiently depleted all non-hair cells in both H and N positions (Figure 3.15E). Therefore, the ectopic non-hair cells in *apum24-2* mutant apparently still rely on formation of the MYB-bHLH-WD40 complex.

RBF mutants affect root hair elongation

In addition to ectopic non-hair cell formation, the *apum23-4* mutant also exhibited a significant reduction in the length of root hairs (Figure 3.1A, Figure 3.16). Compared to wild-type roots, which produced root hairs with mean length around 560 nm, approximately 50% of the *apum23-4* root hairs were shorter than 80 nm (Figure 3.16). The *dim1a* and *prmt3-1* roots also produced significantly shorter root hairs than wild type (Figure 3.16).

The correspondence between shorter root hairs and ectopic non-hair cells in the RBF mutants led us to examine whether the two phenotypes are co-regulated. However, incorporation of the *myb23-1* and/or *anac082-1* mutations into the RBF mutant backgrounds failed to restore normal root hair length (Figure 3.16). Therefore, it is most likely that the effects of RBF mutants on root epidermal cell patterning and root hair growth are regulated by separate pathways.

Discussion

A working model for cell patterning in RBF mutant root epidermis

In this study, we uncovered a new regulatory mechanism mediating a cell fate switch in response to defective ribosome biogenesis. Based on our combined analysis

of ribosome biogenesis mutants (*apum23-4*, *dim1a*, and *prmt3-1*) and CHX-treated

plants that all exhibited ectopic non-hair cell fate establishment, we determined that this

cell fate switch is the result of aberrant induction of *MYB23* gene expression by the

ribosomal stress response mediator ANAC082. Therefore, this work provides evidence

for a molecular linkage between ribosomal status and cell fate specification in plants.

We suggest a model to explain our findings (Figure 3.17). During early

development of the wild-type root epidermis, expression of the *GL2* and *MYB23* genes

is induced by the WER-GL3/EGL3-TTG1 complex, which predominantly occurs in N-

position cells and leads to non-hair cell fate specification (Figure 3.17A). The expression

of *GL2* and *MYB23* is absent (or low) in the H-position cells due to SCM-dependent

inhibition of *WER* expression and CPC-dependent inhibition of WER-GL3/EGL3-TTG1

complex formation, allowing for root-hair cell differentiation in these cells. In *apum23-4*

(and presumably *dim1a*, *prmt3-1*, and CHX-treated plants) (Figure 3.17B), an

ANAC082-dependent pathway is activated in response to impaired ribosome

biogenesis. In addition to the WER-GL3/EGL3-TTG-induced *MYB23* expression in N-

position cells, ANAC082 generates *MYB23* expression in both H- and N-position cells.

In N-position cells, the additional *MYB23* expression further supports WER/MYB23-

dependent gene regulation. In H-position cells, the additional *MYB23* expression leads

to elevated levels of MYB23/WER that, in some cells (approximately 20%), is sufficient

to overcome CPC inhibition and thereby induce *GL2* expression and ectopic non-hair

cell specification.

The novel role of MYB23 in response to ribosome biogenesis defects

The MYB23 protein is most similar to two other Arabidopsis R2R3-type MYB transcription factors, WER and GL1, and it participates with them to specify cell fates in the root epidermis and shoot epidermis. In the developing shoot epidermis, *MYB23* is required for proper trichome branching, and it acts redundantly with *GL1* to control trichome initiation (Kirik et al. 2005; Tominaga et al. 2007; S. F. Li et al. 2009; Balkunde et al. 2010). In the root epidermis, MYB23 acts redundantly with WER to generate the WER-GL3/EGL3-TTG1 complex responsible for non-hair cell fate specification, although the *myb23* mutant exhibits no significant root epidermis defects (Kang et al. 2009). In this study, we expanded our knowledge of MYB23 function by showing that it mediated ectopic non-hair cell specification in response to defective ribosome biogenesis. Specifically, we showed that RBF mutants (*apum23-4*, *dim1a* and *prmt3-1*) exhibited MYB23-dependent ectopic non-hair cell production (Figure 3.5, Figure 3.11), and CHX-treated *wer-1* roots exhibited MYB23-dependent *GL2* expression (Figure 3.14). It is notable that a functionally redundant player in root epidermis cell specification (MYB23) was recruited for this role, rather than the primary R2R3 MYB regulator (WER), suggesting that evolution of new regulatory pathways may take advantage of duplicate genes.

In this respect, our discovery is reminiscent of the role of ETC1 to induce production of ectopic root-hair cells upon phosphate deficiency (Rishmawi et al. 2018). However, under normal growth conditions, ETC1 functions redundantly with CPC, and the *etc1* mutant exhibits no defects in root epidermis cell patterning (V. Kirik et al. 2004; Simon et al. 2007). Thus, our study and the ETC1 study show that redundant regulators

in the root epidermis cell fate network operate as stress responding elements, and they raise the possibility that additional regulators in the network may have similar unrecognized roles in modulating root epidermal cell fate in response to various plant stresses.

This study also has implications for our understanding of *MYB23* transcriptional regulation. A previous study identified WER binding sites in the *MYB23* promoter and showed that WER, GL3/EGL3, and TTG1 were necessary for *MYB23* transcription in the developing root epidermis (Kang et al. 2009). In contrast, our study showed that *MYB23* expression in the root epidermis is WER-independent under conditions of impaired ribosome biogenesis and is instead mediated by ANAC082. It is notable that the ANAC082-dependent *MYB23* expression occurred in both H- and N-position cells and exhibited a later developmental start point within the distal meristematic zone (Figure 3.5). These features suggest a novel regulatory module that induces *MYB23* expression independent of positional cues and following a different developmental timeline. However, it remains unknown whether ANAC082, a potential transcriptional activator (Yamaguchi et al. 2015; Ohbayashi et al. 2017a), induces *MYB23* expression directly or indirectly.

Interestingly, among the RBF mutants we analyzed, the *apum24-2* mutant was unique in generating ectopic non-hair cells in a MYB23-independent manner. Specifically, the *myb23-1* mutation had no significant effect on non-hair cell specification in the *wer-1 apum24-2* or *apum24-2* mutants (Figure 3.15). These findings suggest the possible existence of multiple regulatory mechanisms mediating the effect of impaired ribosome biogenesis on root epidermal cell fate.

Ribosome biogenesis and plant development

Ribosomes are critical for protein synthesis, and developmental processes in general rely on efficient ribosome biogenesis. Accordingly, defective ribosome biogenesis has significant impacts on plant development (Byrne 2009; Weis et al. 2015a). It is proposed that the ribosomal abnormalities in RBF/RP mutants, including insufficient ribosome production and aberrant/unbalanced heterogeneity of ribosome components, differentially affect translation of certain developmental regulator gene transcripts (Horiguchi et al. 2012). Indeed, the translation of several auxin response factors is modulated by particular RPs through the upstream ORF (uORF) in their 5'UTRs (Rosado et al. 2012). ANAC082 has been identified as the mediator of several developmental phenotypes in RBF/RP mutants, connecting ribosomal health with a spectrum of developmental events (Ohbayashi et al. 2017a; Ohbayashi et al. 2017b; Salome 2017). Notably, the *ANAC082* transcript possesses a uORF, and therefore is potentially subject to translational regulation (Ohbayashi et al. 2017a; Salome 2017). In addition, *ANAC082* transcription is reported to be greater in RBF mutants (Ohbayashi et al. 2017a).

Ribosomal defects result from not only RBF/RP mutations, but also challenging conditions such as nutrient deprivation, heat shock and hypoxia (Mayer et al. 2005; Lior Golomb et al. 2014). In animal cells, ribosomal defects trigger ribosomal stress responses mediated by p53 activation and lead to cell cycle arrest and apoptosis (Zhang et al. 2009; L. Golomb et al. 2014; Penzo et al. 2019). As a potential plant version of this p53 pathway, ribosomal defects in plants lead to increased and/or activated ANAC082, which blocks tissue regeneration and delays seed germination

(Figure 3.2, (Ohbayashi et al. 2017a)). Both tissue regeneration and seed germination involve massive cell proliferation and cell growth that rely heavily on ribosome activities. Therefore, the ANAC082-mediated effects on these processes could be a programmed response to contend with ribosomal defects.

In this study, we discovered that a switch of root epidermal cell fate is a common characteristic of several RBF mutants (*APUM23*, *DIM1A*, *PRMT3*, *APUM24*) and plants treated with CHX (Figure 3.1, Figure 3.11, Figure 3.15). The biological rationale for reducing root-hair cell production in response to ribosomal defects is unclear. One possibility is that root-hair cell differentiation requires a relatively high level of ribosome activity. It has been observed that during early developmental stages, cells in the H position show greater cell division rates, higher cytoplasmic densities and delayed vacuolation compared to N-position cells (Galway et al. 1994; Berger et al. 1998b). Further, in this study, we discovered that H-position cells maintained larger nucleolar sizes and relatively greater amounts of APUM23 during later developmental stages (Figure 3.4). All these features suggest that developing H-position cells, committed to root hair production, are more metabolically active so might have a greater demand for ribosomes. Accordingly, we hypothesize that a switch from root-hair to non-hair cell fate is part of a response program to accommodate for ribosomal defects.

In addition to a change in root epidermal cell fate, we also observed reduced root hair length in multiple RBF mutants (*apum23-4*, *dim1a*, *prmt3-1*), which is independent of MYB23 and ANAC082 (Figure 3.16). Notably, the auxin-dependent pathway, which plays an essential role in root hair elongation (S. H. Lee et al. 2009; Overvoorde et al. 2010; Salazar-Henao et al. 2016), responds negatively to ribosomal defects (Rosado et

123

al. 2012). Therefore, it is possible that the defective auxin response elicited by ribosomal abnormalities is responsible for the reduced root hair elongation.

Materials and methods

Plant Material and growth conditions

Arabidopsis seeds were surface sterilized with 30% bleach plus 0.02% Triton X-100, and plated on previously reported mineral mix media (Schiefelbein et al. 1990) containing 0.3% Gelrite. Seedling phenotypes were analyzed after 4 days of growth at 23°C under continuous light. For RBF mutants, older seedlings were used due to slower growth: *apum23-4* mutant, 8 days; *dim1a* mutant, 6 days; *prmt3-1* mutant, 7 days; *mtr4* mutant, 5 days; For RBF mutants carrying the *anac082-1* mutant, seedlings used for analysis were approximately 2 days younger that the corresponding RBF single mutants. For crosses and seed bulking, seedlings were transplanted to soil and grown under long-day light conditions at 22 °C (day) and 18°C (night).

For analysis of cycloheximide (CHX) treated seedlings, seeds were grown on the standard mineral mix media for four days, transferred onto mineral mix media containing CHX (stock solution in ethanol), and grown for an additional 2 days before examination.

The following mutant and reporter lines used in this study have been previously described: *wer-1* (Lee et al. 1999)*, gl3* (Koornneef 1981)*, egl3* (F. Zhang et al. 2003)*, ttg1* (Galway et al. 1994)*, gl2-1* (Koornneef 1981)*, cpc-1* (Wada et al. 1997)*, myb23-1* (Kirik et al. 2005)*, dim1a* (Wieckowski et al. 2012)*, GL2::GUS* (Masucci et al. 1996a)*, MYB23::GUS* (Kang et al. 2009)*, MYB23::MYB23-GFP* (Kang et al. 2009), *GL3::GL3-YFP* (Bernhardt et al. 2005). The *anac082-1* (*sriw1*) seeds were kindly provided by Dr.

Munetaka Sugiyama (the University of Tokyo, Japan). The *MYB23::MYB23-GFP* seeds were kindly provided by Dr. Myeong Min Lee (Yonsei University, Korea).

The following mutant lines were reported previously and obtained from the Arabidopsis Biological Resource Center: *apum23-2* ((Abbasi et al. 2010), *SALK_052992*), *apum24-2* ((Maekawa et al. 2018), *SALK_033623*), *prmt3-1* ((Hang et al. 2014), *SAIL_220_F08*), *prmt3-2* ((Hang et al. 2014), *WISCDSLOX391A01*), *anac082* ((Kim et al. 2018), *GABI_282H08*).

Mutant screening and positional cloning

Mutagenesis of *cpc-1* mutant seeds (Wassilewskija ecotype [Ws]) with ethyl methanesulfonate (EMS) was performed as previously described (Estelle et al. 1987). The *cpc-1 apum23-4* mutant (WS ecotype) was crossed to plants of the Columbia (Col-0) ecotype to generate F2 and F3 offspring for positional cloning. Multiple simple sequence length polymorphism (SSLP) and cleaved amplified polymorphic sequence (CAPS) markers were used (Jander et al. 2002). The responsible mutation was narrowed to a region between the CER481016 (27,196,516) and CER479543 (27,235,489) on chromosome 1. The protein-coding sequences of all genes within this interval were then cloned and sequenced to identify the mutated gene in *apum23-4*.

During later genetic studies, the Derived Cleaved Amplified Polymorphic Sequences (dCAPS, (Neff et al. 2002)) strategy was used to identify the *apum23-4* mutation among individual plants in segregating populations. Genotyping primers are listed in Table 3.2.

Transgenes, and plant transformation

125

To construct the *APUM23::APUM23-GFP* transgene, a 5.5-kb genomic fragment including 1-kb of the 5' promoter region and the full-length genomic sequence of *APUM23* (with the stop codon removed) was cloned and integrated into the Gateway pENTR/SD/TOPO vector (Invitrogen), followed by subcloning into the Gateway binary vector pMDC107 (containing the C-terminal GFP tag). The cloning primers are listed in Table 3.2.

To construct the *35S::APUM23-YFP* transgene, a 4-kb genomic sequence of *APUM23* (from the ATG and excluding the stop codon) was cloned and incorporated into the pCAM binary vector containing the 35S promoter at the 5' end and an in-frame YFP tag at the 3' end, using the HiFi Assembly Cloning kit (NEB).

To construct the *FIB1::FIB1-mcherry* transgene, a 2.2-kb genomic fragment including 1-kb of the 5' promoter region and the full-length *FIB1* genomic sequence (with the stop codon removed), a 0.7-kb mcherry sequence (with a stop codon added), and a 0.5-kb 3' flanking region of *FIB1* were cloned and integrated together into the pCAM binary vector using the HiFi DNA Assembly Cloning kit (NEB). The mcherry tag was added to the C terminus of *FIB1* genomic sequence. The cloning primers are listed in Table 3.2.

Verified constructs were transformed into *Agrobacterium tumefaciens* strain GV3101, which was then used for plant transformation as described previously (Clough et al. 1998). After transformation, T1 seeds were harvested and screened for hygromycin resistance.

Microscopy, quantification and image analysis

Quantification of root-hair cell and non-hair cell frequency were performed with a bright-field compound microscope using seedlings briefly stained with toluidine blue. For each genotype, 10 cells in the H position and 10 cells in the N position were scored per root, and 10 roots were used per replicate. Cell positions were determined according to their location with respect to underlying cortical cells. A cell was scored as a root-hair cell if a visible protrusion was present on its cell surface, regardless of the length. At least 3 replicates were performed for each genotype in one experiment.

Root hair length measurements were performed with a bright-field compound microscope with toluidine-blue-stained seedlings. Only root hairs in the fully mature regions (3-5mm from root tips; marked by relatively universal root hair length) were analyzed. For each genotype, 10 root hairs were measured per root (using ImageJ) and a total of 20 roots were used.

Histochemical analysis of seedling roots containing GUS reporter genes was performed as previously described (Masucci et al. 1996a). For *GL2::GUS*, roots were stained with 0.1 mg/mL X-gluc substrates at 37°C for 20min, while for *MYB23::GUS*, roots were stained with 0.2 mg/mL X-gluc substrates at 37°C for 40-50 min. For quantification of *GL2::GUS* and *MYB23::GUS* expression, 10 continuous cells in the H position and 10 continuous cells in the N position were scored in each root and 10 roots were used for each genotype in each replicate. The 10 cells included the first cell prior to rapid elongation (i.e., cell length > cell width) and extended shootward. A cell was scored as GUS-positive if the GUS signal was visibly greater than the neighboring unstained H-position cells. Cell positions were defined according to their location with

respect to underlying cortical cells. At least 3 replicates were performed for each genotype in one experiment.

Fluorescent images were obtained with a TCS SP5 DM6000B broadband confocal microscope (Leica) with a HCX PL APO CS 20x or 40x dry lens and facilitated with LAS AF software. Before imaging, seedlings were stained with propidium iodide (PI) or DAPI and rinsed with water. For GFP/PI imaging, an argon 488-nm laser was used for excitation. The GFP signal was collected under bandwidth 511-541nm, and the PI signal was collected under bandwidth 620-720nm. For YFP/PI imaging, an argon 514-nm laser was used for excitation. The YFP signal was collected under bandwidth 528-547nm. For DAPI/GFP/mcherry imaging, the 405-nm Diode was used for DAPI excitation and the DPSS 561-nm laser was used for mcherry excitation. The DAPI signal was collected under bandwidth 424-475nm, and the mcherry signal was collected under bandwidth 580-700nm.

In order to examine the expression of both the *GL2::GUS* and *MYB23::MYB23-GFP*/*GL3::GL3-YFP* markers within the same root, seedling roots were first imaged with the confocal microscope, then removed from slides and stained for GUS signals. Special care was taken to place the seedlings in the same posture for GUS examination as for the fluorescent imaging, taking advantage of unique root epidermal cell shapes as landmarks in the viewing window.

Accession numbers

Arabidopsis sequence data from this chapter can be found in the GenBank/EMBL data libraries under the following accession numbers: APUM23 (AT1G72320), DIM1A (At2G47420), PRMT3 (AT3G12270), APUM24 (AT3G16810),

ANAC082 (AT5G09330), CPC (At2G46410), FIB1 (At5G52470), GL2 (At1G79840), GL3 (At5g41315), EGL3 (AT1G63650), MYB23 (At5g40330), TTG1 (At5g24520), and WER (At5g14750).
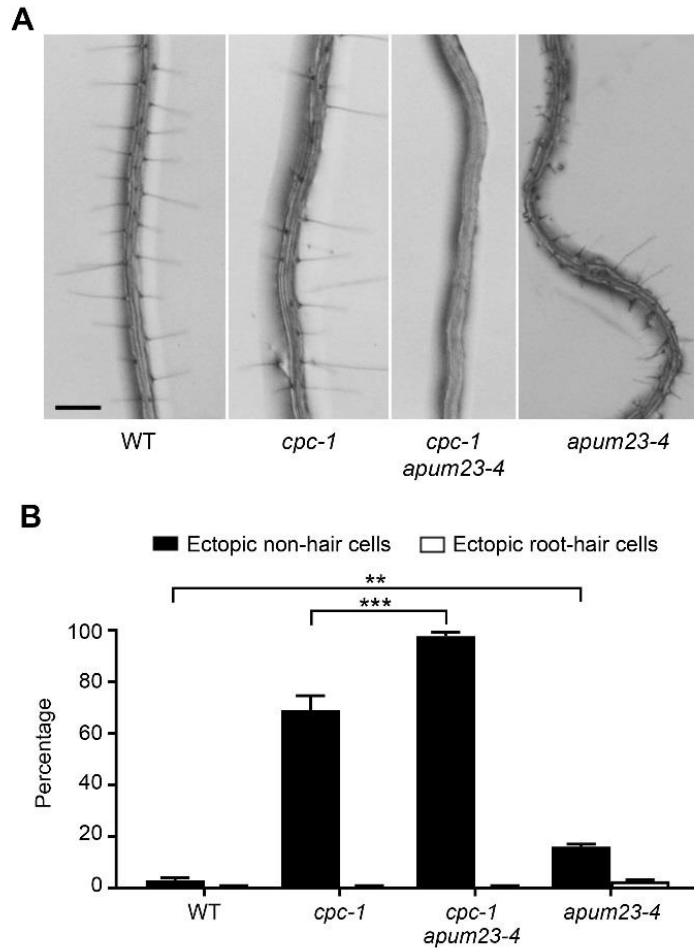
Figure 3.1 The *apum23-4* mutation enhances the *cpc-1* mutant phenotype.
(A) Root hair phenotypes of seedling roots of wild type (WT), *cpc-1*, *cpc-1 apum23-4*, and *apum23-4*. Bar=200μm. (B) Quantification of root epidermal cell specification in seedling roots of WT, *cpc-1*, *cpc-1 apum23-4*, and *apum23-4*. Error bars indicate standard deviations from three replicates. Statistical significance is determined by one-way ANOVA. *** represents $p<0.001$ and ** represents $p<0.01$.
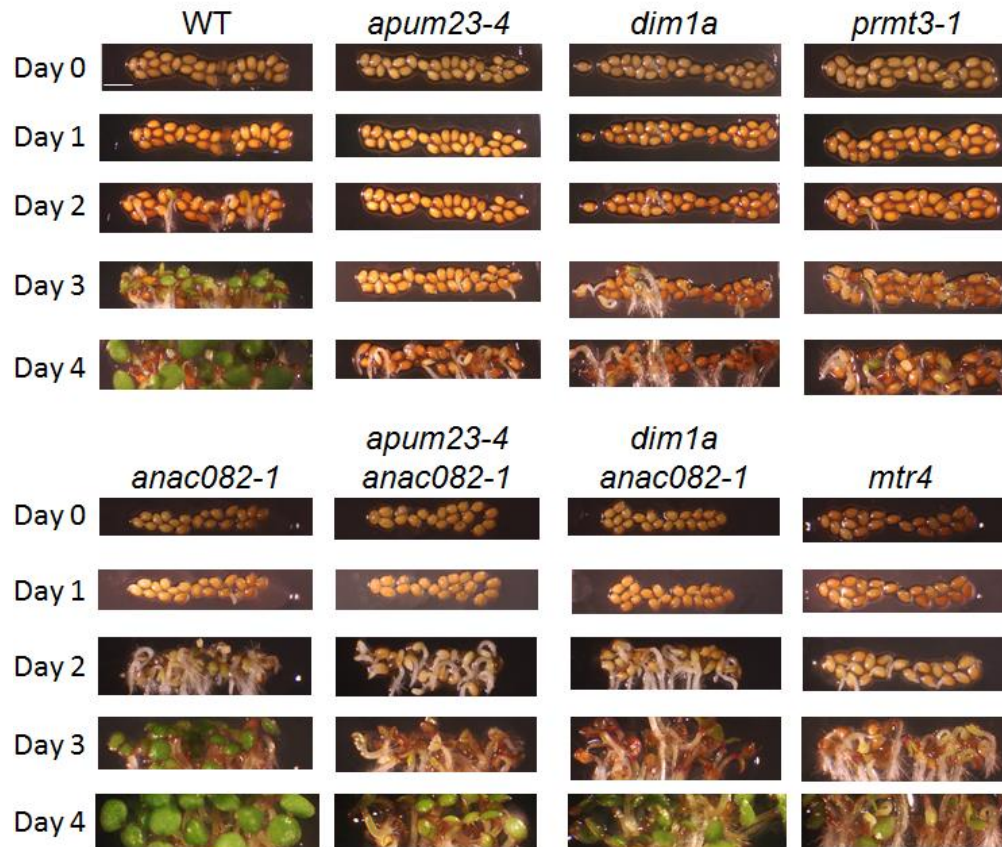
Figure 3.2 RBF mutants exhibited delayed seed germination.
Pictures show germination status of seeds at different time points after sowing.
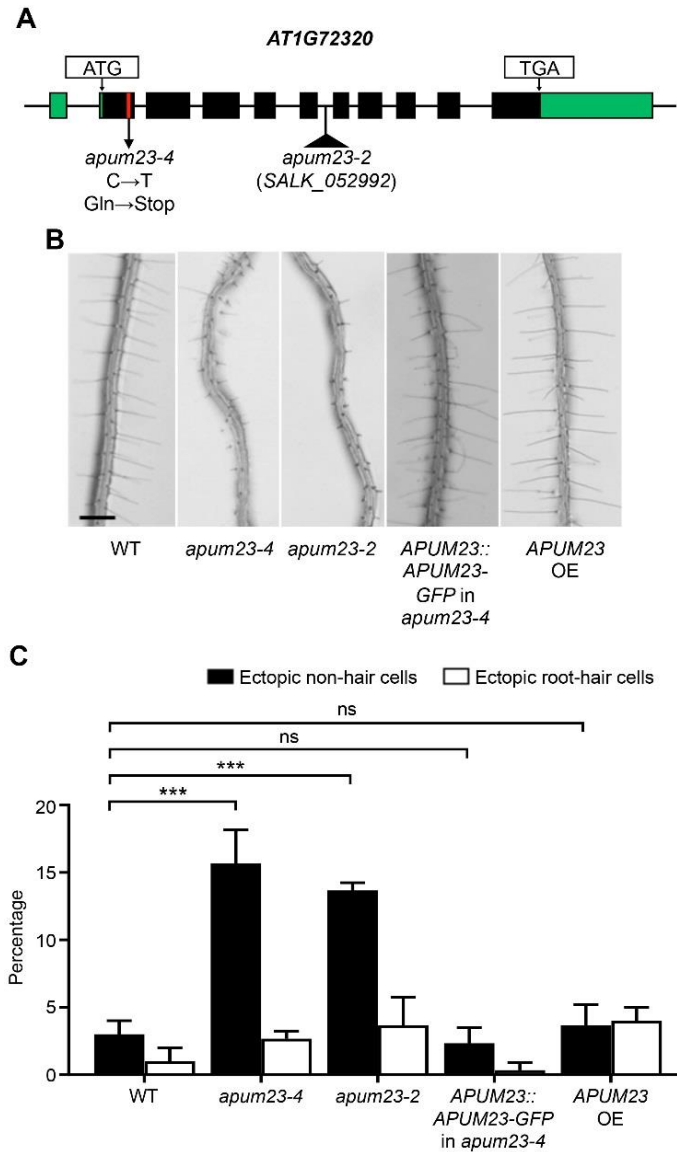
Figure 3.3 The *apum23-4* mutant possesses a nonsense mutation in the *APUM23* gene.
(A) A schematic drawing of the *APUM23* (*AT1G72320*) gene, indicating the position of the mutated nucleotide in the *apum23-4* mutant. The green boxes indicate 5' and 3' UTRs, and the black boxes indicate exons. The single-base substitution in *apum23-4* is indicated by the red line. The position of the T-DNA insertion in the *apum23-2* (*SALK_052992*) mutant is indicated by the black triangle. (B) The root hair phenotypes of seedling roots of wild type (WT), *apum23-4*, *apum23-2, apum23-4* transformed with the *APUM23::APUM23-GFP* transgene, and *apum23-4* transformed with the *35S::APUM23-YFP* transgene (*APUM23* OE). Bar=200µm. (C) Quantification of root epidermal cell specification in seedling roots of wild type, *apum23-4*, *apum23-2*, *apum23-4* transformed with the *APUM23::APUM23-GFP* transgene, and *APUM23* OE. Error bars represent standard deviations from three replicates. Statistical significance is determined by one-way ANOVA. *** represents p<0.001 and ns represents not significant.

Figure 3.4 APUM23 localizes to nucleoli in multiple root tissues.
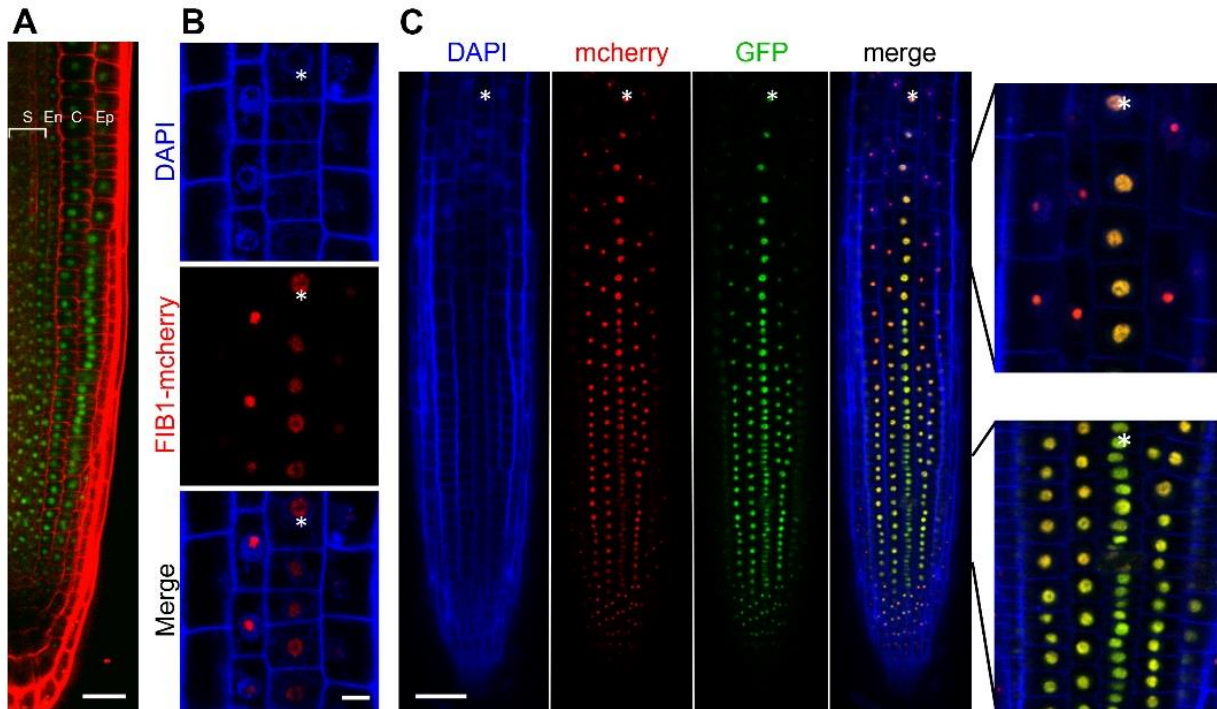(A) Accumulation of APUM23-GFP (green) in tissues of the *APUM23::APUM23-GFP* root. The red color represents propidium iodide staining for cell boundary visualization. Ep: Epidermis; C: Cortex; En: Endodermis; S: Stele. Bar=25µm. (B) Overlay of DAPI staining (blue) and *FIB1::FIB1-mcherry* signals (red) in the root epidermis. Stars indicate H-position cell files. Bar=10µm. (C) Overlay of DAPI staining (blue), *FIB1::FIB1-mcherry* (red), and *APUM23::APUM23-GFP* (green) in the root epidermis. Stars indicate H-position cell files. Bar=50µm. Compared to (B), the root in (C) was only briefly stained with DAPI to enable visualization of cell boundaries.
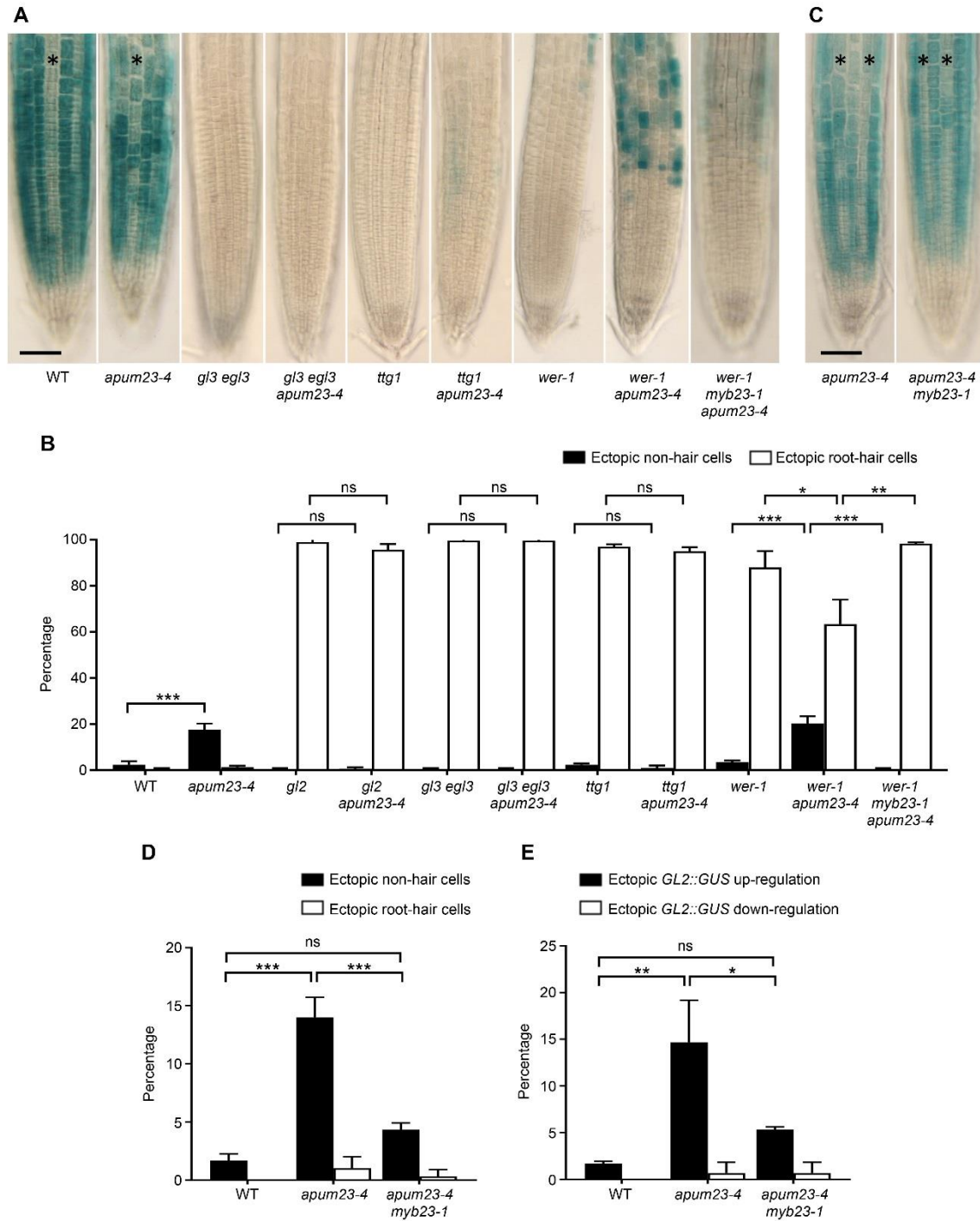
Figure 3.5 MYB23 mediates ectopic non-hair cell fate in the *apum23-4* mutant through up-regulating *GL2*.
(A) Expression of *GL2::GUS* in seedling root tips of wild-type (WT) and various mutant plants. Stars indicate H-position cell files. Bar=50μm. (B) Quantification of epidermal cell specification in seedling roots of WT and mutant plants. Error bars represent standard deviations of three replicates. Statistical significance is determined by one-way ANOVA.

*** represents p<0.001, ** represents p<0.01, * represents p<0.05 and ns represents not significant. (C) Expression of *GL2::GUS* in seedling root tips of *apum23-4* and *apum23-4 myb23-1* plants. Stars indicate H-position cell files. Bar=50μm. (D) Quantification of epidermal cell specification in seedling roots of WT, *apum23-4*, and *apum23-4 myb23-1* plants. Error bars represent standard deviations of three replicates. Statistical significance is determined by one-way ANOVA. *** represents p<0.001 and ns represents not significant. (E) Quantification of *GL2::GUS* signals in seedling root tips of WT, *apum23-4*, and *apum23-4 myb23-1* plants. Error bars represent standard deviations of three replicates. Statistical significance is determined by one-way ANOVA. ** represents p<0.01 and * represents p<0.05 and ns represents not significant.
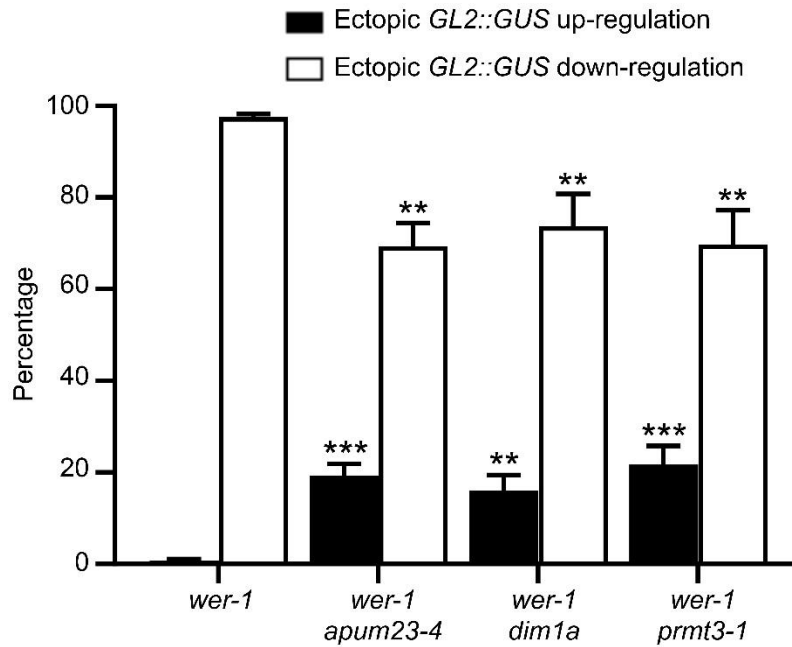
Figure 3.6 Quantification of *GL2::GUS* signals in multiple RBF double mutants with *wer-1*.
The error bars represent standard deviations from three replicates. Statistical significance between either position (H or N) in each double mutant and *wer-1* single mutant is determined by one-way ANOVA. *** indicates $p < 0.001$ and ** indicates $p < 0.01$.
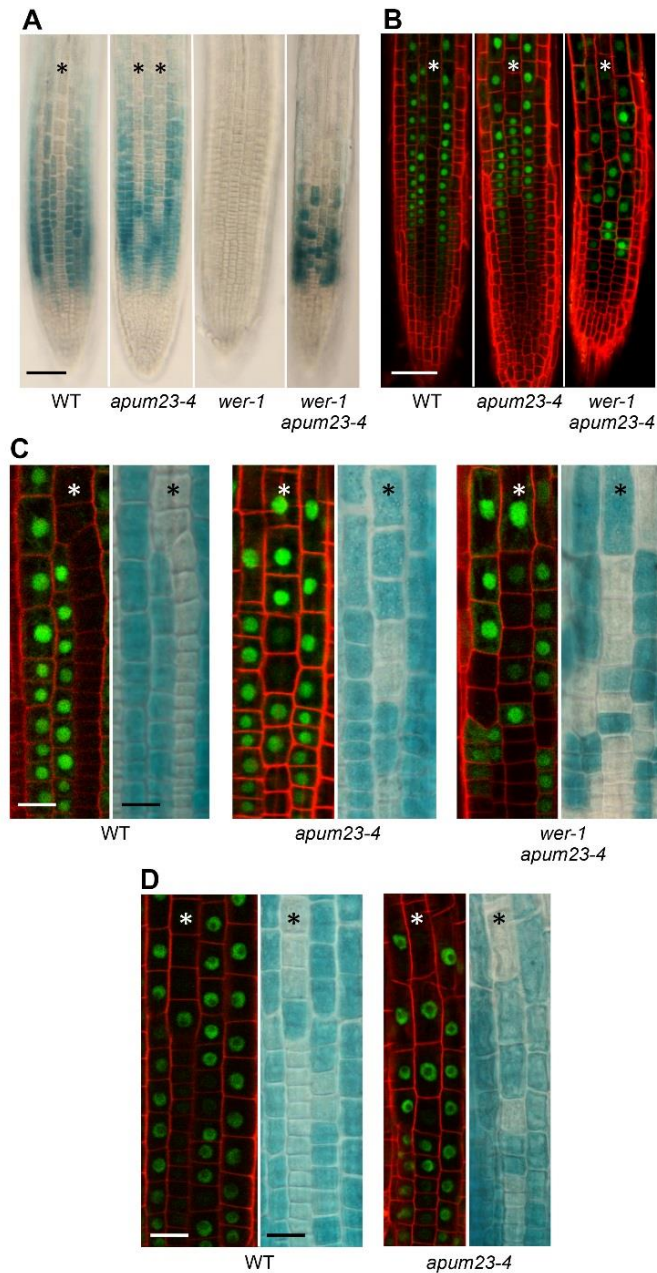
Figure 3.7 The *apum23-4* mutant exhibits ectopic *MYB23* gene expression.
(A) Expression of *MYB23::GUS* in the seedling root epidermis of wild type (WT),
apum23-4, *wer-1*, and *wer-1 apum23-4*. Stars indicate H-position cell files. Bar=50µm.
(B) Expression of *MYB23::MYB23-GFP* in the seedling root epidermis of WT, *apum23-4*, and *wer-1 apum23-4*. The red color represents propidium iodide staining and the
green color represents MYB23-GFP signal. Stars indicate H-position cell files.
Bar=50µm. (C) Expression of *MYB23::MYB23-GFP* (left in each panel) and *GL2::GUS*
(right in each panel) in one single seedling root tip of WT, *apum23-4*, and *wer-1
apum23-4*. Stars indicate H-position cell files. Bar=20µm. (D) Expression of *GL3::GL3-
YFP* (left in each panel) and *GL2::GUS* (right in each panel) in one single seedling root
tip of WT and *apum23-4*. Stars indicate H-position cell files. Bar=20µm.

Figure 3.8 Quantification of *MYB23::GUS* signals in RBF mutants *apum23-4, dim1a* and *prmt3-1*.
Error bars represent standard deviations from three replicates. Statistical significance is determined by one-way ANOVA. ** represents $p<0.01$.
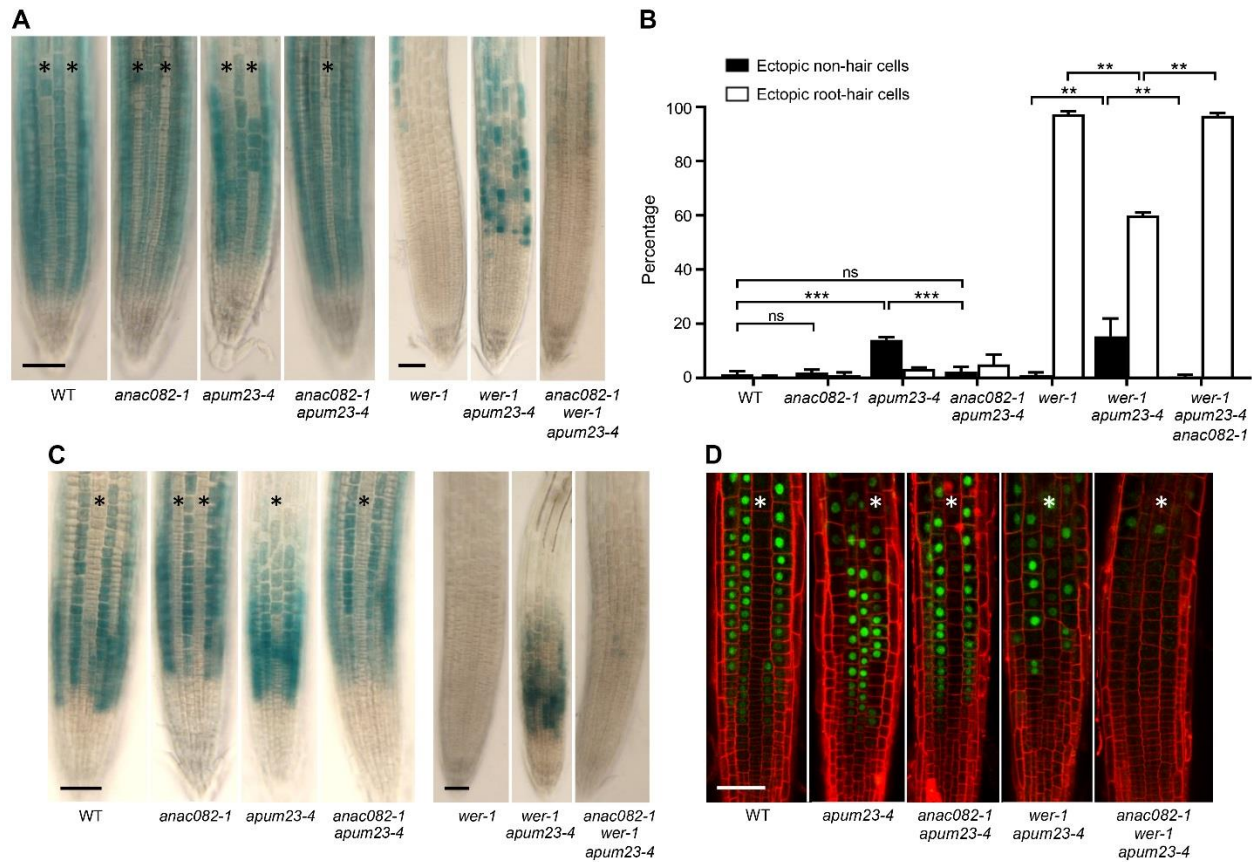
Figure 3.9 ANAC082 is required for ectopic non-hair cells in the *apum23-4* mutant. (A) Expression of *GL2::GUS* in the seedling root epidermis of wild type (WT) and multiple mutants. Stars indicate H-position cell files. Bar=50µm. (B) Quantification of root epidermal cell specification in the seedling roots of WT and multiple mutants. Error bars represent standard deviations from three replicates. Statistical significance is determined by one-way ANOVA. *** represents p<0.001, ** represents p<0.01, ns represents not significant. (C) Expressio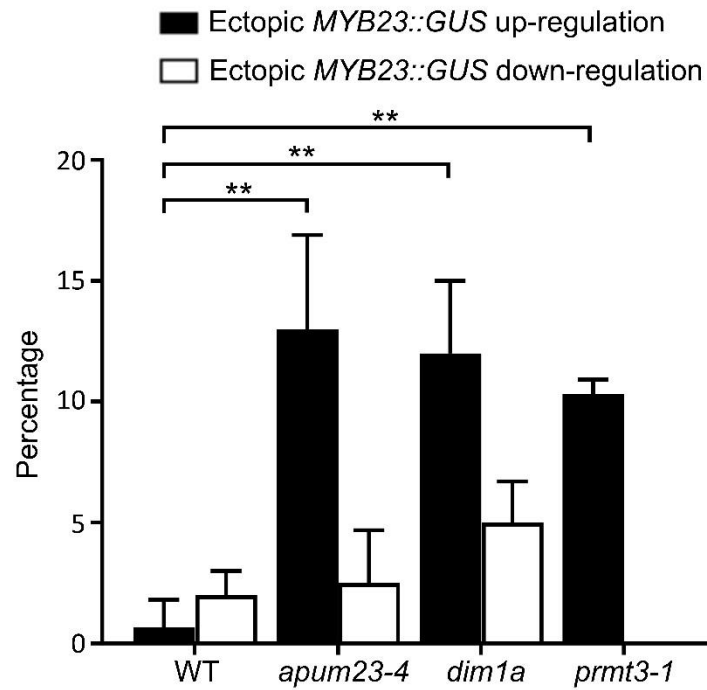n of *MYB23::GUS* in the seedling root epidermis of WT and multiple mutants. Stars indicate H-position cell files. Bar=50µm. (D) Expression of *MYB23::MYB23-GFP* in the seedling root epidermis of WT and multiple mutants. The red color indicates propidium iodide staining and the green color indicates MYB23-GFP signals. Stars indicate H-position cell files. Bar=50µm.
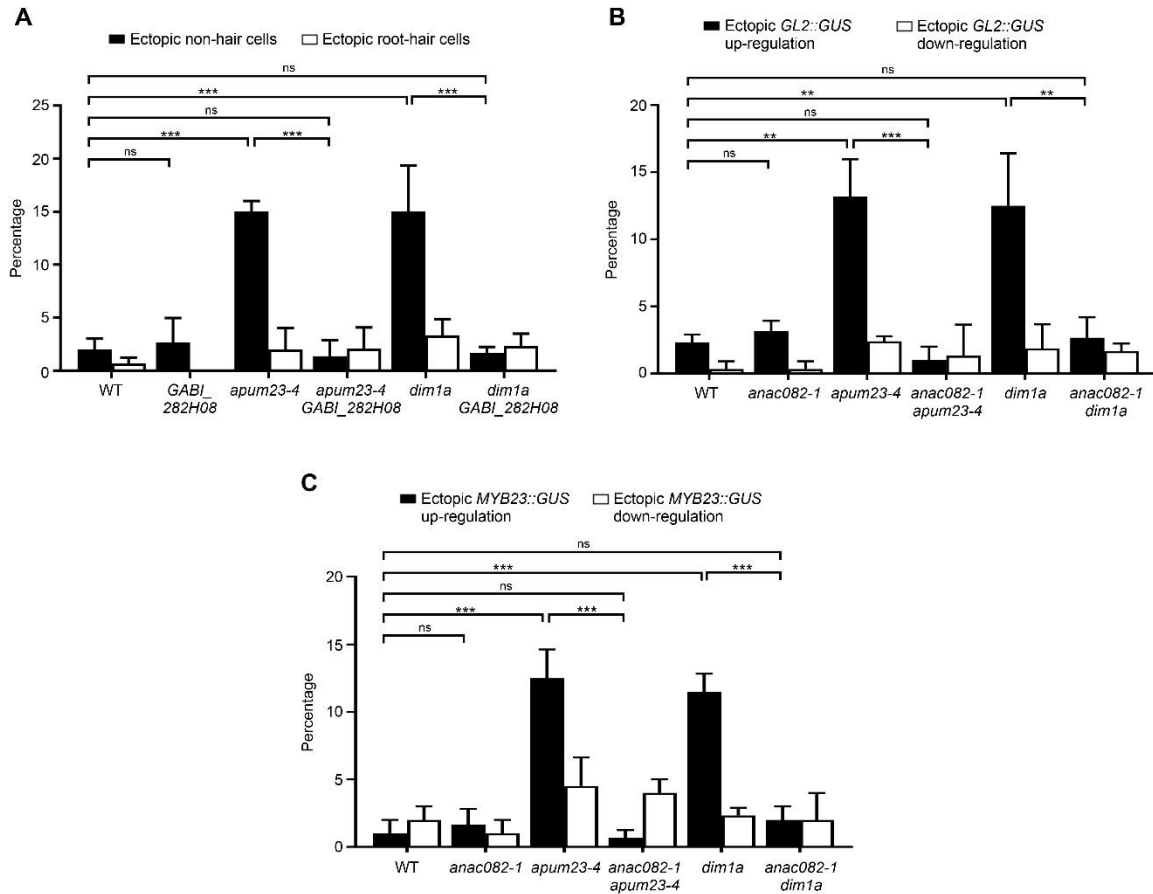
Figure 3.10 ANAC082 is required for ectopic *MYB23* expression and ectopic non-hair cell specification in *apum23-4* and *dim1a* mutants.
(A) Quantification of root epidermal cell specification in seedling roots of wild type and multiple mutants. (B) Quantification of *GL2::GUS* expression of in seedling root tips of wild type and multiple mutants. (C) Quantification of *MYB23::GUS* expression of in seedling root tips of wild type and multiple mutants. For all quantifications, error bar represents standard deviations from three replicates. Statistical significance is determined by one-way ANOVA. ** indicates $p<0.01$, *** represents $p<0.001$, ns represents not significant.
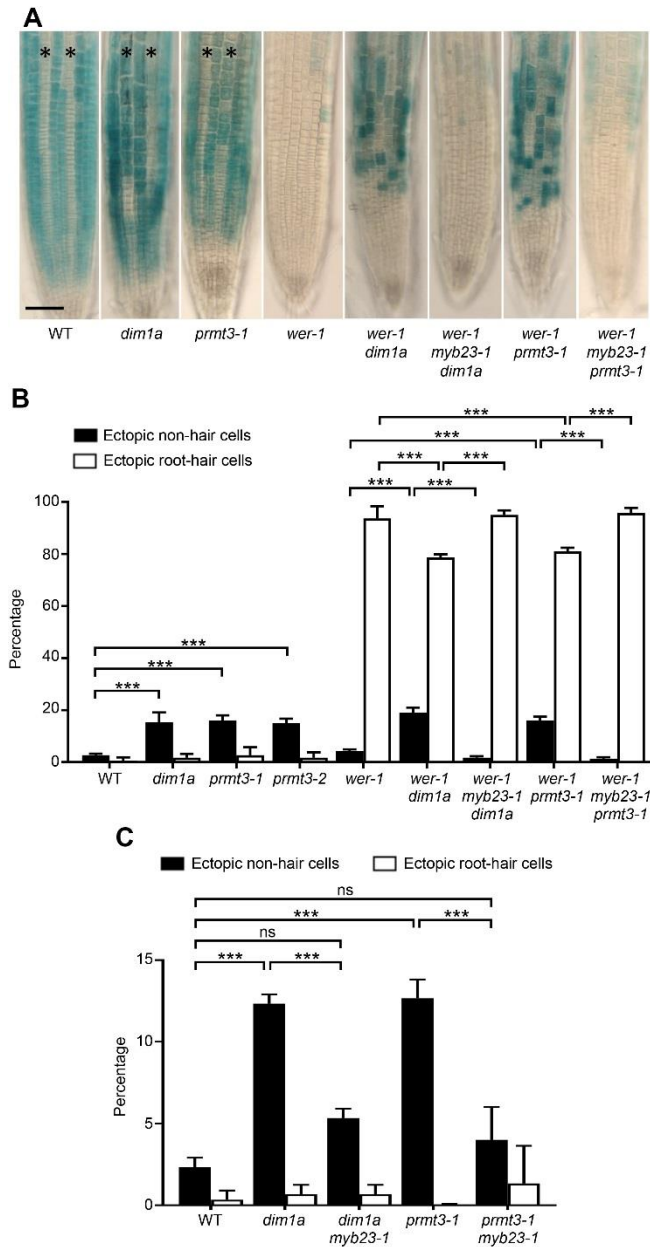
Figure 3.11 The *dim1a* and *prmt3-1* mutants exhibit MYB23-dependent ectopic non-hair cell fate specification.
(A) Expression of *GL2::GUS* in the seedling root epidermis of wild type (WT) and multiple mutants. Stars represent H-position cell files. Bar=50 μm. (B) Quantification of epidermal cell specification in seedling roots of WT and multiple mutants. Error bars represent standard deviations from three replicates. Statistical significance is determined by one-way ANOVA. *** represents $p<0.001$. (C) Quantification of epidermal cell specification in seedling roots of WT and multiple mutants. Error bars represent standard deviations from three replicates. Statistical significance is determined by one-way ANOVA. *** represents $p<0.001$ and ns represents not significant.

141
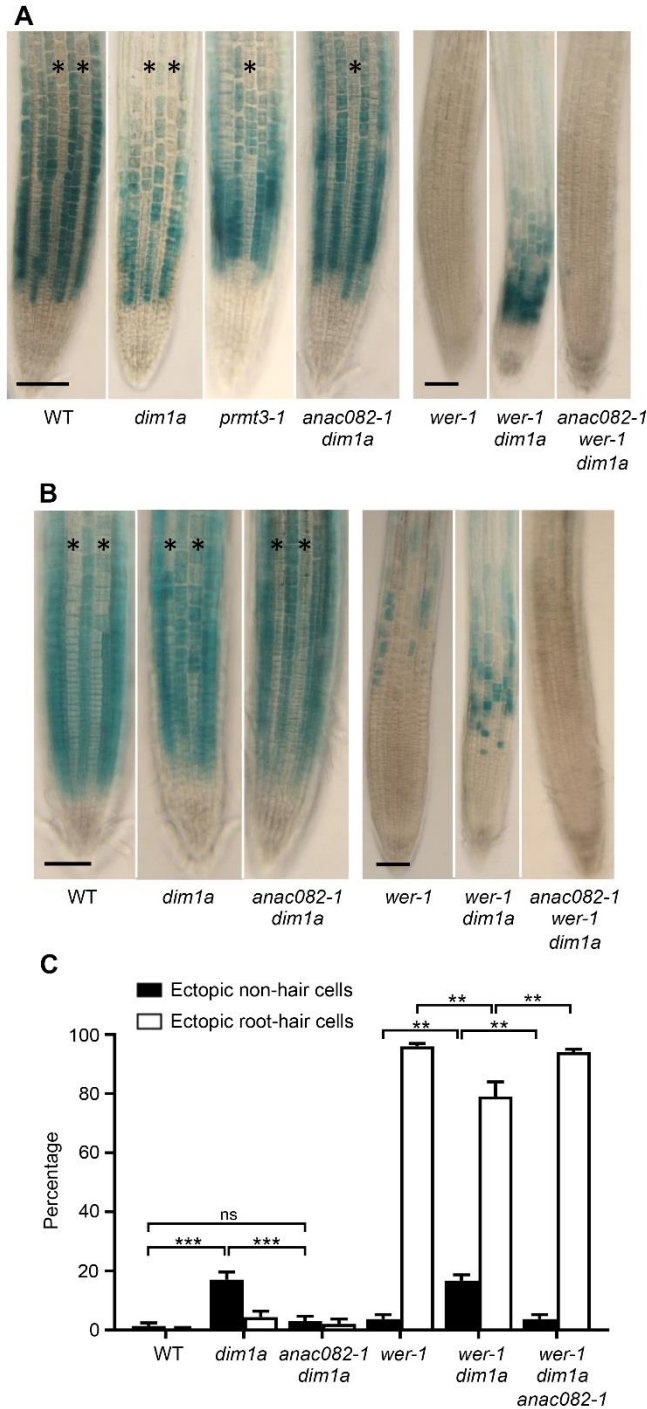
Figure 3.12 ANAC082 is required for ectopic non-hair cells in the *dim1a* mutant. (A) Expression of *MYB23::GUS* in the seedling root epidermis of wild type (WT) and multiple mutants. Stars indicate H-position cell files. Bar=50µm. (B) Expression of *GL2::GUS* in the seedling root epidermis of WT and multiple mutants. Stars indicate H-position cell files. Bar=50µm. (C) Quantification of root epidermal cell specification in seedling roots of WT and multiple mutants. Error bars represent standard deviations from three replicates. Statistical significance is determined by one-way ANOVA. ***

represents p<0.001, ** represents p<0.01, ns represents not significant.
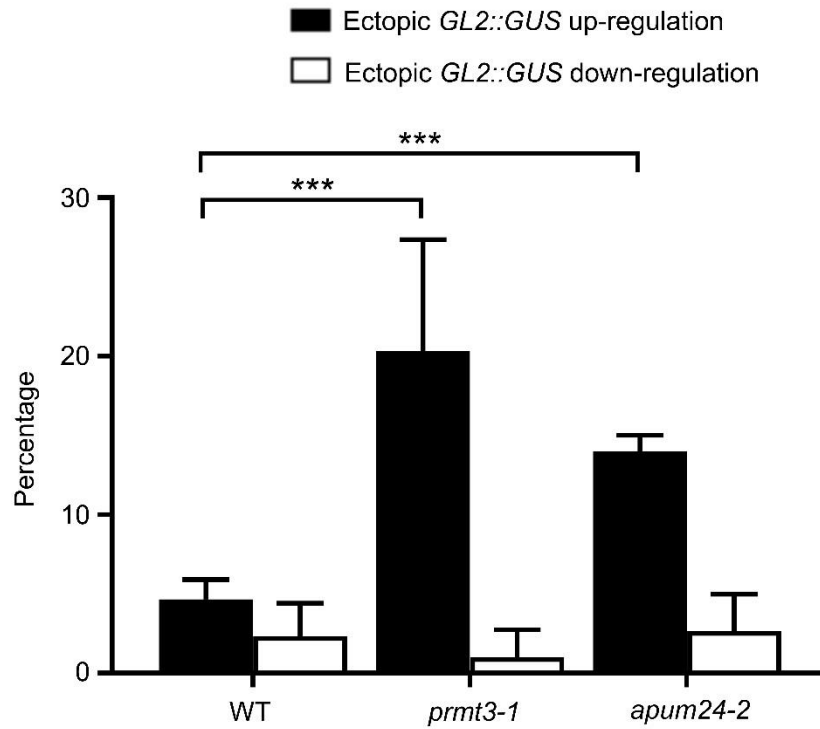
Figure 3.13 Quantification of *GL2::GUS* signals in seedling root tips of wild type, *prmt3-1*, and *apum24-2* mutant.
Error bars represent standard deviation of three replicates. Statistical significance is determined by t-test. *** represents p<0.001.
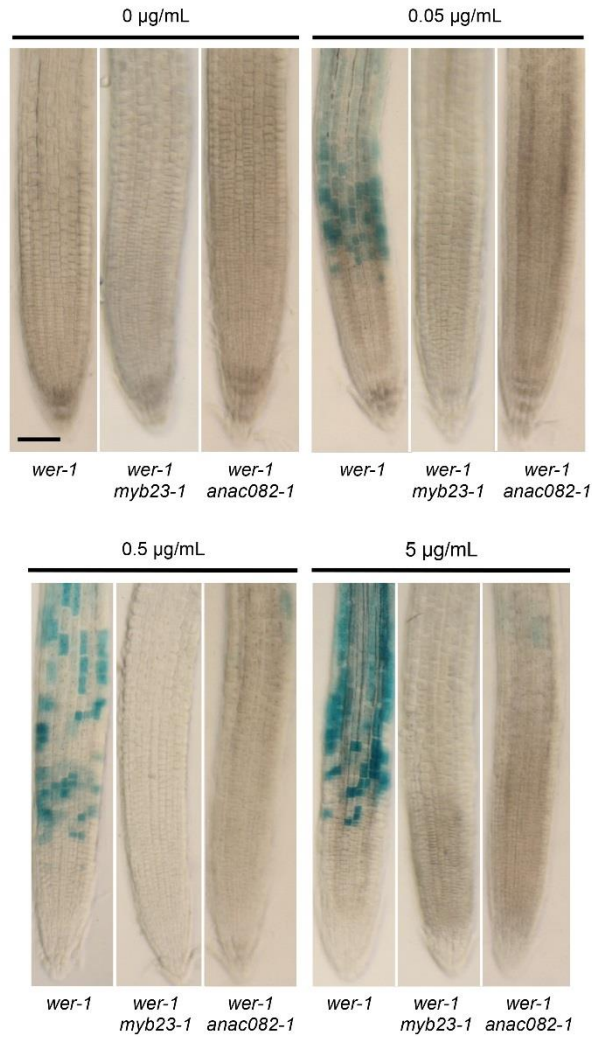
Figure 3.14 MYB23 and ANAC082 mediate WER-independent *GL2* up-regulation triggered by cycloheximide treatment.
Expression of *GL2::GUS* in the root epidermis of *wer-1*, *wer-1 myb23-1*, and *wer-1 anac082-1* seedlings treated with a series of concentrations of cycloheximide. Bar=50µm.
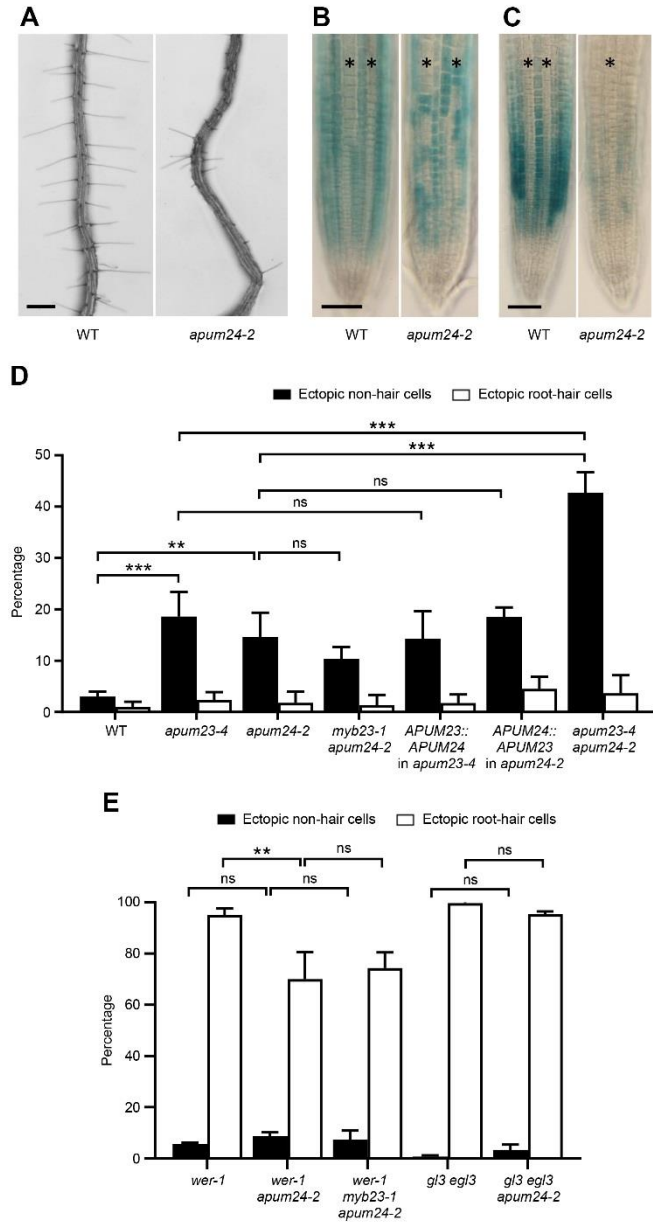
Figure 3.15 The *apum24-2* mutant exhibits MYB23-independent ectopic non-hair cell production.
(A) Root hair phenotypes of wild-type (WT) and *apum24-2* seedling roots. Bar=200µm.
(B) Expression of *GL2::GUS* in the seedling root epidermis of WT and *apum24-2*.
Bar=50µm. Stars indicate H-position cell files. (C) Expression of *MYB23::GUS* in the seedling root epidermis of WT and *apum24-2*. Bar=50µm. Stars indicate H-position cell files. (D) Quantification of root epidermal cell specification in WT and various mutant seedlings. Error bars represent standard deviations from three replicates. Statistical significance is determined by one-way ANOVA. *** represents p<0.001, ** represents p<0.01, ns represents not significant. (E) Quantification of root epidermal cell specification in seedling roots of multiple mutants. Error bars represent standard deviations from three experiments. Statistical significance is determined by one-way ANOVA. ** represents p<0.01, ns represents not significant.
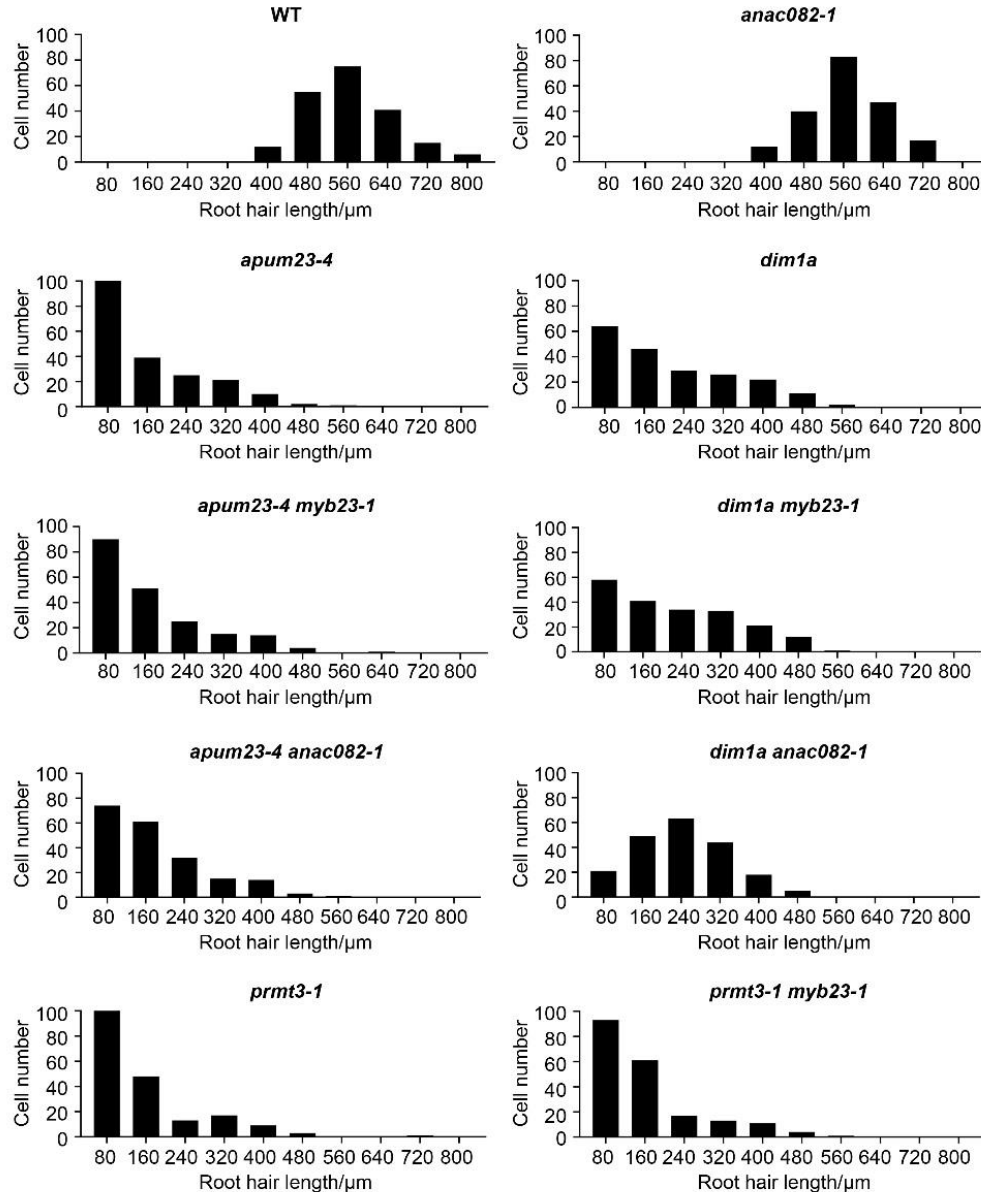
Figure 3.16 RBF mutants affect root hair elongation.
Histograms of root hair length from seedling roots of wild type (WT) and multiple mutants (n=200). For each genotype, 20 seedlings were used, and 10 root hairs were measured for each seedling. Statistical comparisons between different genotypes were conducted using a rank-sum test (Kruskal-Wallis) coupled with Dunn's multiple comparison tests. Specifically, *anac082-1* showed no significant difference from WT (p>0.05); *apum23-4*, *dim1a*, and *prmt3-1* were all significantly different from WT (p<0.001); *apum23-4 myb23-1* and *apum23-4 anac082-1* both showed no significant differences from *apum23-4* (p>0.05); *dim1a myb23-1* and *dim1a anac082-1* both showed no significant differences from *dim1a* (p>0.05); *prmt3-1 myb23-1* showed no significant differences from *prmt3-1* (p>0.05).
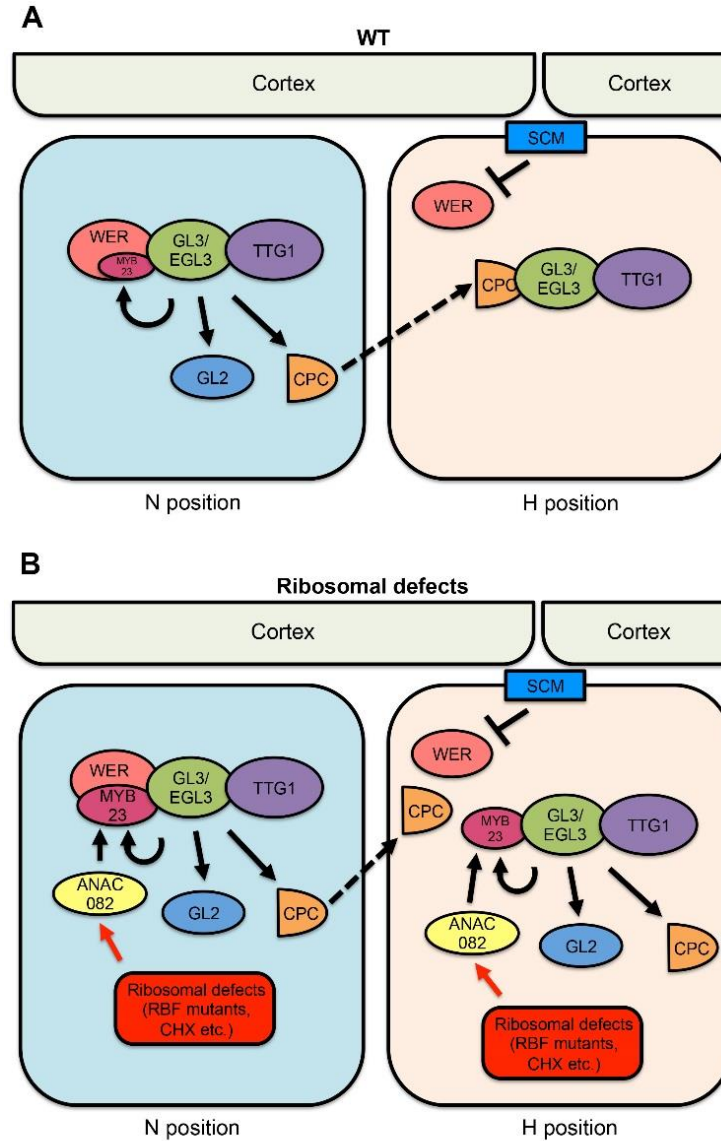
Figure 3.17 Working models for root epidermal cell fate regulation in wild-type (WT) plants and plants with ribosomal defects.
Solid black arrows indicate transcriptional regulation. Dashed black arrows indicate protein translocation. (A) In the wild-type root epidermis, the WER-GL3/EGL3-TTG1 complex preferentially accumulates in N position cells, up-regulating expression of *MYB23*, *GL2* and *CPC*. MYB23 serves in a positive feedback loop to maintain WER function. GL2 promotes non-hair cell fate through repressing root-hair genes. CPC is translocated to the adjacent H-position cell, where it inhibits WER's function by competitively binding to GL3/EGL3. SCM mediates inhibition of WER expression in H-position cells. (B) Ribosomal defects caused by RBF mutants or CHX treatment activate ANAC082, which mediates additional *MYB23* expression in both H and N positions. The additional MYB23 in H-position cells help to outcompete CPC, leading to excessive functional MYB23-GL3/EGL3-TTG1 complex and ectopic non-hair cell fate.

Table 3.1 A list of the RBF mutants tested in this study.

Gene name	Reported phenotype	Ribosomal defects	Tested lines	Root growth and root hair patterns	Reference
BRX1-1	Comparable to wild type	More 27SA/B, 33S; Less P-A3	*SALK_004020*	Comparable to WT	(Weis et al. 2015b)
BRX1-2	Slow growth; pointed leaves	More 27SA/B, 33S; Less P-A3	*SALK_110593C*	Comparable to WT	
LSG1-2	Slow growth; pointed leaves	More P-A3, 18S-A3	*SALK_114083*	Slow growth, normal pattern	(Weis et al. 2014)
MTR4	Slow growth; pointed leaves	More 6S and 7S	*CS842696*	Comparable to WT	(Lange et al. 2011)
			SALK_204906	Slow growth, normal pattern	
NOF1	Increased nucleoli/nuclei proportion;	rDNA promoter methylation	*SAIL_1172_B04*	Comparable to WT	(Harscoet et al. 2010)
			SALK_029968	Slow growth, normal pattern	
NUC1	Slow growth; pointed leaves	rDNA binding; more 35S	*SALK_002764*	Comparable to WT	(Petricka et al. 2007; Pontvianne et al. 2007)
			SALK_053590	Slow growth, normal pattern	
NUFIP	Slow growth; pointed leaves; less seeds production	rRNA methylation; uncertain rRNA intermediate accumulation	*SALK_134962*	Slow growth, normal pattern	(Rodor et al. 2011)
PRMT3	Pointed leaves	More 32S, 27SB, 18S-A, 7S; polyadenylated 18S-A3 and 27SB	*SAIL_220_F08*	Slow growth, ectopic non-hair cells	(Hang et al. 2014)
			WISCDSLOX391A01	Slow growth, ectopic non-hair cells	
RH57	Sensitive to glucose	Uncertain rRNA accumulationi ntermediate	*SALK_008887;*	Slow growth, normal pattern	(Hsu et al. 2014)
			SALK_019721		
RRP6L2	Comparable to WT	More P-P1;	*SALK_113786*	Slow growth, normal pattern	(Lange et al. 2008)
RTL2	NA	3'ETS cleavage	*CS855416*	Comparable to WT	(Comella et al. 2008)

RRP46 (*AT3G46210* in Arabidopsis)	Studied in Barley	More 7S pre-rRNA	*SALK_092163;SALK_109890*	Comparable to WT	(Xi et al. 2009)
XRN2	Comparable to WT	More polyA-rRNA	*SALK_114258*	Slow growth, normal pattern	(Zakrzewska-Placzek et al. 2010)

Table 3.2 Primers used for genotyping and cloning.

Experiment	Name		Primer sequence
Genotyping	*apum23-4*_SspI	FP	tcctgaaaaagatacacccaaa
		RP	gaaacactccgaattcgaatat
Cloning	*APUM23::APUM23-GFP*	FP	caccttaggcggctaattttgt
		RP	gtcgacaattctcattttatttgaatgccg
		P1	ggaaacagctatgaccatgattacgggcaagaactgagcaacttg
		P2	agctccacctccacctcctgaggctgggggtcttttg
		P3	agcctcaggaggtggaggtggagctatggtgagcaagggcga
		P4	ccacagttccttcagttatctacttgtacagctcgtccatg
		P5	cgagctgtacaagtagataactgaaggaactgtggacagtagtg
	FIB1::FIB1-mcherry	P6	acgtgtcagttatctagatccggtgcaatacttaaaaatgcgctaccgatg

Chapter 4

Conclusions and Future Directions

Summary of discoveries

My Ph.D. research began with two *cpc-1* 'enhancer' mutants arising from the

same genetic screening but ended up addressing very different aspects of the root

epidermal cell specification in Arabidopsis.

My first research project, described in Chapter 2, dissects the functions of the

D105 residue of the WER protein. One of my findings is specifically intriguing by

showing that different substitutions of D105 affect WER functions in different ways.

Further functional analysis of the new WER variants (D105E, D105A, and D105Q) in the

future could provide insights into how WER binds to the promoter regions of its target

genes and/or associates with GL3/EGL3. On the other hand, my investigation of the

phenotypes caused by these D105 substitutions reveals the importance of the balanced

production of various cell fate regulators for robust cell fate establishment in root

epidermis. Specifically, my research provides direct evidence for the long-hypothesized

model that the relative protein production of WER versus CPC defines the root-hair or

non-hair cell fate (Song et al. 2011; Schiefelbein et al. 2014): the D105N substitution in

WER weakens *CPC* transcription, and less CPC production leads to insufficient lateral

inhibition in the H-position cells and disrupted distribution of root-hair and non-hair cells;

the D105Q substitution in WER enhances *CPC* transcription, and excessive CPC

production leads to ectopic inhibition of WER function in the N-position cells and ectopic root-hair cell formation.

My second project, described in Chapter 3, explores the molecular connections between root epidermal cell specification and ribosome biogenesis. The ectopic non-hair cell fate establishment in plants carrying ribosomal defects has been observed for many years, since the discovery of the RBF mutant *dim1a* (Wieckowski et al. 2012), but the molecular basis underlying this effect remained unclear. My research initially characterized another RBF mutant *apum23-4* and eventually expanded to multiple RBF mutants (including *dim1a*) and drug-treated plants that show similar root epidermis phenotypes. The ANAC082-MYB23 regulatory module discovered in my research not only provides answers to these phenotypes, but also suggests that the switch from root-hair to non-hair cell fate is programmed as a response to defective ribosome biogenesis. The ribosomal stresses, identified and studied mostly in animal cells, lead to cell division arrest and apoptosis mediated by p53 (Lior Golomb et al. 2014). In plants, reports on cellular responses to defective ribosome biogenesis are largely lacking except the finding of ANAC082 as the critical mediator for cell division arrest (Ohbayashi et al. 2017a; Salome 2017). To our best knowledge, my research provides the first explanation for a cell fate switch as one of the stress-responding events that plants use to cope with ribosomal defects. My study also adds new insights into the function of ANAC082 by showing that it regulates multiple cellular activities. Though there is no direct evidence available yet, *MYB23* could be one direct target gene of ANAC082.

More functional studies of the WER protein

My research in Chapter 2 gives rise to a series of WER variants carrying significant functional alterations, thus providing useful materials for functional studies on the WER protein as a transcription factor. My preliminary characterizations of these variants have revealed several interesting features, but more detailed studies are needed to fully understand them. EMSA and yeast two-hybrid assays would be valuable to test how each D105 substitution alters WER's ability to bind to DNA sequences and/or to associate with its bHLH partners. Given that the D105A and D105Q substitutions enhance induction of *GL2* and *CPC* transcription, these are less likely to impair WER protein functions. It is therefore interesting to determine whether the D105E substitution, which depletes *GL2* and *CPC* expression, abolishes WER-DNA interaction or WER-GL3 interaction (or both). On the other hand, given that both D105A and D105Q substitutions presumably enhance WER function, further analysis could focus on distinguishing whether this enhancement is due to stronger association with GL3 or stronger DNA binding. Quantitative EMSA and yeast two-hybrid experiments may be able to answer this question. Specifically, competitive EMSA experiments can be used to test whether D105A and D105Q substitutions cause greater effects on *CPC* promoter binding compared to *GL2* (which is the case for the D105N substitution).

Critical as it is for root epidermal cell specification, the WER protein has not been studied structurally except through motif swapping (Tominaga et al. 2007; Tominaga-Wada et al. 2012). Nevertheless, the similarity between the R2R3 domain of WER and that of the mammalian c-Myb makes it possible to predict the structure of WER R2R3 domain (Ogata et al. 1994). One potential future study could focus on structural analysis

of WER by employing the iterative threading assembly refinement (I-TASSER) approach, which takes advantage of the crystal structure of closely related proteins (in my case the mammalian c-Myb protein R2R3 domain) to predict the structure and function of unknown proteins (Roy et al. 2010; Yang et al. 2015a; Yang et al. 2015b). The D105 substitutions 'engineered' in Chapter II could then be incorporated into the predicted WER structure model to test their influences on WER structure.

Further investigation of ANAC082 function in root epidermis

My research in Chapter 3 highlights the role of ANAC082 in the root epidermal cell fate switch in response to impaired ribosome biogenesis, but several questions remain to be further addressed.

First, the activation of ANAC082 in the root epidermis in response to ribosomal defects is unclear. As is stated in Chapter III, *ANAC082* transcription in root tissue is elevated by ribosomal defects (Ohbayashi et al. 2017a), but no detailed examination of root epidermis was conducted. Therefore, it remains to be studied whether and how ANAC082 is activated in the root epidermis of RBF mutants (*apum23-4*, *dim1a*, or *prmt3-1*). A combined analysis of the transcriptional and translational reporters of *ANAC082* (i.e. *ANAC082::GUS* and *ANAC082::ANAC082-mcherry*) in the root epidermis of RBF mutants is clearly needed. Specifically, examining *ANAC082::ANAC082-mcherry* and *MYB23::GUS*/*MYB23::MYB23-GFP* within one single root of *apum23-4* or *wer-1 apum23-4* should help to assess the correlation between ANAC082 activation and *MYB23* upregulation.

Additionally, the hypothesized uORF in the *ANAC082* transcript has not been characterized (Ohbayashi et al. 2017b). One interesting experiment would be to

construct an *ANAC082* transgene carrying a mutated start codon in its uORF and transform it into the *anac082* mutants (*anac082-1*, *anac082-6*, or *GABI_282H08*) or wild-type plants. If the role of uORF is to repress *ANAC082* mORF translation when ribosome biogenesis is intact, the transformed plants should have constitutive ANAC082 protein production and therefore exhibit the phenotypes resembling RBF mutants (*apum23-4*, *dim1a*, or *prmt3-1*).

Furthermore, it remains unknown whether and how ANAC082, as a NAC transcription factor family member with transactivation potentials (Ohbayashi et al. 2017a), functions as a transcription factor. ANAC082 activation causes retarded root growth and tissue regeneration (Ohbayashi et al. 2017a). Therefore, ANAC082 is likely to slow down or even arrest cell cycle. However, the potential cell cycle regulator(s) downstream of ANAC082 remains unknown. My research in Chapter III identified an additional role of ANAC082 in mediating non-hair cell specification via upregulating *MYB23* expression. Therefore, an important question would be whether *MYB23* is directly regulated by ANAC082. One previous study made use of *in vitro* protein binding microarrays (PBMs) to identify the DNA-binding specificities of 12 NAC family transcription factors (Lindemose et al. 2014). Among the tested NAC proteins, ANAC082 is closely related to ANAC040 (Podzimska-Sroka et al. 2015), which exhibits a significant specificity to DNA sequences containing the TTTCCTT motif (Lindemose et al. 2014). Notably, the *MYB23* promoter region contains this motif at -792 ~ -798 relative to the transcription start site (Figure 4.1). An electrophoretic mobility shift assay (EMSA) could be used to test whether ANAC082 binds to this *MYB23* promoter region. Follow-up *in vivo* analysis (e.g. chromatin immunoprecipitation, ChIP) could be conducted

156

using the *ANAC082::ANAC082-mcherry* transgenic line under the *apum23-4* or *wer-1*

apum23-4 mutant background. Potentially, this study could be expanded to a search for

ANAC082 target genes using ChIP-seq and might help to identify the potential cell cycle

regulators downstream of ANAC082.

Relationship between ribosome and root epidermis development

In Chapter 3, I argued that the ectopic production of non-hair cells are linked to a

general defect in ribosome biogenesis rather than particular RBF mutants by

demonstrating that mutants of three functionally independent RBFs (APUM23, DIM1A,

and PRMT3) all exhibited this phenotype. However, it notable that mutants of 12 other

RBFs tested in Chapter III exhibited normal root hair patterning. Therefore, it is

interesting to consider why certain RBF mutants disrupt root epidermis patterning while

others do not. One potential answer to this question is that the onset of ectopic non-hair

cell production is dependent on the 'severeness' of ribosomal defects caused by the

RBF mutants. This hypothesis originates from my primary data showing that one RBF

mutants I tested, *mtr4*, showed a slightly increased proportion of ectopic non-hair cells

and a mild increase of *GL2::GUS* expression in its double mutants with *wer-1* (Figure

4.2, A and B). Notably, the *mtr4* mutant exhibited less affected seed germination and

root hair length compared to *apum23-4* (or *dim1a* and *prmt3-1*) (Figure 4.2, C and D).

Several additional experiments are needed to validate these observations, including the

generation of *mtr4 myb23-1*, *mtr4 wer-1 myb23-1*, and *mtr4 anac082-1* mutants.

Nevertheless, the current results suggest that production of ectopic non-hair cells could

be universally triggered in RBF mutant, but is only discernable in these RBF mutants

causing significant impacts in plant growth. To further address this possibility, I

generated the *apum23-4 dim1a* double mutant to test for potential additive or synergic effects. However, this double mutant totally distorted root architecture and made the root epidermis impossible to examine. A possible alternative experiment is to generate the *apum23-4* (or *dim1a* and *prmt3-1*) *mtr4* double mutant and look for synergic interactions between the two RBF mutants.

In the discussion session of Chapter 3, I proposed that the retarded cell division, delayed plant growth, and ectopic production of non-hair cells in roots are mediated by ANAC082 as a strategy to cope with ribosomal defects. However, this hypothesis conflicts with the fact that the *apum23-4 anac082-1* and *dim1a anac082-1* double mutants showed no disadvantageous plant growth or plant flowering phenotypes, therefore casting doubt on the necessity of having a ribosomal stress responding mechanism. One possibility is that the defective ribosome biogenesis in *apum23-4* and *dim1a*, though failing to reach the optimal ribosomal requirements (which triggers ANAC082 activation (Ohbayashi et al. 2017a)), still manages to provide enough ribosomes for plant growth under normal growth conditions. In this case, the *apum23-4 anac082-1* and *dim1a anac082-1* double mutants could be less resistant to challenging growth conditions. Thus, an interesting future study could compare the fitness of *apum23-4 anac082-1* (or *dim1a anac082-1*) to *apum23-4* (or *dim1a*) under ribosome-unfavorable conditions such as nutrition deprivation and heat (Mayer et al. 2005).

My research in Chapter 3 mainly focused on characterizing RBF mutants. As is stated in Chapter I, mutants of RBFs and RPs have highly overlapped developmental impacts, and ANAC082 is also required for the pointed-leaf phenotypes in RP mutants (Ohbayashi et al. 2017a). Therefore, a future study could examine reported RP mutants

for root epidermal patterning disruptions. So far I have tested mutants of 6 RPs but all exhibited wild-type root hair patterning (Table 4.1). Tests on mutants of a wider range of RPs could be conducted in the future.

My examination of the *apum24-2* mutant suggested the existence of a MYB23-independent mechanism to induce ectopic non-hair cell formation. A further study could focus on uncovering the molecular basis underlying this special RBF mutant. The fact that *wer-1 apum24-2* and *gl3 egl3 apum24-2* both depleted non-hair cells in the H position suggested that both WER and GL3/EGL3 could be potential candidates for mediating this phenotype. Meanwhile, the *apum24-2 ttg-1* double mutant needs to be generated to determine whether TTG1 is also a possible candidate. It is still interesting that the *wer-1 apum24-2* double mutant exhibited significant *GL2::GUS* and non-hair cells in the N-position cells, but the biological rationale of additional non-hair cell fate enforcement in the *apum24-2* mutant is unclear.

Materials and methods

The *mtr4* mutant line was obtained from the ABRC (*SALK_204906*). *GL2::GUS* histochemical staining, quantification of root epidermal cell specification, and root hair length measurement were conducted similarly as described in Chapter 3.

159
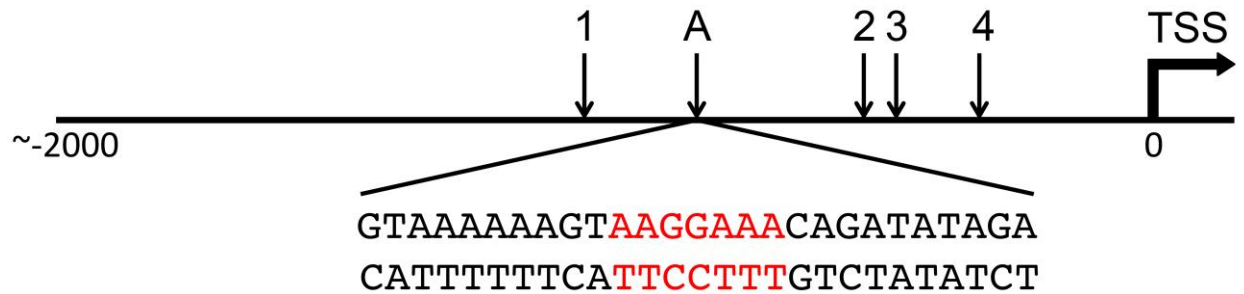
Figure 4.1 The schematic figure showing the promoter region of the *MYB23* gene. TSS stands for transcription start site. The numbers 1-4 indicate the positions of the reported WER binding sites within *MYB23* promoter regions (Kang et al. 2009). Notably, *in vivo* studies reveal that mutation of WER binding site 1 causes dramatic decrease of *MYB23* expression, while mutations of the other three WER binding sites causes no significant affects (Kang et al. 2009). The letter A indicates the position of the optimal binding motif of the ANAC040 protein that is closely related to ANAC082.
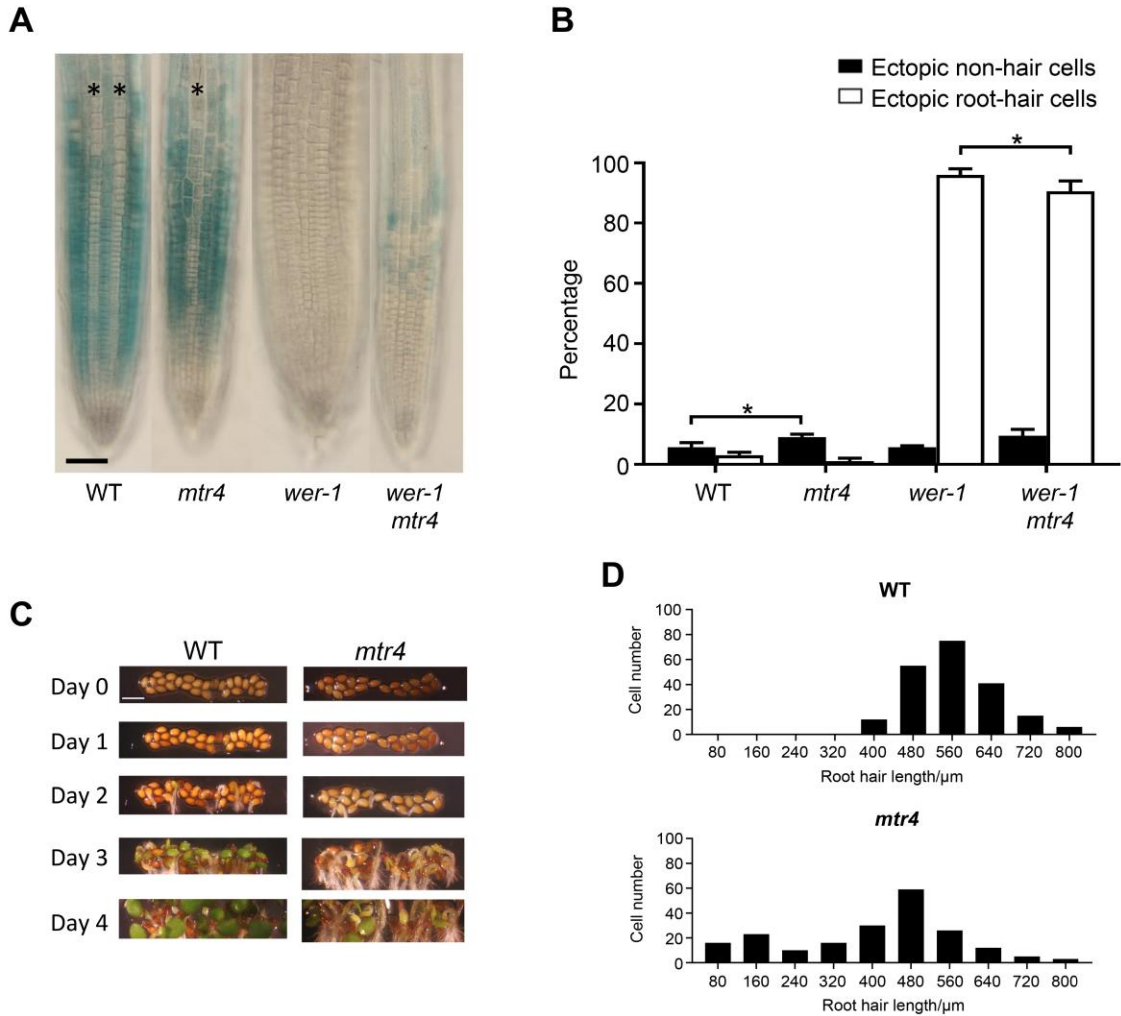
Figure 4.2 Analysis of a RBF mutant *mtr4* showing mild phenotypic impacts.
(A) Expression of *GL2::GUS* in wild-type plants and multiple mutant lines. Bar=50μm.
(B) Quantification of root epidermal cell specification in wild-type plants and multiple
mutant lines. Error bars represent the standard deviations from three replicates. The
statistical significance is determined using one-way ANOVA. * represents $p<0.05$. (C)
Germination of wild-type seeds and *mtr4* seeds at different time points after sowing. (D)
Histograms showing the root hair length distribution of wild-type and *mtr4* plants
(n=200). 10 mature root hairs from each root are measured and 20 roots are measured
for each genotype.

Table 4.1 A list of the RB mutants tested so far (reviewed in (Byrne 2009)).

Gene name*	Reported phenotype	Tested lines	References
RPS18A	Reduced plant size, pointed leaves	*CS5208, CS904411, CS808190*	(Van Lijsebettens et al. 1994)
RPL5A	Reduced male and female transmission, pointed leaves	*SALK_089798*	(Pinon et al. 2008)
RPL10aB	Pointed leaves	*SALK_054323, CS875228*	(Pinon et al. 2008)
RPL23aB	No reported phenotypes	*CS825442, CS807041, CS820434*	(Degenhardt et al. 2008)
RPL24B	Pointed leaves; abnormal cotyledon and leaf vascular patterns	*CS11180, CS6957, CS854347*	(Nishimura et al. 2005)
RPL28A	Pointed leaves	*SALK_138179, CS825981*	(Yao et al. 2008)

* RPS represents ribosomal protein small subunit and RPL represents ribosomal protein large subunit.

REFERENCES

Abbasi N, Kim H B, Park N I, Kim H S, Kim Y K, Park Y I, Choi S B (2010) APUM23, a nucleolar Puf domain protein, is involved in pre-ribosomal RNA processing and normal growth patterning in Arabidopsis. Plant J 64: 960-76

Abou-Ellail M, Cooke R, Saez-Vasquez J (2011) Variations in a team: major and minor variants of Arabidopsis thaliana rDNA genes. Nucleus 2: 294-9

Ahn C S, Cho H K, Lee D H, Sim H J, Kim S G, Pai H S (2016) Functional characterization of the ribosome biogenesis factors PES, BOP1, and WDR12 (PeBoW), and mechanisms of defective cell growth and proliferation caused by PeBoW deficiency in Arabidopsis. J Exp Bot 67: 5217-32

Aitken C E, Lorsch J R (2012) A mechanistic overview of translation initiation in eukaryotes. Nat Struct Mol Biol 19: 568-76

Balkunde R, Pesch M, Hulskamp M (2010) Trichome patterning in Arabidopsis thaliana from genetic to molecular models. Curr Top Dev Biol 91: 299-321

Barakat A, Szick-Miranda K, Chang I F, Guyot R, Blanc G, Cooke R, Delseny M, Bailey-Serres J (2001) The organization of cytoplasmic ribosomal protein genes in the Arabidopsis genome. Plant Physiol 127: 398-415

Bargmann B O, Vanneste S, Krouk G, Nawy T, Efroni I, Shani E, Choe G, Friml J, Bergmann D C, Estelle M, Birnbaum K D (2013) A map of cell type-specific auxin responses. Mol Syst Biol 9: 688

Bates T R, Lynch J P (1996) Stimulation of root hair elongation in Arabidopsis thaliana by low phosphorus availability. Plant, Cell & Environment 19: 529-538

Bell C J, Ecker J R (1994) Assignment of 30 microsatellite loci to the linkage map of Arabidopsis. Genomics 19: 137-44

Benfey P N, Scheres B (2000) Root development. Curr Biol 10: R813-5

Berger F, Haseloff J, Schiefelbein J, Dolan L (1998a) Positional information in root epidermis is defined during embryogenesis and acts in domains with strict boundaries. Curr Biol 8: 421-30

Berger F, Hung C Y, Dolan L, Schiefelbein J (1998b) Control of cell division in the root epidermis of Arabidopsis thaliana. Dev Biol 194: 235-45

Berger F, Linstead P, Dolan L, Haseloff J (1998c) Stomata patterning on the hypocotyl of Arabidopsis thaliana is controlled by genes involved in the control of root epidermis patterning. Dev Biol 194: 226-34

Berna G, Robles P, Micol J L (1999) A mutational analysis of leaf morphogenesis in Arabidopsis thaliana. Genetics 152: 729-42

Bernhardt C, Lee M M, Gonzalez A, Zhang F, Lloyd A, Schiefelbein J (2003) The bHLH genes GLABRA3 (GL3) and ENHANCER OF GLABRA3 (EGL3) specify epidermal cell fate in the Arabidopsis root. Development 130: 6431-9

Bernhardt C, Zhao M, Gonzalez A, Lloyd A, Schiefelbein J (2005) The bHLH genes GL3 and EGL3 participate in an intercellular regulatory circuit that controls cell patterning in the Arabidopsis root epidermis. Development 132: 291-8

Beziat C, Kleine-Vehn J, Feraru E (2017) Histochemical Staining of beta-Glucuronidase and Its Spatial Quantification. Methods Mol Biol 1497: 73-80

Borovjagin A V, Gerbi S A (1999) U3 small nucleolar RNA is essential for cleavage at sites 1, 2 and 3 in pre-rRNA and determines which rRNA processing pathway is taken in Xenopus oocytes. J Mol Biol 286: 1347-63

Boudonck K, Dolan L, Shaw P J (1998) Coiled body numbers in the Arabidopsis root epidermis are regulated by cell type, developmental stage and cell cycle parameters. J Cell Sci 111 (Pt 24): 3687-94

Brown J W, Echeverria M, Qu L H (2003) Plant snoRNAs: functional evolution and new modes of gene expression. Trends Plant Sci 8: 42-9

Brown J W, Shaw P J (1998) Small nucleolar RNAs and pre-rRNA processing in plants. Plant Cell 10: 649-57

Bruex A, Kainkaryam R M, Wieckowski Y, Kang Y H, Bernhardt C, Xia Y, Zheng X, Wang J Y, Lee M M, Benfey P, Woolf P J, Schiefelbein J (2012) A gene regulatory network for root epidermis cell differentiation in Arabidopsis. PLoS Genet 8: e1002446

Byrne M E (2009) A role for the ribosome in development. Trends Plant Sci 14: 512-9

Caparros-Ruiz D, Lahmy S, Piersanti S, Echeverria M (1997) Two ribosomal DNA-binding factors interact with a cluster of motifs on the 5' external transcribed spacer, upstream from the primary pre-rRNA processing site in a higher plant. Eur J Biochem 247: 981-9

Chandrasekhara C, Mohannath G, Blevins T, Pontvianne F, Pikaard C S (2016) Chromosome-specific NOR inactivation explains selective rRNA gene silencing and dosage control in Arabidopsis. Genes Dev 30: 177-90

Chandrika N N, Sundaravelpandian K, Yu S M, Schmidt W (2013) ALFIN-LIKE 6 is involved in root hair elongation during phosphate deficiency in Arabidopsis. New Phytol 198: 709-20

Chau K F, Shannon M L, Fame R M, Fonseca E, Mullan H, Johnson M B, Sendamarai A K, Springel M W, Laurent B, Lehtinen M K (2018) Downregulation of ribosome biogenesis during early forebrain development. Elife 7

Cheng Y, Zhu W, Chen Y, Ito S, Asami T, Wang X (2014) Brassinosteroids control root epidermal cell fate via direct regulation of a MYB-bHLH-WD40 complex by GSK3-like kinases. Elife

Ciganda M, Williams N (2011) Eukaryotic 5S rRNA biogenesis. Wiley Interdiscip Rev RNA 2: 523-33

Cloix C, Tutois S, Mathieu O, Cuvillier C, Espagnol M C, Picard G, Tourmente S (2000) Analysis of 5S rDNA arrays in Arabidopsis thaliana: physical mapping and chromosome-specific polymorphisms. Genome Res 10: 679-90

Cloix C, Yukawa Y, Tutois S, Sugiura M, Tourmente S (2003) In vitro analysis of the sequences required for transcription of the Arabidopsis thaliana 5S rRNA genes. Plant J 35: 251-61

Clough S J, Bent A F (1998) Floral dip: a simplified method for Agrobacterium-mediated transformation of Arabidopsis thaliana. Plant J 16: 735-43

Clowes F A L (2000) Pattern in root meristem development in angiosperms. New Phytologist 146: 83-94

Comella P, Pontvianne F, Lahmy S, Vignols F, Barbezier N, Debures A, Jobet E, Brugidou E, Echeverria M, Saez-Vasquez J (2008) Characterization of a ribonuclease III-like protein required for cleavage of the pre-rRNA in the 3'ETS in Arabidopsis. Nucleic Acids Res 36: 1163-75

Copenhaver G P, Doelling J H, Gens S, Pikaard C S (1995) Use of RFLPs larger than 100 kbp to map the position and internal organization of the nucleolus organizer region on chromosome 2 in Arabidopsis thaliana. Plant J 7: 273-86

Copenhaver G P, Pikaard C S (1996) RFLP and physical mapping with an rDNA-specific endonuclease reveals that nucleolus organizer regions of Arabidopsis thaliana adjoin the telomeres on chromosomes 2 and 4. Plant J 9: 259-72

Costa S, Shaw P (2006) Chromatin organization and cell fate switch respond to positional information in Arabidopsis. Nature 439: 493-6

Creff A, Sormani R, Desnos T (2010) The two Arabidopsis RPS6 genes, encoding for cytoplasmic ribosomal proteins S6, are functionally equivalent. Plant Mol Biol 73: 533-46

Cvrckova F, Bezvoda R, Zarsky V (2010) Computational identification of root hair-specific genes in Arabidopsis. Plant Signal Behav 5: 1407-18

Dalla Venezia N, Vincent A, Marcel V, Catez F, Diaz J-J (2019) Emerging Role of Eukaryote Ribosomes in Translational Control. International Journal of Molecular Sciences 20

Dalla Venezia N, Vincent A, Marcel V, Catez F, Diaz J J (2019) Emerging Role of Eukaryote Ribosomes in Translational Control. Int J Mol Sci 20

de Kloet S R (1966) Ribonucleic acid synthesis in yeast. The effect of cycloheximide on the synthesis of ribonucleic acid in Saccharomyces carlsbergensis. Biochem J 99: 566-81

De Smet I, Lau S, Mayer U, Jurgens G (2010) Embryogenesis - the humble beginnings of plant life. Plant J 61: 959-70

Decatur W A, Fournier M J (2002) rRNA modifications and ribosome function. Trends Biochem Sci 27: 344-51

Degenhardt R F, Bonham-Smith P C (2008) Arabidopsis ribosomal proteins RPL23aA and RPL23aB are differentially targeted to the nucleolus and are disparately required for normal development. Plant Physiol 147: 128-42

Dez C, Tollervey D (2004) Ribosome synthesis meets the cell cycle. Curr Opin Microbiol 7: 631-7

Dieci G, Preti M, Montanini B (2009) Eukaryotic snoRNAs: a paradigm for gene expression flexibility. Genomics 94: 83-8

Doelling J H, Pikaard C S (1995) The minimal ribosomal RNA gene promoter of Arabidopsis thaliana includes a critical element at the transcription initiation site. Plant J 8: 683-92

Doerner P (1998) Root development: quiescent center not so mute after all. Curr Biol 8: R42-4

Dolan L, Janmaat K, Willemsen V, Linstead P, Poethig S, Roberts K, Scheres B (1993) Cellular organisation of the Arabidopsis thaliana root. Development 119: 71-84

Dubos C, Stracke R, Grotewold E, Weisshaar B, Martin C, Lepiniec L (2010) MYB transcription factors in Arabidopsis. Trends Plant Sci 15: 573-81

Duckett C M, Grierson C, Linstead P, Schneider K, Lawson E, Dean C, Poethig S, Roberts K (1994) Clonal relationships and cell patterning in the root epidermis of Arabidopsis. Development 120: 2465

Ebersberger I, Simm S, Leisegang M S, Schmitzberger P, Mirus O, von Haeseler A, Bohnsack M T, Schleiff E (2014) The evolution of the ribosome biogenesis pathway from a yeast perspective. Nucleic Acids Res 42: 1509-23

Ebina I, Takemoto-Tsutsumi M, Watanabe S, Koyama H, Endo Y, Kimata K, Igarashi T, Murakami K, Kudo R, Ohsumi A, Noh A L, Takahashi H, Naito S, Onouchi H (2015) Identification of novel Arabidopsis thaliana upstream open reading frames that control expression of the main coding sequences in a peptide sequence-dependent manner. Nucleic Acids Res 43: 1562-76

Edwards T A, Pyle S E, Wharton R P, Aggarwal A K (2001) Structure of Pumilio reveals similarity between RNA and peptide binding motifs. Cell 105: 281-9

Ernst H A, Olsen A N, Larsen S, Lo Leggio L (2004) Structure of the conserved domain of ANAC, a member of the NAC family of transcription factors. EMBO Rep 5: 297-303

Estelle M A, Somerville C (1987) Auxin-resistant mutants of Arabidopsis thaliana with an altered morphology. Molecular and General Genetics MGG 206: 200-206

Fatica A, Cronshaw A D, Dlakic M, Tollervey D (2002) Ssf1p prevents premature processing of an early pre-60S ribosomal particle. Mol Cell 9: 341-51

Fatica A, Oeffinger M, Dlakic M, Tollervey D (2003) Nob1p is required for cleavage of the 3' end of 18S rRNA. Mol Cell Biol 23: 1798-807

Feng Y, Xu P, Li B, Li P, Wen X, An F, Gong Y, Xin Y, Zhu Z, Wang Y, Guo H (2017) Ethylene promotes root hair growth through coordinated EIN3/EIL1 and RHD6/RSL1 activity in Arabidopsis. Proc Natl Acad Sci U S A 114: 13834-13839

Fisher A P, Sozzani R (2016) Uncovering the networks involved in stem cell maintenance and asymmetric cell division in the Arabidopsis root. Curr Opin Plant Biol 29: 38-43

Fong H K, Hurley J B, Hopkins R S, Miake-Lye R, Johnson M S, Doolittle R F, Simon M I (1986) Repetitive segmental structure of the transducin beta subunit: homology with the CDC4 gene and identification of related mRNAs. Proc Natl Acad Sci U S A 83: 2162-6

Francischini C W, Quaggio R B (2009) Molecular characterization of Arabidopsis thaliana PUF proteins--binding specificity and target candidates. FEBS J 276: 5456-70

Gabrielsen O S, Sentenac A, Fromageot P (1991) Specific DNA binding by c-Myb: evidence for a double helix-turn-helix-related motif. Science 253: 1140-3

Gallie D R, Le H, Caldwell C, Tanguay R L, Hoang N X, Browning K S (1997) The phosphorylation state of translation initiation factors is regulated developmentally and following heat shock in wheat. J Biol Chem 272: 1046-53

Galway M E, Masucci J D, Lloyd A M, Walbot V, Davis R W, Schiefelbein J W (1994) The TTG gene is required to specify epidermal cell fate and cell patterning in the Arabidopsis root. Dev Biol 166: 740-54

Garcia-Gomez J J, Fernandez-Pevida A, Lebaron S, Rosado I V, Tollervey D, Kressler D, de la Cruz J (2014) Final pre-40S maturation depends on the functional integrity of the 60S subunit ribosomal protein L3. PLoS Genet 10: e1004205

Gendreau E, Traas J, Desnos T, Grandjean O, Caboche M, Hofte H (1997) Cellular basis of hypocotyl growth in Arabidopsis thaliana. Plant Physiol 114: 295-305

Gerstberger S, Meyer C, Benjamin-Hong S, Rodriguez J, Briskin D, Bognanni C, Bogardus K, Steller H, Tuschl T (2017) The Conserved RNA Exonuclease Rexo5 Is Required for 3' End Maturation of 28S rRNA, 5S rRNA, and snoRNAs. Cell Rep 21: 758-772

Giavalisco P, Wilson D, Kreitler T, Lehrach H, Klose J, Gobom J, Fucini P (2005) High heterogeneity within the ribosomal proteins of the Arabidopsis thaliana 80S ribosome. Plant Mol Biol 57: 577-91

Golomb L, Volarevic S, Oren M (2014) p53 and ribosome biogenesis stress: the essentials. FEBS Lett 588: 2571-9

Golomb L, Volarevic S, Oren M (2014) p53 and ribosome biogenesis stress: The essentials. FEBS Letters 588: 2571-2579

Gonzalez A, Zhao M, Leavitt J M, Lloyd A M (2008) Regulation of the anthocyanin biosynthetic pathway by the TTG1/bHLH/Myb transcriptional complex in Arabidopsis seedlings. Plant J 53: 814-27

Grandi P, Rybin V, Bassler J, Petfalski E, Strauss D, Marzioch M, Schafer T, Kuster B, Tschochner H, Tollervey D, Gavin A C, Hurt E (2002) 90S pre-ribosomes include the 35S pre-rRNA, the U3 snoRNP, and 40S subunit processing factors but predominantly lack 60S synthesis factors. Mol Cell 10: 105-15

Grant C M, Hinnebusch A G (1994) Effect of sequence context at stop codons on efficiency of reinitiation in GCN4 translational control. Mol Cell Biol 14: 606-18

Grierson C, Schiefelbein J (2002) Root hairs. Arabidopsis Book 1: e0060

Gruendler P, Unfried I, Pascher K, Schweizer D (1991) rDNA intergenic region from Arabidopsis thaliana. Structural analysis, intraspecific variation and functional implications. J Mol Biol 221: 1209-22

Hang R, Liu C, Ahmad A, Zhang Y, Lu F, Cao X (2014) Arabidopsis protein arginine methyltransferase 3 is required for ribosome biogenesis by affecting precursor ribosomal RNA processing. Proc Natl Acad Sci U S A 111: 16190-5

Hang R, Wang Z, Deng X, Liu C, Yan B, Yang C, Song X, Mo B, Cao X (2018) Ribosomal RNA Biogenesis and Its Response to Chilling Stress in Oryza sativa. Plant Physiol 177: 381-397

Hao L, Wei X, Zhu J, Shi J, Liu J, Gu H, Tsuge T, Qu L J (2017) SNAIL1 is essential for female gametogenesis in Arabidopsis thaliana. J Integr Plant Biol 59: 629-641

Harscoet E, Dubreucq B, Palauqui J C, Lepiniec L (2010) NOF1 encodes an Arabidopsis protein involved in the control of rRNA expression. PLoS One 5: e12829

Haupt Y, Maya R, Kazaz A, Oren M (1997) Mdm2 promotes the rapid degradation of p53. Nature 387: 296-9

Henras A K, Soudet J, Gerus M, Lebaron S, Caizergues-Ferrer M, Mougin A, Henry Y (2008) The post-transcriptional steps of eukaryotic ribosome biogenesis. Cell Mol Life Sci 65: 2334-59

Hinnebusch A G (1994) Translational control of GCN4: an in vivo barometer of initiation-factor activity. Trends Biochem Sci 19: 409-14

Hinnebusch A G, Lorsch J R (2012) The mechanism of eukaryotic translation initiation: new insights and challenges. Cold Spring Harb Perspect Biol 4

Horiguchi G, Mollá-Morales A, Pérez-Pérez J M, Kojima K, Robles P, Ponce M R, Micol J L, Tsukaya H (2011) Differential contributions of ribosomal protein genes to Arabidopsis thaliana leaf development. The Plant Journal 65: 724-736

Horiguchi G, Van Lijsebettens M, Candela H, Micol J L, Tsukaya H (2012) Ribosomes and translation in plant developmental control. Plant Sci 191-192: 24-34

Hsu P Y, Calviello L, Wu H L, Li F W, Rothfels C J, Ohler U, Benfey P N (2016) Super-resolution ribosome profiling reveals unannotated translation events in Arabidopsis. Proc Natl Acad Sci U S A 113: E7126-E7135

Hsu Y F, Chen Y C, Hsiao Y C, Wang B J, Lin S Y, Cheng W H, Jauh G Y, Harada J J, Wang C S (2014) AtRH57, a DEAD-box RNA helicase, is involved in feedback inhibition of glucose-mediated abscisic acid accumulation during seedling development and additively affects pre-ribosomal RNA processing with high glucose. Plant J 77: 119-35

Huang L, Schiefelbein J (2015) Conserved Gene Expression Programs in Developing Roots from Diverse Plants. Plant Cell 27: 2119-32

Huang L, Shi X, Wang W, Ryu K H, Schiefelbein J (2017) Diversification of Root Hair Development Genes in Vascular Plants. Plant Physiol 174: 1697-1712

Huang T, Kerstetter R A, Irish V F (2014) APUM23, a PUF family protein, functions in leaf development and organ polarity in Arabidopsis. J Exp Bot 65: 1181-91

Hughes J M, Ares M, Jr. (1991) Depletion of U3 small nucleolar RNA inhibits cleavage in the 5' external transcribed spacer of yeast pre-ribosomal RNA and impairs formation of 18S ribosomal RNA. EMBO J 10: 4231-9

Hulskamp M (2004) Plant trichomes: a model for cell differentiation. Nat Rev Mol Cell Biol 5: 471-80

Hulskamp M, Misra S, Jurgens G (1994) Genetic dissection of trichome cell development in Arabidopsis. Cell 76: 555-66

Hummel M, Dobrenel T, Cordewener J J, Davanture M, Meyer C, Smeekens S J, Bailey-Serres J, America T A, Hanson J (2015) Proteomic LC-MS analysis of Arabidopsis cytosolic ribosomes: Identification of ribosomal protein paralogs and re-annotation of the ribosomal protein genes. J Proteomics 128: 436-49

Hung C Y, Lin Y, Zhang M, Pollock S, Marks M D, Schiefelbein J (1998) A common position-dependent mechanism controls cell-type patterning and GLABRA2 regulation in the root and hypocotyl epidermis of Arabidopsis. Plant Physiol 117: 73-84

Jackson R J, Hellen C U, Pestova T V (2010) The mechanism of eukaryotic translation initiation and principles of its regulation. Nat Rev Mol Cell Biol 11: 113-27

Jander G, Norris S R, Rounsley S D, Bush D F, Levin I M, Last R L (2002) Arabidopsis map-based cloning in the post-genome era. Plant Physiol 129: 440-50

Janes G, von Wangenheim D, Cowling S, Kerr I, Band L, French A P, Bishopp A (2018) Cellular Patterning of Arabidopsis Roots Under Low Phosphate Conditions. Front Plant Sci 9: 735

Jia L, Clegg M T, Jiang T (2004) Evolutionary dynamics of the DNA-binding domains in putative R2R3-MYB genes identified from rice subspecies indica and japonica genomes. Plant Physiol 134: 575-85

Jin H, Martin C (1999) Multifunctionality and diversity within the plant MYB-gene family. Plant Mol Biol 41: 577-85

Jorgensen R A, Dorantes-Acosta A E (2012) Conserved Peptide Upstream Open Reading Frames are Associated with Regulatory Genes in Angiosperms. Front Plant Sci 3: 191

Kalinina N O, Makarova S, Makhotenko A, Love A J, Taliansky M (2018) The Multiple Functions of the Nucleolus in Plant Development, Disease and Stress Responses. Front Plant Sci 9: 132

Kanei-Ishii C, Sarai A, Sawazaki T, Nakagoshi H, He D N, Ogata K, Nishimura Y, Ishii S (1990) The tryptophan cluster: a hypothetical structure of the DNA-binding domain of the myb protooncogene product. J Biol Chem 265: 19990-5

Kang Y H, Kirik V, Hulskamp M, Nam K H, Hagely K, Lee M M, Schiefelbein J (2009) The MYB23 gene provides a positive feedback loop for cell fate specification in the Arabidopsis root epidermis. Plant Cell 21: 1080-94

Kang Y H, Song S K, Schiefelbein J, Lee M M (2013) Nuclear trapping controls the position-dependent localization of CAPRICE in the root epidermis of Arabidopsis. Plant Physiol 163: 193-204

Kidner C, Sundaresan V, Roberts K, Dolan L (2000) Clonal analysis of the Arabidopsis root confirms that position, not lineage, determines cell fate. Planta 211: 191-199

Kim B H, Cai X, Vaughn J N, von Arnim A G (2007) On the functions of the h subunit of eukaryotic initiation factor 3 in late stages of translation initiation. Genome Biol 8: R60

Kim G, Dhar S, Lim J (2017) The SHORT-ROOT regulatory network in the endodermis development of Arabidopsis roots and shoots. Journal of Plant Biology 60: 306-313

Kim H J, Park J H, Kim J, Kim J J, Hong S, Kim J, Kim J H, Woo H R, Hyeon C, Lim P O, Nam H G, Hwang D (2018) Time-evolving genetic networks reveal a NAC troika that negatively regulates leaf senescence in Arabidopsis. Proc Natl Acad Sci U S A 115: E4930-E4939

Kirik V, Lee M M, Wester K, Herrmann U, Zheng Z, Oppenheimer D, Schiefelbein J, Hulskamp M (2005) Functional diversification of MYB23 and GL1 genes in trichome morphogenesis and initiation. Development 132: 1477-85

Kirik V, Simon M, Huelskamp M, Schiefelbein J (2004) The ENHANCER OF TRY AND CPC1 gene acts redundantly with TRIPTYCHON and CAPRICE in trichome and root hair cell patterning in Arabidopsis. Dev Biol 268: 506-13

Kirik V, Simon M, Huelskamp M, Schiefelbein J (2004) The ENHANCER OF TRY AND CPC1 gene acts redundantly with TRIPTYCHON and CAPRICE in trichome and root hair cell patterning in Arabidopsis. Developmental Biology 268: 506-513

Konikkat S, Woolford J L, Jr. (2017) Principles of 60S ribosomal subunit assembly emerging from recent studies in yeast. Biochem J 474: 195-214

Koornneef M (1981) The complex syndrome of ttg mutants. Arab. Inf. Serv. 18: 45-51

Kornprobst M, Turk M, Kellner N, Cheng J, Flemming D, Kos-Braun I, Kos M, Thoms M, Berninghausen O, Beckmann R, Hurt E (2016) Architecture of the 90S Pre-ribosome: A Structural View on the Birth of the Eukaryotic Ribosome. Cell 166: 380-393

171

Kos-Braun I C, Jung I, Kos M (2017) Tor1 and CK2 kinases control a switch between alternative ribosome biogenesis pathways in a growth-dependent manner. PLoS Biol 15: e2000245

Kuai L, Fang F, Butler J S, Sherman F (2004) Polyadenylation of rRNA in Saccharomyces cerevisiae. Proc Natl Acad Sci U S A 101: 8581-6

Kubbutat M H, Jones S N, Vousden K H (1997) Regulation of p53 stability by Mdm2. Nature 387: 299-303

Kuppusamy K T, Chen A Y, Nemhauser J L (2009) Steroids are required for epidermal cell fate establishment in Arabidopsis roots. Proc Natl Acad Sci U S A 106: 8073-6

Kurata T, Ishida T, Kawabata-Awai C, Noguchi M, Hattori S, Sano R, Nagasaka R, Tominaga R, Koshino-Kimura Y, Kato T, Sato S, Tabata S, Okada K, Wada T (2005) Cell-to-cell movement of the CAPRICE protein in Arabidopsis root epidermal cell differentiation. Development 132: 5387-98

Kwak S H, Schiefelbein J (2007) The role of the SCRAMBLED receptor-like kinase in patterning the Arabidopsis root epidermis. Dev Biol 302: 118-31

Kwak S H, Schiefelbein J (2008) A feedback mechanism controlling SCRAMBLED receptor accumulation and cell-type pattern in Arabidopsis. Curr Biol 18: 1949-54

Kwak S H, Shen R, Schiefelbein J (2005) Positional signaling mediated by a receptor-like kinase in Arabidopsis. Science 307: 1111-3

LaCava J, Houseley J, Saveanu C, Petfalski E, Thompson E, Jacquier A, Tollervey D (2005) RNA degradation by the exosome is promoted by a nuclear polyadenylation complex. Cell 121: 713-24

Lam Y W, Trinkle-Mulcahy L, Lamond A I (2005) The nucleolus. J Cell Sci 118: 1335-7

Lange H, Holec S, Cognat V, Pieuchot L, Le Ret M, Canaday J, Gagliardi D (2008) Degradation of a polyadenylated rRNA maturation by-product involves one of the three RRP6-like proteins in Arabidopsis thaliana. Mol Cell Biol 28: 3038-44

Lange H, Sement F M, Gagliardi D (2011) MTR4, a putative RNA helicase and exosome co-factor, is required for proper rRNA biogenesis and development in Arabidopsis thaliana. Plant J 68: 51-63

Lee M M, Schiefelbein J (1999) WEREWOLF, a MYB-related protein in Arabidopsis, is a position-dependent regulator of epidermal cell patterning. Cell 99: 473-83

Lee M M, Schiefelbein J (2001) Developmentally distinct MYB genes encode functionally equivalent proteins in Arabidopsis. Development 128: 1539-46

Lee M M, Schiefelbein J (2002) Cell pattern in the Arabidopsis root epidermis determined by lateral inhibition with feedback. Plant Cell 14: 611-8

Lee S H, Cho H T (2009) 'Auxin and Root Hair Morphogenesis' in Emons, A. M. C. and Ketelaar, T., eds., *Root Hairs*, Berlin, Heidelberg: Springer Berlin Heidelberg, 45-64.

Lee Y Y, Cevallos R C, Jan E (2009) An upstream open reading frame regulates translation of GADD34 during cellular stresses that induce eIF2alpha phosphorylation. J Biol Chem 284: 6661-73

Levine A J (1997) p53, the cellular gatekeeper for growth and division. Cell 88: 323-31

Li D X, Chen W Q, Xu Z H, Bai S N (2015) HISTONE DEACETYLASE6-Defective Mutants Show Increased Expression and Acetylation of ENHANCER OF TRIPTYCHON AND CAPRICE1 and GLABRA2 with Small But Significant Effects on Root Epidermis Cellular Pattern. Plant Physiol 168: 1448-58

Li H D, Zagorski J, Fournier M J (1990) Depletion of U14 small nuclear RNA (snR128) disrupts production of 18S rRNA in Saccharomyces cerevisiae. Mol Cell Biol 10: 1145-52

Li N, Yuan L, Liu N, Shi D, Li X, Tang Z, Liu J, Sundaresan V, Yang W C (2009) SLOW WALKER2, a NOC1/MAK21 homologue, is essential for coordinated cell cycle progression during female gametophyte development in Arabidopsis. Plant Physiol 151: 1486-97

Li S F, Milliken O N, Pham H, Seyit R, Napoli R, Preston J, Koltunow A M, Parish R W (2009) The Arabidopsis MYB5 transcription factor regulates mucilage synthesis, seed coat development, and trichome morphogenesis. Plant Cell 21: 72-89

Li X, Duan X, Jiang H, Sun Y, Tang Y, Yuan Z, Guo J, Liang W, Chen L, Yin J, Ma H, Wang J, Zhang D (2006) Genome-wide analysis of basic/helix-loop-helix transcription factor family in rice and Arabidopsis. Plant Physiol 141: 1167-84

Liang G, He H, Li Y, Ai Q, Yu D (2014) MYB82 functions in regulation of trichome development in Arabidopsis. J Exp Bot 65: 3215-23

Liang W Q, Fournier M J (1995) U14 base-pairs with 18S rRNA: a novel snoRNA interaction required for rRNA processing. Genes Dev 9: 2433-43

Lin-Wang K, Bolitho K, Grafton K, Kortstee A, Karunairetnam S, McGhie T K, Espley R V, Hellens R P, Allan A C (2010) An R2R3 MYB transcription factor associated with regulation of the anthocyanin biosynthetic pathway in Rosaceae. BMC Plant Biol 10: 50

Lin Q, Ohashi Y, Kato M, Tsuge T, Gu H, Qu L J, Aoyama T (2015) GLABRA2 Directly Suppresses Basic Helix-Loop-Helix Transcription Factor Genes with Diverse Functions in Root Hair Development. Plant Cell 27: 2894-906

Lin Y, May G E, Kready H, Nazzaro L, Mao M, Spealman P, Creeger Y, McManus C J (2019) Impacts of uORF codon identity and position on translation regulation. Nucleic Acids Res

Lin Y, Schiefelbein J (2001) Embryonic control of epidermal cell patterning in the root and hypocotyl of Arabidopsis. Development 128: 3697-705

Lindemose S, Jensen M K, Van de Velde J, O'Shea C, Heyndrickx K S, Workman C T, Vandepoele K, Skriver K, De Masi F (2014) A DNA-binding-site landscape and regulatory network analysis for NAC transcription factors in Arabidopsis thaliana. Nucleic Acids Res 42: 7681-93

Liu C, Li L C, Chen W Q, Chen X, Xu Z H, Bai S N (2013) HDA18 affects cell fate in Arabidopsis root epidermis via histone acetylation at four kinase genes. Plant Cell 25: 257-69

Livak K J, Schmittgen T D (2001) Analysis of relative gene expression data using real-time quantitative PCR and the 2(-Delta Delta C(T)) Method. Methods 25: 402-8

Lloyd A M, Schena M, Walbot V, Davis R W (1994) Epidermal cell fate determination in Arabidopsis: patterns defined by a steroid-inducible regulator. Science 266: 436-9

Lofke C, Dunser K, Kleine-Vehn J (2013) Epidermal patterning genes impose non-cell autonomous cell size determination and have additional roles in root meristem size control. J Integr Plant Biol 55: 864-75

Ma Z, Bielenberg D G, Brown K M, Lynch J P (2001) Regulation of root hair density by phosphorus availability in Arabidopsis thaliana. Plant, Cell & Environment 24: 459-467

Maekawa S, Ishida T, Yanagisawa S (2018) Reduced Expression of APUM24, Encoding a Novel rRNA Processing Factor, Induces Sugar-Dependent Nucleolar Stress and Altered Sugar Responses in Arabidopsis thaliana. Plant Cell 30: 209-227

Maher K A, Bajic M, Kajala K, Reynoso M, Pauluzzi G, West D A, Zumstein K, Woodhouse M, Bubb K, Dorrity M W, Queitsch C, Bailey-Serres J, Sinha N, Brady S M, Deal R B (2018) Profiling of Accessible Chromatin Regions across Multiple Plant Species and Cell Types Reveals Common Gene Regulatory Principles and New Control Modules. Plant Cell 30: 15-36

Marechal V, Elenbaas B, Piette J, Nicolas J C, Levine A J (1994) The ribosomal L5 protein is associated with mdm-2 and mdm-2-p53 complexes. Mol Cell Biol 14: 7414-20

Masucci J D, Rerie W G, Foreman D R, Zhang M, Galway M E, Marks M D, Schiefelbein J W (1996a) The homeobox gene GLABRA2 is required for position-dependent cell differentiation in the root epidermis of Arabidopsis thaliana. Development 122: 1253-60

Masucci J D, Schiefelbein J W (1994) The rhd6 Mutation of Arabidopsis thaliana Alters Root-Hair Initiation through an Auxin- and Ethylene-Associated Process. Plant Physiol 106: 1335-1346

Masucci J D, Schiefelbein J W (1996b) Hormones act downstream of TTG and GL2 to promote root hair outgrowth during epidermis development in the Arabidopsis root. Plant Cell 8: 1505-17

Mayer C, Grummt I (2005) Cellular stress and nucleolar function. Cell Cycle 4: 1036-8

Menand B, Yi K, Jouannic S, Hoffmann L, Ryan E, Linstead P, Schaefer D G, Dolan L (2007) An ancient mechanism controls the development of cells with a rooting function in land plants. Science 316: 1477-80

Merchante C, Stepanova A N, Alonso J M (2017) Translation regulation in plants: an interesting past, an exciting present and a promising future. Plant J 90: 628-653

Mineur P, Jennane A, Thiry M, Deltour R, Goessens G (1998) Ultrastructural Distribution of DNA within Plant Meristematic Cell Nucleoli during Activation and the Subsequent Inactivation by a Cold Stress. Journal of Structural Biology 123: 199-210

Missbach S, Weis B L, Martin R, Simm S, Bohnsack M T, Schleiff E (2013) 40S ribosome biogenesis co-factors are essential for gametophyte and embryo development. PLoS One 8: e54084

Misson J, Raghothama K G, Jain A, Jouhet J, Block M A, Bligny R, Ortet P, Creff A, Somerville S, Rolland N, Doumas P, Nacry P, Herrerra-Estrella L, Nussaume L, Thibaud M C (2005) A genome-wide transcriptional analysis using Arabidopsis thaliana Affymetrix gene chips determined plant responses to phosphate deprivation. Proc Natl Acad Sci U S A 102: 11934-9

Mohannath G, Pontvianne F, Pikaard C S (2016) Selective nucleolus organizer inactivation in Arabidopsis is a chromosome position-effect phenomenon. Proc Natl Acad Sci U S A 113: 13426-13431

Morohashi K, Grotewold E (2009) A systems approach reveals regulatory circuitry for Arabidopsis trichome initiation by the GL3 and GL1 selectors. PLoS Genet 5: e1000396

Morohashi K, Zhao M, Yang M, Read B, Lloyd A, Lamb R, Grotewold E (2007) Participation of the Arabidopsis bHLH factor GL3 in trichome initiation regulatory events. Plant Physiol 145: 736-46

Morris D R, Geballe A P (2000) Upstream open reading frames as regulators of mRNA translation. Mol Cell Biol 20: 8635-42

Moss T, Stefanovsky V Y (1995) Promotion and regulation of ribosomal transcription in eukaryotes by RNA polymerase I. Prog Nucleic Acid Res Mol Biol 50: 25-66

Mroue S, Simeunovic A, Robert H S (2018) Auxin production as an integrator of environmental cues for developmental growth regulation. J Exp Bot 69: 201-212

Muller M, Schmidt W (2004) Environmentally induced plasticity of root hair development in Arabidopsis. Plant Physiol 134: 409-19

Muralla R, Lloyd J, Meinke D (2011) Molecular foundations of reproductive lethality in Arabidopsis thaliana. PLoS One 6: e28398

Murata M, Heslop-Harrison J S, Motoyoshi F (1997) Physical mapping of the 5S ribosomal RNA genes in Arabidopsis thaliana by multi-color fluorescence in situ hybridization with cosmid clones. Plant J 12: 31-7

Murata Y, Wharton R P (1995) Binding of pumilio to maternal hunchback mRNA is required for posterior patterning in Drosophila embryos. Cell 80: 747-56

Nadeau J A, Sack F D (2002) Stomatal development in Arabidopsis. Arabidopsis Book 1: e0066

Nazar R N (2004) Ribosomal RNA processing and ribosome biogenesis in eukaryotes. IUBMB Life 56: 457-65

Neff M M, Turk E, Kalishman M (2002) Web-based primer design for single nucleotide polymorphism analysis. Trends Genet 18: 613-5

Nishimura T, Wada T, Yamamoto K T, Okada K (2005) The Arabidopsis STV1 protein, responsible for translation reinitiation, is required for auxin-mediated gynoecium patterning. Plant Cell 17: 2940-53

Nocedal I, Johnson A D (2015) How Transcription Networks Evolve and Produce Biological Novelty. Cold Spring Harb Symp Quant Biol 80: 265-74

Ogata K, Morikawa S, Nakamura H, Sekikawa A, Inoue T, Kanai H, Sarai A, Ishii S, Nishimura Y (1994) Solution structure of a specific DNA complex of the Myb DNA-binding domain with cooperative recognition helices. Cell 79: 639-48

Ohashi Y, Oka A, Ruberti I, Morelli G, Aoyama T (2002) Entopically additive expression of GLABRA2 alters the frequency and spacing of trichome initiation. Plant J 29: 359-69

Ohbayashi I, Konishi M, Ebine K, Sugiyama M (2011) Genetic identification of Arabidopsis RID2 as an essential factor involved in pre-rRNA processing. Plant J 67: 49-60

Ohbayashi I, Lin C Y, Shinohara N, Matsumura Y, Machida Y, Horiguchi G, Tsukaya H, Sugiyama M (2017a) Evidence for a Role of ANAC082 as a Ribosomal Stress Response Mediator Leading to Growth Defects and Developmental Alterations in Arabidopsis. Plant Cell 29: 2644-2660

Ohbayashi I, Sugiyama M (2017b) Plant Nucleolar Stress Response, a New Face in the NAC-Dependent Cellular Stress Responses. Front Plant Sci 8: 2247

Olson M O, Hingorani K, Szebeni A (2002) Conventional and nonconventional roles of the nucleolus. Int Rev Cytol 219: 199-266

Ooka H, Satoh K, Doi K, Nagata T, Otomo Y, Murakami K, Matsubara K, Osato N, Kawai J, Carninci P, Hayashizaki Y, Suzuki K, Kojima K, Takahara Y, Yamamoto K, Kikuchi S (2003) Comprehensive analysis of NAC family genes in Oryza sativa and Arabidopsis thaliana. DNA Res 10: 239-47

Overvoorde P, Fukaki H, Beeckman T (2010) Auxin control of root development. Cold Spring Harb Perspect Biol 2: a001537

Pajerowska-Mukhtar K M, Wang W, Tada Y, Oka N, Tucker C L, Fonseca J P, Dong X (2012) The HSF-like transcription factor TBF1 is a major molecular switch for plant growth-to-defense transition. Curr Biol 22: 103-12

Palm D, Streit D, Ruprecht M, Simm S, Scharf C, Schleiff E (2018) Late ribosomal protein localization in Arabidopsis thaliana differs to that in Saccharomyces cerevisiae. FEBS Open Bio 8: 1437-1444

Palm D, Streit D, Shanmugam T, Weis B L, Ruprecht M, Simm S, Schleiff E (2019) Plant-specific ribosome biogenesis factors in Arabidopsis thaliana with essential function in rRNA processing. Nucleic Acids Res 47: 1880-1895

Patel S B, Bellini M (2008) The assembly of a spliceosomal small nuclear ribonucleoprotein particle. Nucleic Acids Res 36: 6482-93

Pattanaik S, Patra B, Singh S K, Yuan L (2014) An overview of the gene regulatory network controlling trichome development in the model plant, Arabidopsis. Front Plant Sci 5: 259

Payne C T, Zhang F, Lloyd A M (2000) GL3 encodes a bHLH protein that regulates trichome development in arabidopsis through interaction with GL1 and TTG1. Genetics 156: 1349-62

Paz-Ares J, Ghosal D, Wienand U, Peterson P A, Saedler H (1987) The regulatory c1 locus of Zea mays encodes a protein with homology to myb proto-oncogene products and with structural similarities to transcriptional activators. EMBO J 6: 3553-8

Penzo M, Montanaro L, Trere D, Derenzini M (2019) The Ribosome Biogenesis-Cancer Connection. Cells 8

Pesch M, Schultheiss I, Klopffleisch K, Uhrig J F, Koegl M, Clemen C S, Simon R, Weidtkamp-Peters S, Hulskamp M (2015) TRANSPARENT TESTA GLABRA1 and GLABRA1 Compete for Binding to GLABRA3 in Arabidopsis. Plant Physiol 168: 584-97

Petricka J J, Nelson T M (2007) Arabidopsis nucleolin affects plant development and patterning. Plant Physiol 144: 173-86

Petricka J J, Winter C M, Benfey P N (2012) Control of Arabidopsis root development. Annu Rev Plant Biol 63: 563-90

Phipps K R, Charette J M, Baserga S J (2011) The small subunit processome in ribosome biogenesis—progress and prospects. Wiley Interdisciplinary Reviews: RNA 2: 1-21

Pih K T, Yi M J, Liang Y S, Shin B J, Cho M J, Hwang I, Son D (2000) Molecular cloning and targeting of a fibrillarin homolog from Arabidopsis. Plant Physiol 123: 51-8

Pillitteri L J, Dong J (2013) Stomatal development in Arabidopsis. Arabidopsis Book 11: e0162

Pinon V, Etchells J P, Rossignol P, Collier S A, Arroyo J M, Martienssen R A, Byrne M E (2008) Three PIGGYBACK genes that specifically influence leaf patterning encode ribosomal proteins. Development 135: 1315-24

Planta R J, Mager W H (1998) The list of cytoplasmic ribosomal proteins of Saccharomyces cerevisiae. Yeast 14: 471-7

Podzimska-Sroka D, O'Shea C, Gregersen P L, Skriver K (2015) NAC Transcription Factors in Senescence: From Molecular Structure to Function in Crops. Plants (Basel) 4: 412-48

Pontvianne F, Abou-Ellail M, Douet J, Comella P, Matia I, Chandrasekhara C, Debures A, Blevins T, Cooke R, Medina F J, Tourmente S, Pikaard C S, Saez-Vasquez J (2010) Nucleolin is required for DNA methylation state and the expression of rRNA gene variants in Arabidopsis thaliana. PLoS Genet 6: e1001225

Pontvianne F, Blevins T, Chandrasekhara C, Mozgova I, Hassel C, Pontes O M, Tucker S, Mokros P, Muchova V, Fajkus J, Pikaard C S (2013) Subnuclear partitioning of rRNA genes between the nucleolus and nucleoplasm reflects alternative epiallelic states. Genes Dev 27: 1545-50

Pontvianne F, Matia I, Douet J, Tourmente S, Medina F J, Echeverria M, Saez-Vasquez J (2007) Characterization of AtNUC-L1 reveals a central role of nucleolin in nucleolus organization and silencing of AtNUC-L2 gene in Arabidopsis. Mol Biol Cell 18: 369-79

Qiu C, McCann K L, Wine R N, Baserga S J, Hall T M (2014) A divergent Pumilio repeat protein family for pre-rRNA processing and mRNA localization. Proc Natl Acad Sci U S A 111: 18554-9

Rabiger D S, Drews G N (2013) MYB64 and MYB119 are required for cellularization and differentiation during female gametogenesis in Arabidopsis thaliana. PLoS Genet 9: e1003783

Ramakrishnan V (2002) Ribosome structure and the mechanism of translation. Cell 108: 557-72

Ramsay N A, Glover B J (2005) MYB-bHLH-WD40 protein complex and the evolution of cellular diversity. Trends Plant Sci 10: 63-70

Ren M, Venglat P, Qiu S, Feng L, Cao Y, Wang E, Xiang D, Wang J, Alexander D, Chalivendra S, Logan D, Mattoo A, Selvaraj G, Datla R (2012) Target of rapamycin signaling regulates metabolism, growth, and life span in Arabidopsis. Plant Cell 24: 4850-74

Rerie W G, Feldmann K A, Marks M D (1994) The GLABRA2 gene encodes a homeo domain protein required for normal trichome development in Arabidopsis. Genes Dev 8: 1388-99

Revenkova E, Masson J, Koncz C, Afsar K, Jakovleva L, Paszkowski J (1999) Involvement of Arabidopsis thaliana ribosomal protein S27 in mRNA degradation triggered by genotoxic stress. EMBO J 18: 490-9

Rishmawi L, Wolff H, Schrader A, Hulskamp M (2018) Sub-epidermal Expression of ENHANCER OF TRIPTYCHON AND CAPRICE1 and Its Role in Root Hair Formation Upon Pi Starvation. Front Plant Sci 9: 1411

Rodor J, Jobet E, Bizarro J, Vignols F, Carles C, Suzuki T, Nakamura K, Echeverria M (2011) AtNUFIP, an essential protein for plant development, reveals the impact of snoRNA gene organisation on the assembly of snoRNPs and rRNA methylation in Arabidopsis thaliana. Plant J 65: 807-19

Rosado A, Li R, van de Ven W, Hsu E, Raikhel N V (2012) Arabidopsis ribosomal proteins control developmental programs through translational regulation of auxin response factors. Proc Natl Acad Sci U S A 109: 19537-44

Rosato M, Kovarik A, Garilleti R, Rossello J A (2016) Conserved Organisation of 45S rDNA Sites and rDNA Gene Copy Number among Major Clades of Early Land Plants. PLoS One 11: e0162544

Rovere F D, Fattorini L, Ronzan M, Falasca G, Altamura M M (2016) The quiescent center and the stem cell niche in the adventitious roots of Arabidopsis thaliana. Plant Signal Behav 11: e1176660

Roy A, Kucukural A, Zhang Y (2010) I-TASSER: a unified platform for automated protein structure and function prediction. Nat Protoc 5: 725-38

Ryu K H, Kang Y H, Park Y H, Hwang I, Schiefelbein J, Lee M M (2005) The WEREWOLF MYB protein directly regulates CAPRICE transcription during cell fate specification in the Arabidopsis root epidermis. Development 132: 4765-75

Saez-Vasquez J, Caparros-Ruiz D, Barneche F, Echeverria M (2004a) Characterization of a crucifer plant pre-rRNA processing complex. Biochem Soc Trans 32: 578-80

Saez-Vasquez J, Caparros-Ruiz D, Barneche F, Echeverria M (2004b) A plant snoRNP complex containing snoRNAs, fibrillarin, and nucleolin-like proteins is competent for both rRNA gene binding and pre-rRNA processing in vitro. Mol Cell Biol 24: 7284-97

Saez-Vasquez J, Delseny M (2019) Ribosome Biogenesis in Plants: from Functional 45S Ribosomal DNA Organization to Ribosome Assembly Factors. Plant Cell

Saikumar P, Murali R, Reddy E P (1990) Role of tryptophan repeats and flanking amino acids in Myb-DNA interactions. Proc Natl Acad Sci U S A 87: 8452-6

Sakura H, Kanei-Ishii C, Nagase T, Nakagoshi H, Gonda T J, Ishii S (1989) Delineation of three functional domains of the transcriptional activator encoded by the c-myb protooncogene. Proc Natl Acad Sci U S A 86: 5758-62

Salazar-Henao J E, Velez-Bermudez I C, Schmidt W (2016) The regulation and plasticity of root hair patterning and morphogenesis. Development 143: 1848-58

Salome P A (2017) Proliferate at Your Own Risk: Ribosomal Stress and Regeneration. Plant Cell 29: 2318

Sanchez C G, Teixeira F K, Czech B, Preall J B, Zamparini A L, Seifert J R, Malone C D, Hannon G J, Lehmann R (2016) Regulation of Ribosome Biogenesis and Protein Synthesis Controls Germline Stem Cell Differentiation. Cell Stem Cell 18: 276-90

Savage N, Yang T J, Chen C Y, Lin K L, Monk N A, Schmidt W (2013) Positional signaling and expression of ENHANCER OF TRY AND CPC1 are tuned to increase root hair density in response to phosphate deficiency in Arabidopsis thaliana. PLoS One 8: e75452

Schafer T, Strauss D, Petfalski E, Tollervey D, Hurt E (2003) The path from nucleolar 90S to cytoplasmic 40S pre-ribosomes. EMBO J 22: 1370-80

Schellmann S, Schnittger A, Kirik V, Wada T, Okada K, Beermann A, Thumfahrt J, Jurgens G, Hulskamp M (2002a) TRIPTYCHON and CAPRICE mediate lateral inhibition during trichome and root hair patterning in Arabidopsis. EMBO J 21: 5036-46

Schellmann S, Schnittger A, Kirik V, Wada T, Okada K, Beermann A, Thumfahrt J, Jürgens G, Hülskamp M (2002b) TRIPTYCHON and CAPRICE mediate lateral inhibition during trichome and root hair patterning in Arabidopsis. The EMBO Journal 21: 5036

Scheres B, Wolkenfelt H, Willemsen V, Terlouw M, Lawson E, Dean C, Weisbeek P (1994) Embryonic origin of the Arabidopsis primary root and root meristem initials. Development 120: 2475

Schiefelbein J, Huang L, Zheng X (2014) Regulation of epidermal cell fate in Arabidopsis roots: the importance of multiple feedback loops. Front Plant Sci 5: 47

Schiefelbein J, Kwak S H, Wieckowski Y, Barron C, Bruex A (2009) The gene regulatory network for root epidermal cell-type pattern formation in Arabidopsis. J Exp Bot 60: 1515-21

Schiefelbein J W, Somerville C (1990) Genetic Control of Root Hair Development in Arabidopsis thaliana. Plant Cell 2: 235-243

Schikora A, Schmidt W (2001) Acclimative changes in root epidermal cell fate in response to Fe and P deficiency: a specific role for auxin? Protoplasma 218: 67-75

Schmidt S, Dethloff F, Beine-Golovchuk O, Kopka J (2013) The REIL1 and REIL2 proteins of Arabidopsis thaliana are required for leaf growth in the cold. Plant Physiol 163: 1623-39

Schmidt W, Schikora A (2001) Different pathways are involved in phosphate and iron stress-induced alterations of root epidermal cell development. Plant Physiol 125: 2078-84

Sergiev P V, Aleksashin N A, Chugunova A A, Polikanov Y S, Dontsova O A (2018) Structural and evolutionary insights into ribosomal RNA methylation. Nat Chem Biol 14: 226-235

Serna L (2008) CAPRICE positively regulates stomatal formation in the Arabidopsis hypocotyl. Plant Signal Behav 3: 1077-82

Shahbazian M D, Grunstein M (2007) Functions of site-specific histone acetylation and deacetylation. Annu Rev Biochem 76: 75-100

Shanmugam T, Abbasi N, Kim H S, Kim H B, Park N I, Park G T, Oh S A, Park S K, Muench D G, Choi Y, Park Y I, Choi S B (2017) An Arabidopsis divergent pumilio protein, APUM24, is essential for embryogenesis and required for faithful pre-rRNA processing. Plant J 92: 1092-1105

Shi D Q, Liu J, Xiang Y H, Ye D, Sundaresan V, Yang W C (2005) SLOW WALKER1, essential for gametogenesis in Arabidopsis, encodes a WD40 protein involved in 18S ribosomal RNA biogenesis. Plant Cell 17: 2340-54

Sidrauski C, McGeachy A M, Ingolia N T, Walter P (2015) The small molecule ISRIB reverses the effects of eIF2alpha phosphorylation on translation and stress granule assembly. Elife 4

Simon M, Lee M M, Lin Y, Gish L, Schiefelbein J (2007) Distinct and overlapping roles of single-repeat MYB genes in root epidermal patterning. Dev Biol 311: 566-78

Sloan K E, Warda A S, Sharma S, Entian K D, Lafontaine D L J, Bohnsack M T (2017) Tuning the ribosome: The influence of rRNA modification on eukaryotic ribosome biogenesis and function. RNA Biol 14: 1138-1152

Slomnicki L P, Chung D H, Parker A, Hermann T, Boyd N L, Hetman M (2017) Ribosomal stress and Tp53-mediated neuronal apoptosis in response to capsid protein of the Zika virus. Sci Rep 7: 16652

Slomovic S, Laufer D, Geiger D, Schuster G (2006) Polyadenylation of ribosomal RNA in human cells. Nucleic Acids Res 34: 2966-75

Smith S, De Smet I (2012) Root system architecture: insights from Arabidopsis and cereal crops. Philos Trans R Soc Lond B Biol Sci 367: 1441-52

Sonenberg N, Hinnebusch A G (2009) Regulation of translation initiation in eukaryotes: mechanisms and biological targets. Cell 136: 731-45

Song S K, Ryu K H, Kang Y H, Song J H, Cho Y H, Yoo S D, Schiefelbein J, Lee M M (2011) Cell fate in the Arabidopsis root epidermis is determined by competition between WEREWOLF and CAPRICE. Plant Physiol 157: 1196-208

Srivastava A K, Schlessinger D (1991) Structure and organization of ribosomal DNA. Biochimie 73: 631-8

Stepinski D (2010) Organization of the nucleoli of soybean root meristematic cells at different states of their activity. Micron 41: 283-8

Stepinski D (2014) Functional ultrastructure of the plant nucleolus. Protoplasma 251: 1285-306

Stępiński D (2008) Nucleolar vacuolation in soybean root meristematic cells during recovery after chilling. Biologia Plantarum 52: 507-512

Stoyanova B B, Hadjiolov A A (1979) Alterations in the processing of rat-liver ribosomal RNA caused by cycloheximide inhibition of protein synthesis. Eur J Biochem 96: 349-56

Stracke R, Werber M, Weisshaar B (2001) The R2R3-MYB gene family in Arabidopsis thaliana. Curr Opin Plant Biol 4: 447-56

Strunk B S, Karbstein K (2009) Powering through ribosome assembly. RNA 15: 2083-104

Szakonyi D, Byrne M E (2011) Involvement of ribosomal protein RPL27a in meristem activity and organ development. Plant Signal Behav 6: 712-4

Szamecz B, Rutkai E, Cuchalova L, Munzarova V, Herrmannova A, Nielsen K H, Burela L, Hinnebusch A G, Valasek L (2008) eIF3a cooperates with sequences 5' of uORF1 to

promote resumption of scanning by post-termination ribosomes for reinitiation on GCN4 mRNA. Genes Dev 22: 2414-25

Szostak E, Gebauer F (2013) Translational control by 3'-UTR-binding proteins. Brief Funct Genomics 12: 58-65

Szymanski D B, Jilk R A, Pollock S M, Marks M D (1998) Control of GL2 expression in Arabidopsis leaves and trichomes. Development 125: 1161-71

Tam P P, Barrette-Ng I H, Simon D M, Tam M W, Ang A L, Muench D G (2010) The Puf family of RNA-binding proteins in plants: phylogeny, structural modeling, activity and subcellular localization. BMC Plant Biol 10: 44

Tanimoto M, Roberts K, Dolan L (1995) Ethylene is a positive regulator of root hair development in Arabidopsis thaliana. Plant J 8: 943-8

ten Hove C A, Lu K J, Weijers D (2015) Building a plant: cell fate specification in the early Arabidopsis embryo. Development 142: 420-30

Thomson E, Ferreira-Cerca S, Hurt E (2013) Eukaryotic ribosome biogenesis at a glance. J Cell Sci 126: 4815-21

Thomson E, Rappsilber J, Tollervey D (2007) Nop9 is an RNA binding protein present in pre-40S ribosomes and required for 18S rRNA synthesis in yeast. RNA 13: 2165-74

Tombuloglu H, Kekec G, Sakcali M S, Unver T (2013) Transcriptome-wide identification of R2R3-MYB transcription factors in barley with their boron responsive expression analysis. Mol Genet Genomics 288: 141-55

Tomecki R, Sikorski P J, Zakrzewska-Placzek M (2017) Comparison of preribosomal RNA processing pathways in yeast, plant and human cells - focus on coordinated action of endo- and exoribonucleases. FEBS Lett 591: 1801-1850

Tominaga-Wada R, Nukumizu Y, Sato S, Kato T, Tabata S, Wada T (2012) Functional divergence of MYB-related genes, WEREWOLF and AtMYB23 in Arabidopsis. Biosci Biotechnol Biochem 76: 883-7

Tominaga R, Iwata M, Okada K, Wada T (2007) Functional analysis of the epidermal-specific MYB genes CAPRICE and WEREWOLF in Arabidopsis. Plant Cell 19: 2264-77

Troncoso-Ponce M A, Barthole G, Tremblais G, To A, Miquel M, Lepiniec L, Baud S (2016) Transcriptional Activation of Two Delta-9 Palmitoyl-ACP Desaturase Genes by MYB115 and MYB118 Is Critical for Biosynthesis of Omega-7 Monounsaturated Fatty Acids in the Endosperm of Arabidopsis Seeds. Plant Cell 28: 2666-2682

Tzafrir I, Pena-Muralla R, Dickerman A, Berg M, Rogers R, Hutchens S, Sweeney T C, McElver J, Aux G, Patton D, Meinke D (2004) Identification of genes required for embryo development in Arabidopsis. Plant Physiol 135: 1206-20

Uechi T, Tanaka T, Kenmochi N (2001) A complete map of the human ribosomal protein genes: assignment of 80 genes to the cytogenetic map and implications for human disorders. Genomics 72: 223-30

van den Berg C, Weisbeek P, Scheres B (1998) Cell fate and cell differentiation status in the Arabidopsis root. Planta 205: 483-91

van den Berg C, Willemsen V, Hendriks G, Weisbeek P, Scheres B (1997) Short-range control of cell differentiation in the Arabidopsis root meristem. Nature 390: 287-9

van Hengel A J, Barber C, Roberts K (2004) The expression patterns of arabinogalactan-protein AtAGP30 and GLABRA2 reveal a role for abscisic acid in the early stages of root epidermal patterning. Plant J 39: 70-83

van Hoof A, Lennertz P, Parker R (2000) Three conserved members of the RNase D family have unique and overlapping functions in the processing of 5S, 5.8S, U4, U5, RNase MRP and RNase P RNAs in yeast. EMBO J 19: 1357-65

Van Lijsebettens M, Vanderhaeghen R, De Block M, Bauw G, Villarroel R, Van Montagu M (1994) An S18 ribosomal protein gene copy at the Arabidopsis PFL locus affects plant development by its specific expression in meristems. EMBO J 13: 3378-88

Vaughan-Hirsch J, Goodall B, Bishopp A (2018) North, East, South, West: mapping vascular tissues onto the Arabidopsis root. Curr Opin Plant Biol 41: 16-22

Venkateswarlu K, Lee S W, Nazar R N (1991) Conserved upstream sequence elements in plant 5S ribosomal RNA-encoding genes. Gene 105: 249-54

Verbelen J P, De Cnodder T, Le J, Vissenberg K, Baluska F (2006) The Root Apex of Arabidopsis thaliana Consists of Four Distinct Zones of Growth Activities: Meristematic Zone, Transition Zone, Fast Elongation Zone and Growth Terminating Zone. Plant Signal Behav 1: 296-304

Visser E J, Pierik R (2007) Inhibition of root elongation by ethylene in wetland and non-wetland plant species and the impact of longitudinal ventilation. Plant Cell Environ 30: 31-8

Wada T, Kurata T, Tominaga R, Koshino-Kimura Y, Tachibana T, Goto K, Marks M D, Shimura Y, Okada K (2002) Role of a positive regulator of root hair development, CAPRICE, in Arabidopsis root epidermal cell differentiation. Development 129: 5409-19

Wada T, Tachibana T, Shimura Y, Okada K (1997) Epidermal cell differentiation in Arabidopsis determined by a Myb homolog, CPC. Science 277: 1113-6

Walker A R, Davison P A, Bolognesi-Winfield A C, James C M, Srinivasan N, Blundell T L, Esch J J, Marks M D, Gray J C (1999) The TRANSPARENT TESTA GLABRA1 locus, which regulates trichome differentiation and anthocyanin biosynthesis in Arabidopsis, encodes a WD40 repeat protein. Plant Cell 11: 1337-50

Wang M, Oge L, Perez-Garcia M D, Hamama L, Sakr S (2018) The PUF Protein Family: Overview on PUF RNA Targets, Biological Functions, and Post Transcriptional Regulation. Int J Mol Sci 19

Wang S, Chen J G (2008) Arabidopsis transient expression analysis reveals that activation of GLABRA2 may require concurrent binding of GLABRA1 and GLABRA3 to the promoter of GLABRA2. Plant Cell Physiol 49: 1792-804

Wang W, Ryu K H, Barron C, Schiefelbein J (2019) Root Epidermal Cell Patterning is Modulated by a Critical Residue in the WEREWOLF Transcription Factor. Plant Physiol

Wang Z, Tang J, Hu R, Wu P, Hou X L, Song X M, Xiong A S (2015) Genome-wide analysis of the R2R3-MYB transcription factor genes in Chinese cabbage (Brassica rapa ssp. pekinensis) reveals their stress and hormone responsive patterns. BMC Genomics 16: 17

Warner J R (1999) The economics of ribosome biosynthesis in yeast. Trends Biochem Sci 24: 437-40

Watkins N J, Bohnsack M T (2012) The box C/D and H/ACA snoRNPs: key players in the modification, processing and the dynamic folding of ribosomal RNA. Wiley Interdiscip Rev RNA 3: 397-414

Weis B L, Kovacevic J, Missbach S, Schleiff E (2015a) Plant-Specific Features of Ribosome Biogenesis. Trends Plant Sci 20: 729-740

Weis B L, Missbach S, Marzi J, Bohnsack M T, Schleiff E (2014) The 60S associated ribosome biogenesis factor LSG1-2 is required for 40S maturation in Arabidopsis thaliana. Plant J 80: 1043-56

Weis B L, Palm D, Missbach S, Bohnsack M T, Schleiff E (2015b) atBRX1-1 and atBRX1-2 are involved in an alternative rRNA processing pathway in Arabidopsis thaliana. RNA 21: 415-25

Wester K, Digiuni S, Geier F, Timmer J, Fleck C, Hulskamp M (2009) Functional diversity of R3 single-repeat genes in trichome development. Development 136: 1487-96

Wickens M, Bernstein D S, Kimble J, Parker R (2002) A PUF family portrait: 3'UTR regulation as a way of life. Trends Genet 18: 150-7

Wieckowski Y, Schiefelbein J (2012) Nuclear ribosome biogenesis mediated by the DIM1A rRNA dimethylase is required for organized root growth and epidermal patterning in Arabidopsis. Plant Cell 24: 2839-56

Wilson D N, Doudna Cate J H (2012) The structure and function of the eukaryotic ribosome. Cold Spring Harb Perspect Biol 4

Woo H R, Richards E J (2008) Natural variation in DNA methylation in ribosomal RNA genes of Arabidopsis thaliana. BMC Plant Biol 8: 92

Xi L, Moscou M J, Meng Y, Xu W, Caldo R A, Shaver M, Nettleton D, Wise R P (2009) Transcript-based cloning of RRP46, a regulator of rRNA processing and R gene-independent cell death in barley-powdery mildew interactions. Plant Cell 21: 3280-95

Xiang C, Han P, Lutziger I, Wang K, Oliver D J (1999) A mini binary vector series for plant transformation. Plant Mol Biol 40: 711-7

Xiong Y, McCormack M, Li L, Hall Q, Xiang C, Sheen J (2013) Glucose-TOR signalling reprograms the transcriptome and activates meristems. Nature 496: 181-6

Xu C, Min J (2011) Structure and function of WD40 domain proteins. Protein Cell 2: 202-14

Xu C R, Liu C, Wang Y L, Li L C, Chen W Q, Xu Z H, Bai S N (2005) Histone acetylation affects expression of cellular patterning genes in the Arabidopsis root epidermis. Proc Natl Acad Sci U S A 102: 14469-74

Xu G, Greene G H, Yoo H, Liu L, Marques J, Motley J, Dong X (2017a) Global translational reprogramming is a fundamental layer of immune regulation in plants. Nature 545: 487-490

Xu G, Yuan M, Ai C, Liu L, Zhuang E, Karapetyan S, Wang S, Dong X (2017b) uORF-mediated translation allows engineered plant disease resistance without fitness costs. Nature 545: 491-494

Yamaguchi M, Nagahage I S P, Ohtani M, Ishikawa T, Uchimiya H, Kawai-Yamada M, Demura T (2015) Arabidopsis NAC domain proteins VND-INTERACTING1 and ANAC103 interact with multiple NAC domain proteins. Plant Biotechnology advpub

Yang J, Yan R, Roy A, Xu D, Poisson J, Zhang Y (2015a) The I-TASSER Suite: protein structure and function prediction. Nat Methods 12: 7-8

Yang J, Zhang Y (2015b) I-TASSER server: new development for protein structure and function predictions. Nucleic Acids Res 43: W174-81

Yao H, Wang G, Guo L, Wang X (2013) Phosphatidic acid interacts with a MYB transcription factor and regulates its nuclear localization and function in Arabidopsis. Plant Cell 25: 5030-42

Yao Y, Ling Q, Wang H, Huang H (2008) Ribosomal proteins promote leaf adaxial identity. Development 135: 1325-34

Yi K, Menand B, Bell E, Dolan L (2010) A basic helix-loop-helix transcription factor controls cell growth and size in root hairs. Nat Genet 42: 264-7

Yoshihama M, Uechi T, Asakawa S, Kawasaki K, Kato S, Higa S, Maeda N, Minoshima S, Tanaka T, Shimizu N, Kenmochi N (2002) The human ribosomal protein genes: sequencing and comparative analysis of 73 genes. Genome Res 12: 379-90

Young S K, Wek R C (2016) Upstream Open Reading Frames Differentially Regulate Gene-specific Translation in the Integrated Stress Response. J Biol Chem 291: 16927-35

Zakrzewska-Placzek M, Souret F F, Sobczyk G J, Green P J, Kufel J (2010) Arabidopsis thaliana XRN2 is required for primary cleavage in the pre-ribosomal RNA. Nucleic Acids Res 38: 4487-502

Zamore P D, Williamson J R, Lehmann R (1997) The Pumilio protein binds RNA through a conserved domain that defines a new class of RNA-binding proteins. RNA 3: 1421-33

Zeiger E (1983) The Biology of Stomatal Guard Cells. Annual Review of Plant Physiology 34: 441-474

Zhang C, Feng R, Ma R, Shen Z, Cai Z, Song Z, Peng B, Yu M (2018) Genome-wide analysis of basic helix-loop-helix superfamily members in peach. PLoS One 13: e0195974

Zhang C, Muench D G (2015) A Nucleolar PUF RNA-binding Protein with Specificity for a Unique RNA Sequence. J Biol Chem 290: 30108-18

Zhang F, Gonzalez A, Zhao M, Payne C T, Lloyd A (2003) A network of redundant bHLH proteins functions in all TTG1-dependent pathways of Arabidopsis. Development 130: 4859-69

Zhang H, Wang Y, Lu J (2019) Function and Evolution of Upstream ORFs in Eukaryotes. Trends Biochem Sci 44: 782-794

Zhang J, Harnpicharnchai P, Jakovljevic J, Tang L, Guo Y, Oeffinger M, Rout M P, Hiley S L, Hughes T, Woolford J L, Jr. (2007) Assembly factors Rpf2 and Rrs1 recruit 5S rRNA and ribosomal proteins rpL5 and rpL11 into nascent ribosomes. Genes Dev 21: 2580-92

Zhang J, McCann K L, Qiu C, Gonzalez L E, Baserga S J, Hall T M (2016) Nop9 is a PUF-like protein that prevents premature cleavage to correctly process pre-18S rRNA. Nat Commun 7: 13085

Zhang Y, Li B, Huai D, Zhou Y, Kliebenstein D J (2015) The conserved transcription factors, MYB115 and MYB118, control expression of the newly evolved benzoyloxy glucosinolate pathway in Arabidopsis thaliana. Front Plant Sci 6: 343

Zhang Y, Lu H (2009) Signaling to p53: ribosomal proteins find their way. Cancer Cell 16: 369-77

Zhang Y, Wolf G W, Bhat K, Jin A, Allio T, Burkhart W A, Xiong Y (2003) Ribosomal protein L11 negatively regulates oncoprotein MDM2 and mediates a p53-dependent ribosomal-stress checkpoint pathway. Mol Cell Biol 23: 8902-12

Zhao H, Lu S, Li R, Chen T, Zhang H, Cui P, Ding F, Liu P, Wang G, Xia Y, Running M P, Xiong L (2015) The Arabidopsis gene DIG6 encodes a large 60S subunit nuclear export GTPase 1 that is involved in ribosome biogenesis and affects multiple auxin-regulated development processes. J Exp Bot 66: 6863-75

Zhao H, Wang X, Zhu D, Cui S, Li X, Cao Y, Ma L (2012) A single amino acid substitution in IIIf subfamily of basic helix-loop-helix transcription factor AtMYC1 leads to trichome and root hair patterning defects by abolishing its interaction with partner proteins in Arabidopsis. J Biol Chem 287: 14109-21

Zhao M, Morohashi K, Hatlestad G, Grotewold E, Lloyd A (2008) The TTG1-bHLH-MYB complex controls trichome cell fate and patterning through direct targeting of regulatory loci. Development 135: 1991-9

Zhou X, Liao W J, Liao J M, Liao P, Lu H (2015) Ribosomal proteins: functions beyond the ribosome. J Mol Cell Biol 7: 92-104

Zhu P, Wang Y, Qin N, Wang F, Wang J, Deng X W, Zhu D (2016) Arabidopsis small nucleolar RNA monitors the efficient pre-rRNA processing during ribosome biogenesis. Proc Natl Acad Sci U S A 113: 11967-11972

Zhu Z, An F, Feng Y, Li P, Xue L, A M, Jiang Z, Kim J M, To T K, Li W, Zhang X, Yu Q, Dong Z, Chen W Q, Seki M, Zhou J M, Guo H (2011) Derepression of ethylene-stabilized transcription factors (EIN3/EIL1) mediates jasmonate and ethylene signaling synergy in Arabidopsis. Proc Natl Acad Sci U S A 108: 12539-44

Zimmermann I M, Heim M A, Weisshaar B, Uhrig J F (2004) Comprehensive identification of Arabidopsis thaliana MYB transcription factors interacting with R/B-like BHLH proteins. Plant J 40: 22-34

Zsogon A, Szakonyi D, Shi X, Byrne M E (2014) Ribosomal Protein RPL27a Promotes Female Gametophyte Development in a Dose-Dependent Manner. Plant Physiol 165: 1133-1143